(4)

SECOND QUARTERLY REPORT

FOR THE PROJECT

"COMPOSITE CERAMIC SUPERCONDUCTING
WIRES FOR ELECTRIC MOTOR APPLICATIONS"

PRIME CONTRACTOR

CERAMICS PROCESS SYSTEMS CORPORATION
840 MEMORIAL DRIVE
CAMBRIDGE, MASSACHUSETTS 02139

30 DECEMBER 1988

CERAMICS PROCESS SYSTEMS

(4)

SECOND QUARTERLY REPORT

FOR THE PROJECT

"COMPOSITE CERAMIC SUPERCONDUCTING
WIRES FOR ELECTRIC MOTOR APPLICATIONS"

PRIME CONTRACTOR

CERAMICS PROCESS SYSTEMS CORPORATION
840 MEMORIAL DRIVE
CAMBRIDGE, MASSACHUSETTS 02139

30 DECEMBER 1988

CPS 89-001

DARPA ORDER NO: 9525
CONTRACT NO: N00014-88-C-0512
CONTRACT EFFECTIVE DATE: 30 JUNE 1988
CONTRACT EXPIRATION DATE: 31 MARCH 1991
PRINCIPAL INVESTIGATOR: JOHN W. HALLORAN
(617) 354-2020

Prepared for
DEFENSE ADVANCED RESEARCH PROJECTS AGENCY
1400 Wilson Boulevard
Arlington, VA 22209

OFFICE OF NAVAL RESEARCH
800 North Quincy Street
Arlington, VA 22217-5000

APPROVED FOR PUBLIC RELEASE: DISTRIBUTION IS UNLIMITED

SECURITY CLASSIFICATION OF THIS PAGE

ADA204532

REPORT DOCUMENTATION PAGE

1a. REPORT SECURITY CLASSIFICATION: UNCLASSIFIED	1b. RESTRICTIVE MARKINGS: N/A
2a. SECURITY CLASSIFICATION AUTHORITY: N/A	3. DISTRIBUTION/AVAILABILITY OF REPORT: Approved for public release, Distribution Unlimited
2b. DECLASSIFICATION/DOWNGRADING SCHEDULE: N/A	
4. PERFORMING ORGANIZATION REPORT NUMBER(S): N/A	5. MONITORING ORGANIZATION REPORT NUMBER(S): N/A
6a. NAME OF PERFORMING ORGANIZATION: Ceramics Process Systems Corporation; 6b. OFFICE SYMBOL (If applicable): N/A	7a. NAME OF MONITORING ORGANIZATION: Office of Naval Research
6c. ADDRESS (City, State and ZIP Code): 840 Memorial Drive, Cambridge, MA 02139	7b. ADDRESS (City, State and ZIP Code): 800 North Quincy Street, Arlington, VA 22217-5000
8a. NAME OF FUNDING/SPONSORING ORGANIZATION: Defense Advanced Research Projects Agency; 8b. OFFICE SYMBOL (If applicable): N/A	9. PROCUREMENT INSTRUMENT IDENTIFICATION NUMBER: Contract N00014-88-C-0512
8c. ADDRESS (City, State and ZIP Code): 1400 Wilson Boulevard, Arlington, VA 22209	10. SOURCE OF FUNDING NOS. — PROGRAM ELEMENT NO.: ; PROJECT NO.: ; TASK NO.: ; WORK UNIT NO.:
11. TITLE (Include Security Classification): Composite Ceramic Superconducting Wires..	
12. PERSONAL AUTHOR(S): John W. Halloran	
13a. TYPE OF REPORT: Technical Report; 13b. TIME COVERED: 9/30/88 to 12/30/88; 14. DATE OF REPORT (Yr., Mo., Day): 88/12/30; 15. PAGE COUNT: 143	
16. SUPPLEMENTARY NOTATION: N/A	
17. COSATI CODES — FIELD: ; GROUP: ; SUB. GR.:	18. SUBJECT TERMS (Continue on reverse if necessary and identify by block number): Superconductor, Ceramic, Motor

19. ABSTRACT (Continue on reverse if necessary and identify by block number)

SEE ATTACHED

20. DISTRIBUTION/AVAILABILITY OF ABSTRACT: UNCLASSIFIED/UNLIMITED ☒ SAME AS RPT. ☐ DTIC USERS ☐	21. ABSTRACT SECURITY CLASSIFICATION: UNCLASSIFIED
22a. NAME OF RESPONSIBLE INDIVIDUAL: John W. Halloran	22b. TELEPHONE NUMBER (Include Area Code): 617-354-2020; 22c. OFFICE SYMBOL: N/A

DD FORM 1473, 83 APR — EDITION OF 1 JAN 73 IS OBSOLETE.

COMPOSITE CERAMIC SUPERCONDUCTING WIRES FOR ELECTRIC MOTOR APPLICATIONS

Second Quarterly Report on
Contract Number N00014-88-C-0512
December 30, 1988
Ceramics Process Systems Corporation
Cambridge, MA 02139

ABSTRACT

This is the Second Quarterly Report on a project to develop HTSC wire for an HTSC motor. The wire fabrication task at CPSS and AIResCo is making progress in each separate process step. The raw material for fiber production is an improved $YBa_2Cu_3O_{7-x}$ powder, made at CPSS in adequate quantities to support the program. Continuous spools of green $YBa_2Cu_3O_{7-x}$ fiber are being produced. The major effort in fiber spinning is aimed at improving fiber/quality and reducing fiber diameter. Binder burnout and sintering has been intensively investigated. Fiber sintering fibers is done rapid zone sintering method. A continuous furnace recieved near the end of this Quarter will be used for continuous sintering. Continuous silver coated green fiber are produced. We have made progress toward continuous cladding using the mechanical cladding concept.

The melt spinning process was successfully applied to $YBa_2Cu_3O_{7-x}$ powders at 50 volt solids loadings. Spools of continuous fiber were produced with diameters ranging between 3 and 15 mils, with several carrier polymer systems. The $YBa_2Cu_3O_{7-x}$ was found to react with polymers and processing aids during binder burnout under certain conditions. With fast heating, however, these reactions can be avoided, producing sintered filaments with no apparent degradation. Analysis of sintered fiber shows carbon levels at 0.18%, which is the same as the starting powder.

The sintering of variety of $YBa_2Cu_3O_{7-x}$ powders was examined in form of dry spun fibers. Melt spun fibers sinter well, achieving a microstructure consistent with the particle size. Fibers from different carrier polymers sinter similarly, although EVA fibers have less shape retention than HDPE fibers.

The cladding work centered on mechanical cladding of silver treated filaments by solder bonding to copper strips. Thin silver alloy coatings are co-fired with the fiber. Components for a continuous cladding module are being evaluated.

Aluminum deposits on $YBa_2Cu_3O_{7-x}$ filament surfaces were produced by MOCVD at ATM, but the superconductivity was degraded. Lashmore and Stafford at NIST produced Al-Mn electrodeposits on filaments from molten salt. The clad filaments were superconducting, but an insulating layer formed between the $YBa_2Cu_3O_{7-x}$ substrate and the metal deposit. Electroless copper was deposited on $YBa_2Cu_3O_{7-x}$ filaments at SUNY-Buffalo, but the superconductivity was degraded.

Electrical characterization work focused on methods of making low resistance contacts on $YBa_2Cu_3O_{7-x}$ filaments. Contact resistance was reduced to as low as 20 microohm/cm2. New software was written for measuring critical current and resistive transition.

Emerson Motor Division has begun work on DC heteropolar and homopolar motor designs. The mechanical stresses on conventional copper wires during winding have been characterized to determine the mechanical parameters of motor building. A materials property database is being assembled for $YBa_2Cu_3O_{7-x}$, with the major uncertainties being the material's tolerance of time varying magnetic fields and critical current in magnetic fields.

Keywords: Yttrium Compounds, Barium Copper Oxides. (JES/AW)

COMPOSITE CERAMIC SUPERCONDUCTING WIRES FOR ELECTRIC MOTOR APPLICATIONS

EXECUTIVE SUMMARY

The program is now fully underway, as the Emerson Motor Division design activities have begun. The wire fabrication task at CPSS and AIResCo is making progress in each separate process step. The raw material for fiber production is now CPSS $YBa_2Cu_3O_{7-x}$ powder, which is produced in adequate quantities to support the program. The quality of the $YBa_2Cu_3O_{7-x}$ powder has improved. Green $YBa_2Cu_3O_{7-x}$ fiber is being continuously produced on spools, with adequate strength for handling. Green fiber diameters are still larger than desired, but are steadily being reduced. We have improved understanding of binder burnout and sintering as a result of some intensive investigations. Fiber sintering is still being done in a batch mode, using the rapid zone sintering method. The arrival of a continuous furnace at the end of this Quarter places us on the verge of continuous sintering. Continuous silver coated green fiber can be produced. We have made progress toward continuous cladding using the mechanical cladding concept.

An extensive powder optimization study was undertaken to provide an improved $YBa_2Cu_3O_{7-x}$ powder feedstock for the program. Eleven different powders, representing variations in calcination, raw materials, and milling conditions, were prepared and spun into fibers. Particle sizes varied from 0.69 to more than 3 microns. The study uncovered some deleterious effects of anticaking aids used in dry milling. Jet milling was identified as the preferred particle size reduction method, and has been adopted for $YBa_2Cu_3O_{7-x}$ powder production.

The melt spinning process was successfully applied to $YBa_2Cu_3O_{7-x}$ powders at 50 vol% solids loadings. Spools of continuous fiber were produced with diameters ranging between 3 and 15 mils, depending upon drawing conditions. $YBa_2Cu_3O_{7-x}$ fibers were melt spun with several carrier polymer systems, including high density polyethylene, and ethylene vinylacetate. Spinning and drawing behavior was found to be sensitive to the milling aids used in powder preparation.

The $YBa_2Cu_3O_{7-x}$ was found to be reactive with organic polymers and processing aids during binder burnout. These reactions were studied in detail. Under certain conditions the reaction can destroy the specimen, as the copper oxide in $YBa_2Cu_3O_{7-x}$ oxidizes the organic polymers. The reaction of $YBa_2Cu_3O_{7-x}$ powders with 2% stearic acid milling aid is particularly bad. Ethylene glycol milling aid is benign. In fibers, the carrier polymer can react with the $YBa_2Cu_3O_{7-x}$, especially under conditions of slow heating.

Ethylene vinyl acetate is more reactive than polyethylene. Stearic acid exacerbates the reaction between the polymers and $YBa_2Cu_3O_{7-x}$. With fast heating, however, these reactions can be avoided, producing sintered filaments with no apparent degradation. Analysis of sintered fiber shows carbon levels at 0.18%, which is the same as the starting powder.

The sintering of a variety of $YBa_2Cu_3O_{7-x}$ powders was examined in the form of dry spun fibers. Melt spun fibers sinter well, achieving a microstructure consistent with the particle size. Fibers from different carrier polymers sinter similarly, although EVA fibers have less shape retention than HDPE fibers.

The cladding work centered on mechanical cladding of silver treated filaments by solder bonding to copper strips. The silver treatment is now done continuously. The thin silver coating is co-fired with the $YBa_2Cu_3O_{7-x}$ fiber. Silver-palladium alloy coatings were developed further for higher sintering temperature. Solder run-out during the reflow bonding was eliminated by using a channel shaped copper strip. The components for the surrogate cladding module are still being evaluated.

Aluminum was deposited on $YBa_2Cu_3O_{7-x}$ filament surfaces were produced by MOCVD at ATM, but the superconductivity was degraded. Lashmore and Stafford at NIST deposited Al-Mn alloys on filaments by molten salt electrodeposition. The Meissner effect proved that superconductivity was retained, but no resistive transition was found by the transport method, due to a resistive layer between the $YBa_2Cu_3O_{7-x}$ substrate and the metal deposit. Electroless plated copper deposits were obtained on $YBa_2Cu_3O_{7-x}$ filaments at SUNY-Buffalo, but the superconductivity was degraded.

Electrical characterization work focused on methods of making low resistance contacts. A new method has reduced contact resistance of silver pads on $YBa_2Cu_3O_{7-x}$ filaments three orders of magnitude, down to as low as 20 micro ohm/cm2. New software was written for computer controlled determination of critical current and resistive transition.

Emerson Motor Division has begun work on DC heteropolar motor designs and, through Professor Novotny at U. Wisconsin, DC homopolar machines. The mechanical stresses on conventional copper wires during winding have been characterized to determine the mechanical parameters of motor building. A materials property database is being assembled for $YBa_2Cu_3O_{7-x}$, with the major uncertainties being the material's tolerance of time varying magnetic fields and, of course, critical current in magnetic fields.

TABLE OF CONTENTS

LIST OF FIGURES

LIST OF TABLES

COMPOSITE CERAMIC SUPERCONDUCTING WIRES FOR ELECTRIC MOTOR APPLICATIONS

JOHN W. HALLORAN
PRINCIPAL INVESTIGATOR
CERAMICS PROCESS SYSTEMS CORPORATION
CAMBRIDGE, MASSACHUSETTS

SECTION 1

GENERAL INTRODUCTION

This Second Quarterly Report covers activities during October through December 1988, on a program to develop high temperature superconducting wire by metal cladding $YBa_2Cu_3O_{7-x}$ ceramic fiber, and to use this wire to build a superconducting motor. This program is being carried out by three subcontractors: an affiliate of Ceramics Process Systems, CPS Superconductor Corporation (CPSS) is charged with development of the wire; Albany International Research Corporation (AIResCo) develops fiber spinning processes; and the Emerson Motor Division (EMD) of Emerson Electric will design and build superconducting motors. During this period work continued at CPSS and AIResCo on the wire fabrication task, and work commenced at Emerson Motor Division on the motor design task.

The status of the program is compared with the planned statement of work in Table 1.1. We are on target in the powder production subtask in terms of quantity of $YBa_2Cu_3O_{7-x}$ produced. A significant portion of our efforts this quarter was devoted to producing improved powder, an activity planned as a powder optimization task. As we moved to continuous melt spinning for producing $YBa_2Cu_3O_{7-x}$ green fiber, our consumption of powder increased and we discovered attributes of the powder which were undesirable for fiber spinning. The powder optimization study became an intensive project to look at particle size effects and milling methods. This led to an interim switch to a better ball milled

$YBa_2Cu_3O_{7-x}$ powder, and identified jet milling as the preferred comminution method.

The green fiber spinning activities are progressing ahead of schedule. The early melt spinning experiments were fruitful and have been further developed. This makes continuous spools of green fiber available. The success of the early melt spinning encouraged us to continue with it, so we have postponed work on more novel "advanced" spinning concepts. Unfortunately, we have not been able to produce grain-oriented green fiber, since this requires platy shaped powder particles. Only equiaxed $YBa_2Cu_3O_{7-x}$ powders have been available to date.

Fiber sintering activities were primarily in support of the powder optimization study. Consequently we largely evaluated materials rather than developed the fiber sintering process. This not only helped the development of powder, but also drew attention to several important aspects of the sintering behavior of $YBa_2Cu_3O_{7-x}$. Further progress was made on co-firing of silver alloy coated $YBa_2Cu_3O_{7-x}$ green fiber. No continuous fiber sintering was done this quarter. The continuous belt furnace, ordered last quarter for this work, was not received by the end of December.

The cladding area received more attention. Three different deposition methods were explored by outside collaboration. None of these appeared ready for adoption in the in-house activity, so our main thrust remained in the mechanical cladding. Activities centered around further developments of the thin silver alloy surface coatings and on the solder reflow method of assembling the clad composite. The continuous cladding module is not ready yet. Several components of the prototype cladding module have been

received, and many of the design features have been identified. The assembly and testing of the prototype module will be delayed until the next quarter.

Most of the effort in the Characterization task was devoted to improving testing methods for resistivity and critical current. Both of these now are fully controlled by software written during this quarter. Methods for mounting the $YBa_2Cu_3O_{7-x}$ filaments for testing received much attention. The previous silver epoxy electrodes were not reproducible, and a new method was developed which significantly decreased contact resistance. Emphasis was on refining technique, rather than routine testing of $YBa_2Cu_3O_{7-x}$ filaments. Detailed characterization of sintered filaments was largely deferred until next quarter, when it will focus on the continuously sintered silver-coated filaments from the new $YBa_2Cu_3O_{7-x}$ powder.

Activities began at Emerson Motor Division during this quarter. The project was conducted with engineers currently on staff, while recruitment of new engineers continues. Design activities began on a homopolar motor and heteropolar motor. The applications study, originally scheduled for this quarter was postponed. The field of applications will be predominantly determined by the electromagnetic and mechanical performance of the HTSC wire, which is yet to be determined. The applications study will be deferred until more data is available.

TABLE 1.1
PROGRESS AGAINST STATEMENT OF WORK
SECOND REPORT PERIOD: FOURTH QUARTER 1988

TASK I: COMPOSITE WIRE MANUFACTURING

SUBTASK IA) POWDER PRODUCTION

1) Supply improved powder at least 4 kilograms per month
STATUS: WE ARE AT THIS RATE

2) Continue to define optimum particle size distribution for fiber spinning and sintering.
STATUS: THIS HAS BECOME A MAJOR EFFORT THIS QUARTER

3) Continuing improvement of powder production
STATUS: IN PROGRESS

SUBTASK IB) GREEN FIBER DEVELOPMENT

1) Supply continuous green fiber from AIRC
STATUS: THIS IS BEING DONE

2) Define and optimize spinning conditions
STATUS: IN PROGRESS

3) Define advanced spinning concepts at AIRC
STATUS: LITTLE WORK, SINCE PRESENT MELT SPINNING APPEARS SATISFACTORY

4) Continue to characterize green textures
STATUS: DELAYED UNTIL PLATY PARTICLES ARE AVAILABLE

SUBTASK IC) FIBER SINTERING AND MICROSTRUCTURE DEVELOPMENT

1) Continue directional recrystallization process development
STATUS: SINTERING DEVELOPMENT FOCUSED ON POWDER EVALUATION

2) Achieve continuous fiber sintering and annealing
STATUS: BELT FURNACE NOT RECEIVED YET, EXPECTED IN JANUARY

3) Correlate sintered filament texture with critical current
STATUS: TEXTURED FILAMENTS DELAYED

SUBTASK ID) FILAMENT CLADDING DEVELOPMENT

1) Select cladding process for further development, either electroplating or mechanical cladding
STATUS: MECHANICAL CLADDING CHOSEN

2) Continue development of continuous cladding facility using surrogate filament
STATUS: DELAYED--COMPONENTS AND MATERIALS FOR FACILITY ARE NOW BEING ACQUIRED, ASSEMBLY NEXT QUARTER

TASK II: CHARACTERIZATION

1) Electrical and magnetic properties
Determine resistance vs. temperature for sintered filaments and early clad wires
STATUS: CONTINUING ACTIVITY, METHODS IMPROVED

2) Determine critical current density at liquid nitrogen temperature on sintered filaments and clad wires as a function of magnetic field, and correlate with microstructure
STATUS: CONTINUING ACTIVITY, WITH EMPHASIS ON SELF-FIELD

2) Mechanical and physical properties
Determine tensile strength of green, fired, and clad filaments
STATUS: GREEN FIBERS TESTED

TASK III: MOTOR DESIGN AND CONSTRUCTION

1) Assign motor design engineer and mechanical engineer to project on full time basis.
STATUS: KEY ENGINEER HAS BEEN RECRUITED, NOW STAFFED WITH EXISTING EMD ENGINEERS

2) Conduct detailed literature research on superconductive motors and mechanical systems that can operate at liquid nitrogen temperature.
STATUS: IN PROGRESS AT U. WISCONSIN

3) Begin Application Study - Engage consultants to evaluate motor technologies that are potential candidates for HTSC.
STATUS: LOWER ACTIVITY UNTIL PROPERTIES OF HTSC MOTORS ARE DEFINED

4) Define initial wire property targets for design database.
STATUS: DONE

5) Engage consultant to study and report on physical properties, effect of environment, test requirements and test methods for HTSC conductors.
STATUS: DR. HILLAL, U. WISCONSIN-MADISON

SECTION 2

WIRE FABRICATION

ZONGYI CHEN, JOHN HALLORAN, JAMES HODGE, LORI JO KLEMPTNER,
MATTHEW NEAL, MARK PARISH, VIREN PATHARE, AND RAYSHA PICERNO
CPS SUPERCONDUCTOR CORPORATION

GEORGE BAKIS, DANA EAGLES, WESLEY ISHIDA, AND STEPHEN TIERNAN
ALBANY INTERNATIONAL RESEARCH CORPORATION

2.1 Introduction and General Comments

The wire fabrication task is divided into several subtasks concerned with preparation of the $YBa_2Cu_3O_{7-x}$ powder, production of green fiber, sintering of the fiber to make $YBa_2Cu_3O_{7-x}$ filaments, metal cladding the filaments to produce prototype wire, and electrical characterization. The use of the term "production" emphasizes that the output of each subtask is the feedstock of the next subtask, but does not imply that any of the subtasks are fully developed. Indeed every step is still under development, so at this stage the wire fabrication task is a set of five parallel development projects. Each subtask develops processes in its own area to upgrade capability and improve quality. It also evaluates the output of the preceding subtask and supplies feed stock for the following subtask, which provides the major threads of continuity between subtasks. We believe there is a good deal of coordination between the subtasks. But there are at any time several different types of powder, made into several different kinds of fiber, etc., which naturally lead to a highly ramified program.

2.2 Fiber Preparation

2.2.1 Introduction

During this quarter there were important activities in three areas related to fiber preparation. The main thrust was in melt spinning of green fiber. Melt spun $YBa_2Cu_3O_{7-x}$ fibers were prepared from several carrier polymer systems. Continuous green fiber was collected on spools at lengths up to 300 meters, limited only by sample size. Figure 2.2.1 is a photograph of two small spools of $YBa_2Cu_3O_{7-x}$ and barium titanate melt spun fibers. Diameter control was exercised through the spinnerette die diameter, elongation during melt drawing, and occasionally further elongation via a separate cold drawing step. Activity was aimed at defining favorable powder characteristics, powder/polymer blend compositions, and spinning conditions. The processing aids used in preparing the powder were found to strongly influence melt spinning. Melt spun fibers made with CPSS $YBa_2Cu_3O_{7-x}$ powder are now the standard feedstock for subsequent processing. These are presently available in 4-10 mil diameters. Efforts are now underway to reduce the diameter to below one mil.

Phenomena related to binder burnout were examined in some detail. This was motivated by observations of degradation of $YBa_2Cu_3O_{7-x}$ during binder burnout. An intensive series of experiments has clarified the behavior of $YBa_2Cu_3O_{7-x}$ during binder removal as influenced by the carrier polymer, heating conditions, and especially, the powder processing aids. Conditions have been defined for binder burnout without degradation of the superconductor.

Dry spinning is no longer the preferred method for preparing fibers as feedstock for further processing. This process is now used only for preparing small quantities of fiber from small lots of experimental powders.

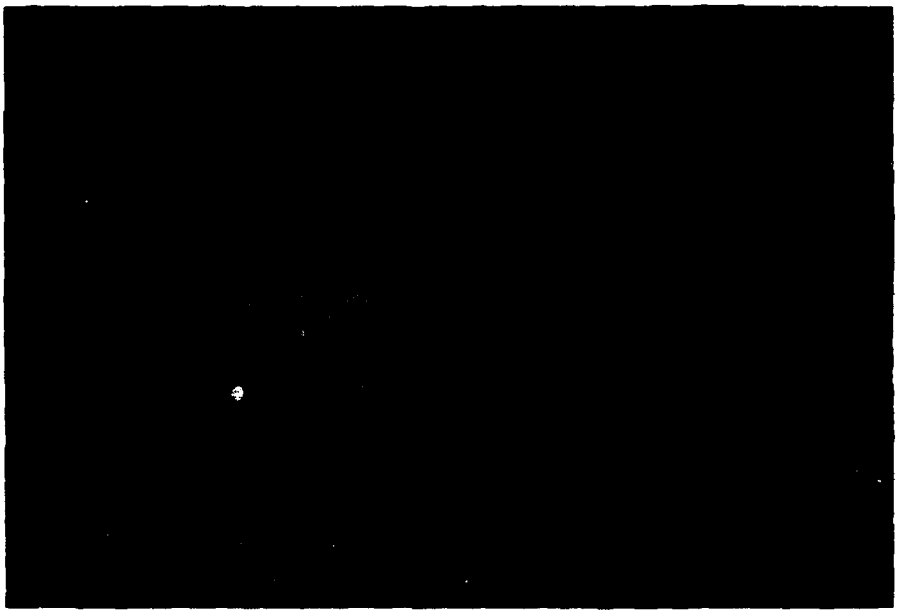

Figure 2.2.1: Typical Spools of Melt Spun $YBa_2Cu_3O_{7-x}$ and Barium Titanate Fiber

Since a major powder optimization study was undertaken during this report period, a wide variety of dry spun fibers was prepared.

2.2.2 Preparation of Dry Spun Fibers from Experimental $YBa_2Cu_3O_{7-x}$ Powders

One of the major activities of the program this quarter was examining a variety of $YBa_2Cu_3O_{7-x}$ powders of different characteristics for sintering behavior and microstructure development. Dry spun polymethylmethacrylate (PMMA)-based fibers were prepared from twelve experimental powders, as specified in Table 2.2.1.

The dry spinning dope had to be adjusted for each powder in order to make fibers with a smooth surface and a diameter acceptable for sintering work. Substantial problems were encountered in achieving well dispersed dopes from some of the powders. For example, if a stearic acid processing aid had been used for making the $YBa_2Cu_3O_{7-x}$ powder, the dope viscosity increased too rapidly to achieve a well-mixed dope. This problem was traced to the stearic acid catalyzing the cross-linking reaction in the dry spinning dope. This problem was avoided by preparing powders in wet milled cyclohexane dispersed with 2 wt% sorbitan trioleate, eliminating the need for stearic acid. To prevent agglomeration during evaporation of solvent, the toluene was removed by cryo-granulating the milled powder slurry and freeze drying the granules. The powders made by this process were friable and did not agglomerate as badly as the stearic acid containing powders. However, dopes made from these powders were still not dispersed well enough. Changes were made in the dope mixing method to increase shear during the mixing process. The fibers so made were passed on for evaluation of the sintering behavior of these experimental powders. This work is reported in Section 2.3.

TABLE 2.2.1

YBCO POWDERS USED TO MAKE DRY SPUN PMMA FIBERS
FOR SINTERING, MICROSTRUCTURE, AND CRITICAL CURRENT EVALUATION.

POWDER CODE	FIBER CODE	POWDER DESCRIPTION	PROCESSING AID	HRS. MILLED
00271A-27	02182	YBCO	2 WT% SPAN 85	27
00271B-27	02183	YBCO + 5 WT% CuO	2 WT% SPAN 85	27
00271A-70	02179	YBCO	2 WT% SPAN 85	70
00271B-70	02181	YBCO + 5 WT% CuO	2 WT% SPAN 85	70
00271A-143	02195	YBCO	2 WT% SPAN 85	143
00271B-143	02196	YBCO + 5 WT% CuO	2 WT% SPAN 85	143
00271A-242	02197	YBCO	2 WT% SPAN 85	242
01377	02186	PHASE IMPURE YBCO	0.5 WT% EG	214
01395	02185	PREMILLED Y_2O_3/YBCO	0.5 WT% EG	62
00272	02184	TETRAGONAL YBCO	0.5 WT% EG	92
02318	02199	YBCO FROM $Ba(OH)_2$	0.8 WT% EG	104
02317	02198	YBCO FROM K_2CO_3	0.6 WT% EG	104

YBCO = $YBa_2Cu_3O_{7-x}$

EG = ETHYLENE GYLCOL

2.2.3 Development of Melt Spinning Process

Activities in melt spinning were aimed at evaluating new carrier polymers using barium titanate as a surrogate, and fabricating a variety of $YBa_2Cu_3O_{7-x}$ fibers. These were done both to develop the melt spinning process and to supply green fiber as feedstock for further processing.

Two different extrusion systems were used. The Hobbs unit was the preferred machine, since it had been previously used for highly loaded fiber and provides higher shear mixing. However, since it was not available for part of this report period, the larger NRM extrusion system was used in its place. The NRM is an adequate substitute, but has a less intense shear mixing. This makes it less desirable for small scale experiments with the costly $YBa_2Cu_3O_{7-x}$ feedstock.

2.2.3.1 Screening of carrier polymers by extrusion behavior

An attempt was made to spin 50 vol% loaded fibers using polypropylene (PP) as the carrier polymer. As before, carrier polymer screening tests were performed with barium titanate powder. Based on the successful melt spun trials with 50 vol% loadings of $BaTiO_3$ in high density polyethylene (HDPE) and ethylene vinylacetate (EVA), a similar 50 vol% $BaTiO_3$ blend was compounded with PP on the sigma blade mixer to produce a PP feedstock analogous to the HDPE and EVA feedstocks. The Hobbs extrusion system, which had been previously used for this work was unavailable, so this blend was processed on the NRM extruder fitted with a conventional screw and the stream-lined die assembly previously reported. Attempts to fabricate fiber from this PP blend were unsuccessful as flow was lost before any extrudate formed through the die. It was not clear if

this was related to the new PP blend, or whether it was the different extrusion equipment. To determine if a 50 vol% powder blend could be extruded on the NRM machine, a previously successful barium titanate/HDPE composition was tried. Extrusion of this blend on the NRM through a 20 mil die resulted in fiber as thin as 4.7 mil, which was similar to the minimum diameter attainable on the Hobbs machine for this blend. Tenacity of this fiber was also similar, 2,400 psi vs. 3,200 psi for the Hobbs fiber, suggesting the change in extrusion systems was not responsible for the unsuccessful trial with PP. This grade of PP was judged to be not useful for melt spinning loaded fibers by the present process. Preliminary trials of a lower melt index (higher molecular weight) grade of PP, however, have been encouraging. Successful melt spinning of a PP-based fiber is expected in the next quarter.

2.2.3.2 Fabrication of $YBa_2Cu_3O_{7-x}$ melt spun fibers

HDPE and EVA were chosen as carrier polymers for the next phase of the feasibility study which was to fabricate $YBa_2Cu_3O_{7-x}$ green fibers. Due to $YBa_2Cu_3O_{7-x}$'s sensitivity to moisture, the method of preparing the feedstock after compounding was modified. Upon removal from the sigma blade, the $BaTiO_3$ melts were removed, allowed to solidify and cryogenically ground. During the grinding process, moisture condensed from the atmosphere onto the granulated product. This resulted in a water soaked feedstock, which would be detrimental to $YBa_2Cu_3O_{7-x}$. The process was modified for $YBa_2Cu_3O_{7-x}$ blends by allowing the removed melts to solidify, compression molding the solids into approximately 10 mil plaques, and cutting and granulating the plaques in a chopper at ambient conditions.

A blend of 50 vol% $YBa_2Cu_3O_{7-x}$ (lot #01701 milled with stearic acid) with HDPE was compounded and prepared into feedstock for the NRM extruder. The blend was successfully processed into green fibers of several diameters. Fibers as thin as 15.5 mil were drawn from a 20 mil die, 9.5 mil from a 13.5 mil die, 7.5 mil from a 9 mil die, and 7.0 mil from a 7 mil die. Notice that the fiber diameters were not much finer than the die diameter, indicating that little "spin draw" could be supported by these melts. The samples processed on the 9 mil and 7 mil die were fabricated by reprocessing green fiber extruded through the 20 mil and 13.5 mil die, so that this material had been previously extruded.

Table 2.2.2 reports the tensile properties of this batch of fibers. Tenacity (tensile strength) was relatively similar for all these fiber samples regardless of gauge or number of passes through the extruder. This reflects the absence of significant spin draw, which typically produces stronger fibers. TGA revealed that multiple passes did not result in significantly different compositions.

An analogous $YBa_2Cu_3O_{7-x}$ blend was produced to evaluate EVA as the carrier polymer. This and subsequent spins were conducted on the Hobbs extruder. The EVA blend was likewise successfully converted into a 50 vol% $YBa_2Cu_3O_{7-x}$ green fiber. The blend was processed on the Hobbs extruder through a 22.5 mil die to fabricate fiber as thin as 16.5 mil. A 50 vol% $YBa_2Cu_3O_{7-x}$/CuO green fiber was produced for use in sintering studies. The ceramic component was 95 wt% $YBa_2Cu_3O_{7-x}$ (Lot # 01704, with stearic acid) and 5 wt% CuO. An HDPE blend was compounded in a 50 vol% ceramic loading and extruded into 8 to 9 mil fiber from a 13.5 mil die.

These early fibers with stearic acid milled-$YBa_2Cu_3O_{7-x}$ had relatively low tensile strength and could not be cold drawn. Microstructure examination

TABLE 2.2.2

TENSILE PROPERTIES OF GREEN FIBERS

SAMPLE #	COMPOSITION	GAUGE (mils)	TENSILE STRENTGH (psi)	MODULUS (psi)	% ELONGATION
3498-61-1	46 VOL % BARIUM TITANATE IN HDPE BLEND	4.4	3,200	120,000	27
3498-69-4	50 VOL % BARIUM TITANATE IN HDPE BLEND	4.7	2,350	77,600	33.6
3498-73-2	50 VOL % YBCO/SA IN HDPE BLEND	17.3	1,250	44,400	13.2
3498-74-1		14.2	1,530	52,400	10.6
3498-75-2		10.1	1,420	65,700	10.2
3498-77-7		6.9	1,240	65,900	11.9
3498-80-2	50 VOL % YBCO/SA IN EVA BLEND	16.8	1,490	22,600	18.8
3498-84-2	50 VOL % YBCO/CuO/SA IN HDPE BLEND	8.1	1,950	88,400	8.5
3498-84-3		6.6	1,190	81,400	10.7
3498-86-1	50 VOL % YBCO/EG IN HDPE BLEND	6.6	1,670	158,000	6.1
3498-87-2		5.8	1,800	178,000	16.4
3498-92-1		5.4	5,910	101,600	14.2
3498-93-1		3.9	15,770	176,200	11.1
3498-90-3	40 VOL % YBCO/EG IN HDPE BLEND	9.0	1,820	126,000	9.1
3498-95-1	50 VOL % YBCO/EG IN EVA BLEND	12.6	1,070	29,400	20.9

NOTE: SA = STEARIC ACID
EG = ETHYLENE GLYCOL

of these green fibers revealed that the ceramic and polymer had poor adherence. Figure 2.2.2 illustrates a ruptured cross section of a green fiber, showing that the polymer pulls cleanly away from the ceramic particles, indicating little wetting or adherence. The stearic acid, used as a processing aid in the production of the $YBa_2Cu_3O_{7-x}$ powder, was suspected to be responsible for the poor adherence between the polymer and the powder. The literature reports stearic acid to be relatively incompatible with polyolefins. This also accounts for the low strength and drawability of these compositions.

To determine the effect of processing aid on minimum fiber diameter, a lot of $YBa_2Cu_3O_{7-x}$ powder was made with ethylene glycol as the processing aid (Lot # 01394). The HDPE based $YBa_2Cu_3O_{7-x}$ composition was compounded and processed on the Hobbs system into fiber as thin as 4.5 mil from a 13.5 mil die. The spin draw of this blend is comparable to the barium titanate blends. This achievement suggests that ethylene glycol is a more compatible processing aid for use with HDPE than stearic acid. A successful experiment was performed to determine if this fiber could be subsequently post drawn to decrease diameter and increase orientation. Fibers as thin as 3 mil were drawn from a 7 mil initial fiber diameter, suggesting that additional processing will result in thinner diameters than the current spin drawn fibers.

To determine the effect of ceramic loading on the spin drawability of green fibers and shape retention upon sintering, a lower ceramic content 40 vol% $YBa_2Cu_3O_{7-x}$ in the HDPE blend was compounded and extruded on the Hobbs system. Processing of this blend through the 13.5 mil die revealed insufficient melt strength to draw fibers thinner than 8 mil. This was surprising, since lower ceramic loading was expected to improve drawability. Apparently the additives in the HDPE blend were inappropriate for the lower solids loading,

Figure 2.2.2: Ruptured Green Fiber Prepared With Stearic Acid-Milled Powder, Showing Poor Adherence

suggesting that the carrier polymer blend composition needs to be adjusted when solids content changes.

The final spin for this reporting period was based on EVA as a carrier for the 50 vol% $YBa_2Cu_3O_{7-x}$ containing ethylene glycol processing aid. The 50 vol% $YBa_2Cu_3O_{7-x}$ in an EVA carrier compound was extruded on the Hobbs system to produce fiber as thin as 10 mil diameter. Tensile strength and microstructure analysis suggests that although ethylene glycol appears to have aided the spin drawability in HDPE based green fiber, its effect is not as favorable in EVA.

In comparing the green fiber tensile properties of the blends made with $YBa_2Cu_3O_{7-x}$ ceramic in Table 2.2.2, it is apparent that the fibers with the highest tensile strength and modulus are those made with HDPE and ethylene glycol processing aid. Fibers with similar composition and diameter using stearic acid processing aid showed a 25% lower tensile strength and 58% lower modulus value than the fibers using ethylene glycol processing aid. Fibers made with EVA polymer showed lower tensile strength and modulus values than their HDPE counterparts. Table 2.2.3 contains a summary of all melt processed blends reported in this progress report.

2.2.4 Polymer-$YBa_2Cu_3O_{7-x}$ Interactions During Binder Burnout

In this section we present results related to polymer-$YBa_2Cu_3O_{7-x}$ interactions associated with binder burnout. While we discuss these results together, many of the observations were initially obtained as rather surprising results of diverse experiments aimed either at sintering of simple pellets, or screening of new carrier polymers. Some of the first melt spun processing trial fibers using CPSS powder were used to examine binder burnout with slow heating.

TABLE 2.2.3

SUMMARY MATRIX OF MELT SPUN EXPERIMENTS
(50 VOL% CERAMIC UNLESS OTHERWISE NOTED)

POLYMER	CERAMIC	COMMENTS
PP	TAM BaTiO3	NOT EXTRUDABLE
HDPE	TAM BaTiO3	SPUN INTO 3498-69 SERIES ON NRM EXTRUDER
HDPE	01701 YBCO	SPUN INTO 3498-73 THROUGH 3498-77 SERIES ON NRM EXTRUDER
EVA	01701 YBCO	SPUN INTO 3498-80 SEREIES ON NRM EXTRUDER
HDPE	01704 YBCO/CuO	SPUN INTO 3498-83 THROUGH 3498-84 SERIES ON HOBBS EXTRUDER
HDPE	01394 YBCO	SPUN INTO 3498-86 THROUGH 3498-88 SERIES ON HOBBS EXTRUDER
HDPE	01394 YBCO	SPUN ON HOBBS EXTRUDER AND POST DRAWN INTO 3498-92 THROUGH 3498-93 SERIES
HDPE	01394 YBCO	SPUN INTO 3498-90 SERIES ON HOBBS EXTRUDER 40 VOL% CERAMIC
EVA	01394 YBCO	SPUN INTO 3498-95 AND 3498-96 SERIES ON HOBBS EXTRUDER

To our unpleasant surprise, the $YBa_2Cu_3O_{7-x}$ was seriously degraded. This motivated an intensive study of $YBa_2Cu_3O_{7-x}$ interactions with melt spinning carrier polymers. At the same time a series of sintering experiments were conducted using pressed and molded shapes of the $YBa_2Cu_3O_{7-x}$ powder with no added binder other than the processing aid. These tests revealed a series of spectacular failures associated with heating through the "binder burnout" temperature range. This led to a similarly intensive sintering study.

2.2.4.1 Reaction of $YBa_2Cu_3O_{7-x}$ with carrier polymers

The purpose of this binder burnout study was to test the chemical compatibility and extent of reactivity of the candidate polymers with $YBa_2Cu_3O_{7-x}$ ceramic. Thermal gravimetric analysis data, taken in both nitrogen and air atmospheres, showed complete burnout at 500°C of the polymers listed in Table 2.2.4. During initial melt spin processing trials, fiber samples of 10, 30, and 50 vol% $YBa_2Cu_3O_{7-x}$ were made from polypropylene, high density polyethylene, polypropylene carbonate (PPC), and Celcon. The $YBa_2Cu_3O_{7-x}$ was an early CPSS powder processed with stearic acid (Lot # 00165). This powder was not as phase pure as the other CPSS powder lots, containing detectable amounts of barium cuprate, barium carbonate, and copper oxide. The fibers were heated in either air or in a nitrogen atmosphere. The temperature profile consisted of a one hour ramp from room temperature to 500°C (heating rate of 8°C/min.), followed by a one hour hold at 500°C and power shut-off, for a gradual cool down to room temperature. After burnout the samples were ground into fine powders and examined by x-ray powder diffraction. Table 2.2.5 summarizes the x-ray powder diffraction results.

TABLE 2.2.4

DECOMPOSITION TEMPERATURE FOR CANDIDATE POLYMERS

POLYMER	NITROGEN ATMOSPHERE DECOMPOSITION TEMP. RANGE	AIR ATMOSPHERE DECOMPOSITION TEMP. RANGE
POLYPROPYLENE CARBONATE	192 - 323°C	184 - 297°C
POLYMETHYL METHACRYLATE	213 - 426°C	244 - 400°C
POLYACETAL	305 - 434°C	244 - 286°C
POLYPROPYLENE	347 - 482°C	221 - 403°C
HIGH DENSITY POLYETHYLENE	378 - 483°C	257 - 496°C
ETHYLENE VINYL ACETATE	300 - 496°C	239 - 521°C

TABLE 2.2.5

XRD RESULTS OF BINDER BURNOUT STUDY

SAMPLE	DESCRIPTION	BINDER BURNOUT IN NITROGEN	BINDER BURNOUT IN AIR
3498-9-3	10 vol% CPSS YBCO in melt spun PP	Reference: CPSS 01405 major phases: $BaCO_3$, Cu, Y_2BaCuO_5 minor phases: Y_2O_3, $Cu_2Y_2O_5$	Reference: CPSS 01406 major phase: $YBa_2Cu_3O_7$ (orthorhombic) minor phases: Y_2O_3, $BaCO_3$, CuO
3498-11-1	30 vol% CPSS YBCO in melt spun PP	Omitted due to sample limitation	Reference: CPSS 01452 major phase: $YBa_2Cu_3O_7$ (orthorhombic) minor phases: Y_2O_3, $BaCO_3$, CuO
30206B	49.8 vol% RP YBCO in dry spun PMMA	Reference: CPSS 01409 phases present: $BaCO_3$, Y_2O_3, Cu, CuO, BaY_2O_4, $Ba_2Y_2O_5$	References: CPSS 01410 & 01422 phases present: Y_2O_3, $BaCO_3$, CuO
3498-4-1	10 vol% CPSS YBCO in melt spun HDPE	Omitted due to sample limitation	Reference: CPSS 01453 phases present: Y_2O_3, $BaCO_3$, CuO
3498-5-4	30 vol% CPSS YBCO in melt spun HDPE	Reference: CPSS 01434 phases present: Y_2O_3, $BaCO_3$, Cu	Reference: CPSS 01435 phases present: Y_2O_3, $BaCO_3$, CuO
3498-28-3	50 vol% CPSS YBCO in melt spun QPAC-40M	Reference: CPSS 01481 major phase: $YBa_2Cu_3O_6$(tetr.) minor phases: Y_2O_3, $BaCO_3$, Cu	Reference: CPSS 01480 major phase: $YBa_2Cu_3O_7$(orthorhombic) minor phases: Y_2O_3, $BaCO_3$, CuO
3498-21-1	30 vol% CPSS YBCO in melt spun Celcon	Reference: CPSS 01483 major phase: $YBa_2Cu_3O_6$(tetr.) minor phases: Y_2O_3, $BaCO_3$, Cu	Reference: CPSS 01482 major phase: $YBa_2Cu_3O_7$(orthorhombic) minor phases: Y_2O_3, $BaCO_3$, CuO

NOTE: CPSS YBCO powder lot #00165 was used. This powder contained $YBa_2Cu_3O_{7-x}$ as the major phase, $BaCuO_2$ as a secondary phase and Y_2O_3, $BaCO_3$, and CuO as minor phases.

RP stands for Rhone-Poulenc Superamic Y123 YBCO powder, lot #S41416CI. This powder was similar to CPSS YBCO lot #00165.

All the samples exposed to nitrogen atmosphere during binder burnout showed the presence of metallic copper. This indicates that in the absence of atmospheric oxygen the CuO component of $YBa_2Cu_3O_{7-x}$ acts as an oxidizing agent to the polymer. For samples containing PP, PMMA, and HDPE polymers the $YBa_2Cu_3O_{7-x}$ ceramic showed complete degradation in nitrogen atmosphere burnout. The samples containing PPC and Celcon did not show major degradation of the $YBa_2Cu_3O_{7-x}$, instead there was a transformation of $YBa_2Cu_3O_{7-x}$ phase from orthorhombic to tetragonal. This indicates that both PPC and Celcon do not use a thermal oxidative mechanism for polymer thermal degradation, and so are not detrimental to $YBa_2Cu_3O_{7-x}$ ceramic by that process. The products of the thermal oxidative degradation of PP, PMMA, and HDPE polymers by CuO were different for each polymer. This suggests that the mechanism for CuO polymer oxidation in each case could be different.

The PP, PPC, and Celcon samples exposed to air atmosphere during binder burnout retained the $YBa_2Cu_3O_{7-x}$ orthorhombic phase with minor phases of Y_2O_3, $BaCO_3$, and CuO, which may have been initially present in this powder. In sharp contrast, the samples containing HDPE and PMMA polymers showed complete degradation of the $YBa_2Cu_3O_{7-x}$ to Y_2O_3, $BaCO_3$, and CuO phases.

Complete $YBa_2Cu_3O_{7-x}$ degradation in PMMA polymer was a surprising result. We have been sintering dry spun PMMA fibers in air for some time, and have only detected the $YBa_2Cu_3O_{7-x}$ phase after sintering. The zone sintered $YBa_2Cu_3O_{7-x}$ filaments are superconducting, with no evidence of extensive decomposition. There is apparently an important kinetic effect which determines whether $YBa_2Cu_3O_{7-x}$ decomposition occurs during binder burnout. The binder burnout schedule for zone sintered fibers is very rapid in comparison to the one hour soak time, at 500°C, used in this study.

The differences observed in the air binder burnout of PP and HDPE samples were also unexpected. Both PP and HDPE are polyolefins. The literature reports that the thermal degradation mechanism in both polymers is similar. Yet, they had a very different effect on the $YBa_2Cu_3O_{7-x}$ ceramic.

The mechanism for thermal decomposition of a polymer is determined by the chemical structure of the polymer, the oxygen partial pressures and by the traces of unstable impurities. Thermal degradation does not occur until the temperature is high enough to separate primary chemical bonds. Both HDPE and PP are susceptible to oxidative degradation at tertiary hydrogen sites in the polymer chain. Since PP has more tertiary hydrogen sites than HDPE, it is more susceptible to oxidative degradation. In oxidative degradation free radicals are generated which react with oxygen and eventually lead to polymer chain degradation.

It could be that, similar to the PMMA/$YBa_2Cu_3O_{7-x}$ sample, there is a difference in the kinetics of polymer degradation between PP and HDPE in the presence of $YBa_2Cu_3O_{7-x}$ ceramic. A Differential Thermal Analysis (DTA) of the 30 vol% $YBa_2Cu_3O_{7-x}$ melt spun HDPE and PP samples was done in flowing air to discern any differences in thermal profiles of both samples upon thermal degradation of the polymer. The data is presented in Figure 2.2.3. The temperature profile used consisted of a heating rate of 5°C/min to 500°C followed by a one hour hold at 500°C.

A super heating effect was observed with both samples resulting from the exothermic oxidative degradation reactions. It is apparent from this data that the HDPE exothermic reaction is twice as energetic as that of PP. The bond dissociation energy of a carbon-carbon bond is less than that of a carbon-

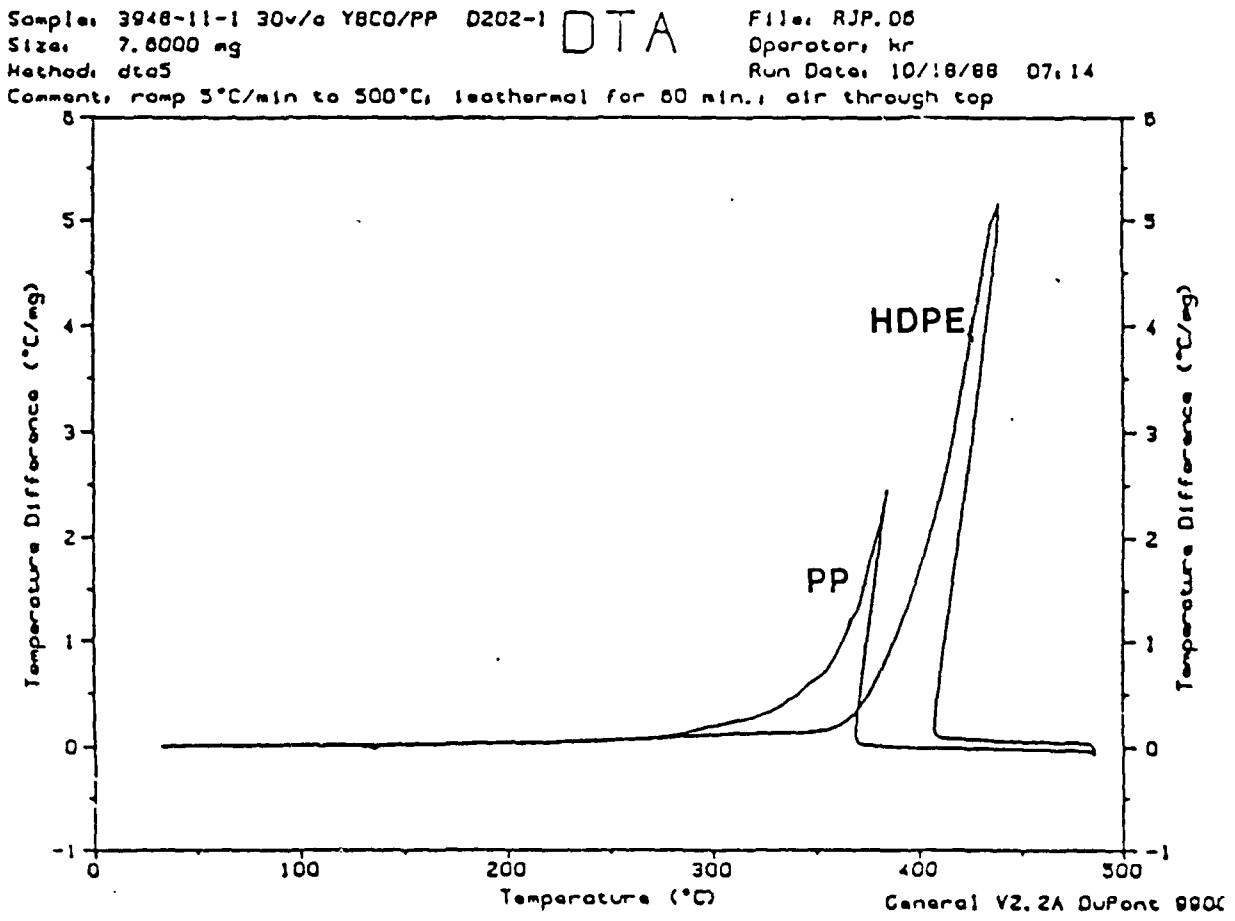

Figure 2.2.3: DTA of PP and HDPE

hydrogen bond. Since PP has many more carbon-carbon bonds than PE, PP has a lower total dissociation energy than PE.

The results of this binder burnout study indicate that of the polymers tested for reactivity with $YBa_2Cu_3O_{7-x}$ ceramic, PPC and Celcon show no reactivity towards the $YBa_2Cu_3O_{7-x}$ ceramic upon burnout and would be safest to use in the processing of the $YBa_2Cu_3O_{7-x}$ ceramic. Larger samples of these polymers are on order for further evaluation. When using any of the other polymer candidates, strict attention must be paid to the binder burnout process to prevent reactivity of the polymer with the $YBa_2Cu_3O_{7-x}$ ceramic.

2.2.4.2 Thermal analysis of $YBa_2Cu_3O_{7-x}$ green fiber and their constituents

Green fiber samples were analyzed by DSC to elucidate the reactions during binder burnout. The procedure was to heat 10 mg of fiber at 20°C/min to 695K (422°C) in both air and nitrogen. The upper temperature was limited by the aluminum specimen pans. A second heat was performed to determine whether any polymer material remained after the first heat cycle. Table 2.2.6 describes the DSC collected and their respective figure numbers in this report.

Figures 2.2.4 through 2.2.6 are scans of the $YBa_2Cu_3O_{7-x}$ powder (Lot #01701, made with stearic acid) and the HDPE and EVA fibers made from this powder in both air and nitrogen. The scans of the air studies for both EVA and HDPE reveal complete reaction is not obtained in the first heat cycle. The scans in nitrogen reveal that although no atmospheric oxygen is present, both green fibers show an exotherm on the first cycle and an endotherm on the second cycle.

To determine the effect of each component, the base polymers were analyzed in air and nitrogen, as shown in Figures 2.2.7 and 2.2.8. The scans

TABLE 2.2.6

DSC DATA ON YBCO GREEN FIBERS

FIGURE #	DSC#	DESCRIPTION
2.2.4	3497-76-4	YBCO POWDER (LOT# 01701) WITH 2 WT% STEARIC ACID PROCESSING AID
2.2.5	3497-76-1	MELT SPUN FIBER 3498-77-7, 01701 YBCO IN HDPE
2.2.6	3497-76-2	MELT SPUN FIBER 3498-80-2, 01701 YBCO IN EVA
2.2.7	3497-76-3	HDPE POLYMER USED IN MELT SPUN FIBERS
2.2.8	3497-76-5	EVA POLYMER USED IN MELT SPUN FIBERS
2.2.9	3497-80-1	YBCO POWDER (LOT# 01394) WITH 0.5 WT% ETHYLENE GLYCOL PROCESSING AID
2.2.10	3497-80-2	MELT SPUN FIBER 3498-86-5, 01394 YBCO IN HDPE
2.2.11	3497-80-3	MELT SPUN FIBER 3498-95-1, 01394 YBCO IN EVA

for both base polymers in air reveal that complete combustion is not achieved in either during the two heat cycles. This may explain why the first cycles of the green fiber do not provide complete exotherms of reaction. The nitrogen scans for HDPE reveal no change in the polymer whereas the nitrogen scans of EVA suggest a volatilization in the first cycle with an endotherm at 378°C. The second cycle for EVA shows no further changes in the polymer.

Analysis of the DSC for $YBa_2Cu_3O_{7-x}$ powder with 2 wt% stearic acid processing in air, Figure 2.2.4, shows on first heat a large, broad exotherm which peaks at 299°C. This exotherm is due to the oxidation of stearic acid by atmospheric oxygen in air and also by CuO in the $YBa_2Cu_3O_{7-x}$ ceramic. Both reactions consume the stearic acid and are not readily reversible. Upon second heat in air there is a broad exotherm which peaks at 362°C. This is believed due to the lower concentration of stearic acid available for oxidation in the powder.

The amount of stearic acid and CuO available in the 10 mg of $YBa_2Cu_3O_{7-x}$ reagent powder is 70.3 micromoles of stearic acid and 44.1 micromoles of CuO. To completely oxidize this quantity of stearic acid using CuO as the oxidizer would require 36.6 micromoles of CuO. Thus, 2 wt% stearic acid processing aid in the $YBa_2Cu_3O_{7-x}$ powder is sufficient in principle to reduce to copper metal about 70% of all the CuO present in the $YBa_2Cu_3O_{7-x}$.

On first heat in nitrogen there is a very large exotherm with a maximum at 398°C. Without atmospheric oxygen, the only oxidizing species available to combust the stearic acid is CuO in the $YBa_2Cu_3O_{7-x}$ powder. It appears that this reaction has a higher heat of activation than that of stearic acid combustion with atmospheric oxygen. This accounts for the shift to higher temperature observed for the $YBa_2Cu_3O_{7-x}$ exotherm in nitrogen gas.

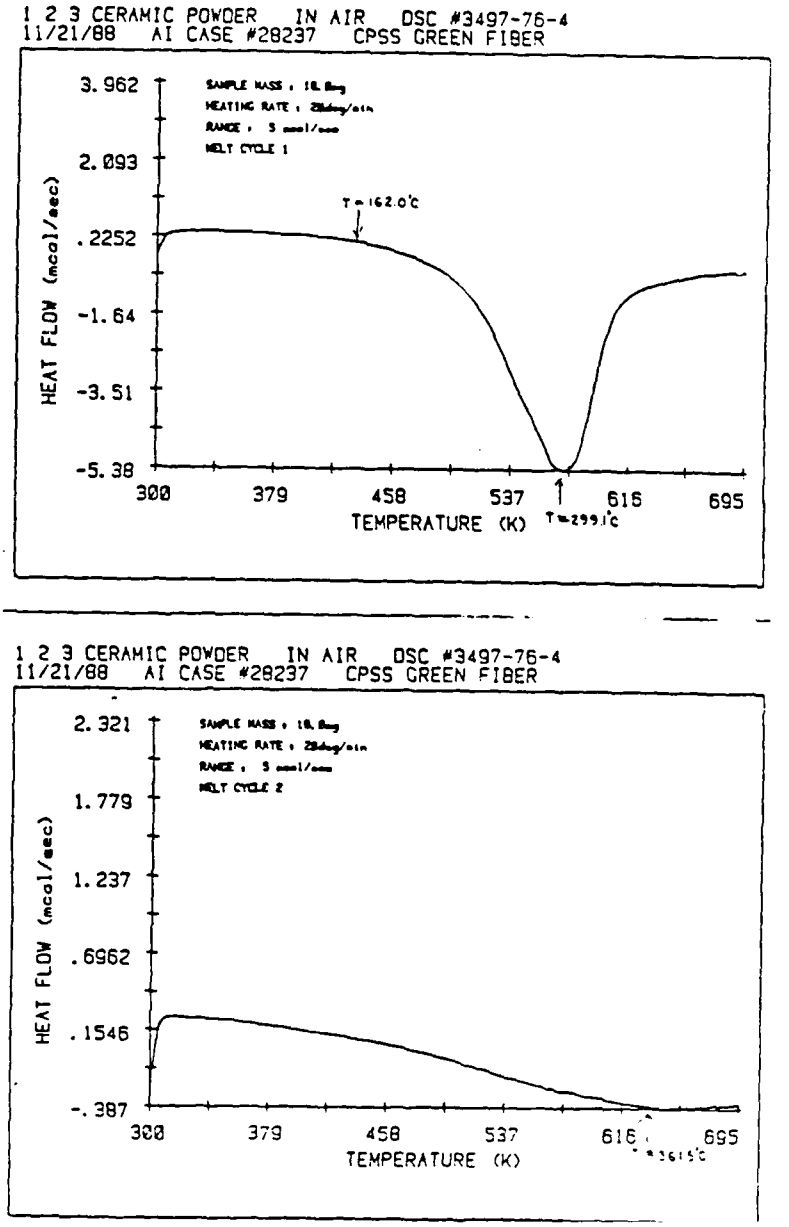

Figure 2.2.4(A): Thermal Analysis of $YBa_2Cu_3O_{7-x}$ Powder
With 2 wt% Stearic Acid
Above: First Heating Cycle in Air
Below: Second Heating Cycle in Air

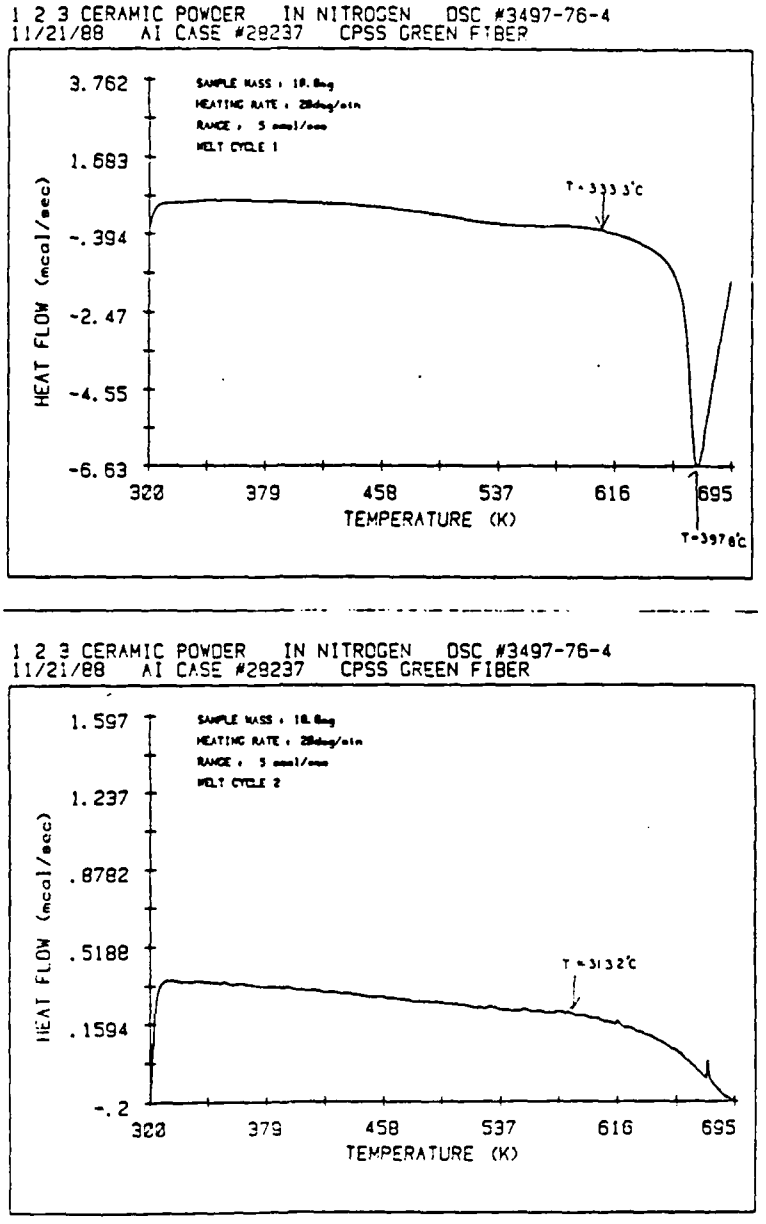

Figure 2.2.4(B): Thermal Analysis of $YBa_2Cu_3O_{7-x}$ Powder With 2 wt% Stearic Acid
Above: First Heating Cycle in Nitrogen
Below: Second Heating Cycle in Nitrogen

The DSC for the HDPE polymer, Figure 2.2.7, shows a large endotherm peak at 140°C in air due to the melting of the polymer. This is followed by several exotherms, the largest and broadest of which occurs at 422°C. These exotherms correspond to thermal oxidative degradation of the HDPE polyolefin. During thermal oxidative degradation, the molecular weight distribution of the polymer is reduced, volatile products form, and changes in the polymer composition occur. The second heat shows that the HDPE polymer is not totally decomposed at 422°C in air as evidenced by an endotherm at 132°C corresponding to the polymer melting temperature. The drop in T_m from 140°C in first heat to 132°C in second heat indicates that this polymer does have some ordering resulting from processing history.

In nitrogen the HDPE polymer does not decompose when heated to 422°C. This indicates that an oxidizing species must be present for thermal degradation of HDPE to occur at these temperatures.

The DSC for the $YBa_2Cu_3O_{7-x}$/HDPE fiber, Figure 2.2.5, shows an exotherm due to thermal oxidative degradation in air at 410°C. This exotherm is broader and at a lower temperature than that observed for the unfilled polymer. This suggests reaction of the HDPE polymer with the $YBa_2Cu_3O_{7-x}$ ceramic. The most probable reaction is oxidation of the HDPE polymer by CuO in the $YBa_2Cu_3O_{7-x}$ powder.

The amount of HDPE and CuO available in the 10 mg fiber sample is 32.3 micromoles of HDPE monomer and 39.2 micromoles of CuO. To completely oxidize this ethylene monomer using CuO from the $YBa_2Cu_3O_{7-x}$ would require as much as 193.8 micromoles of CuO, about five times more than is present in the $YBa_2Cu_3O_{7-x}$. Thus, the HDPE in this $YBa_2Cu_3O_{7-x}$ fiber is sufficient to reduce all of the CuO in the $YBa_2Cu_3O_{7-x}$ to metallic copper, with excess polymer remaining.

This explains why in nitrogen on first heat this sample shows a sharp exotherm at 362°C and on second heat an endotherm at 386°C. The exotherm observed on first heat is due to the oxidation of ethylene by CuO, the only oxidizing species available to this sample in the absence of oxygen. On second heat an endotherm is observed due to the formation of volatile products from the remaining HDPE. A second exotherm is observed on first heat in nitrogen at 392°C. This is due to the oxidation of stearic acid processing aid by CuO in the $YBa_2Cu_3O_{7-x}$ powder.

"Ethylene vinylacetate" describes a family of thermoplastic polymers ranging from 5 to 50 wt% vinyl acetate incorporated into an ethylene chain. EVA is a highly branched, random copolymer with acetoxy groups positioned randomly along the carbon chain. The DSC for the EVA polymer, Figure 2.2.8, in air on first heat shows a complex series of endotherms and exotherms which correspond to volatile product formation, thermal oxidative degradation and change in the polymer composition. The second heat shows that the EVA polymer is not totally decomposed at 422°C in air as evidenced by an endotherm at 102°C, corresponding to polymer melting. In nitrogen the EVA polymer releases volatile products in the first heat. This is represented by a large endotherm at 378°C. However, the second heat shows that EVA is not completely degraded when subjected to 422°C.

The DSC for the $YBa_2Cu_3O_{7-x}$/EVA fiber, Figure 2.2.6, shows a series of exotherms in air due to oxidative degradation. These exotherms are at higher temperature than those observed for the unfilled polymer. This suggests reaction of the EVA with the $YBa_2Cu_3O_{7-x}$ ceramic. The DSC data for this sample in nitrogen supports this belief. In nitrogen on first heat this sample shows a large exotherm at 354°C and on second heat an endotherm at 390°C. The

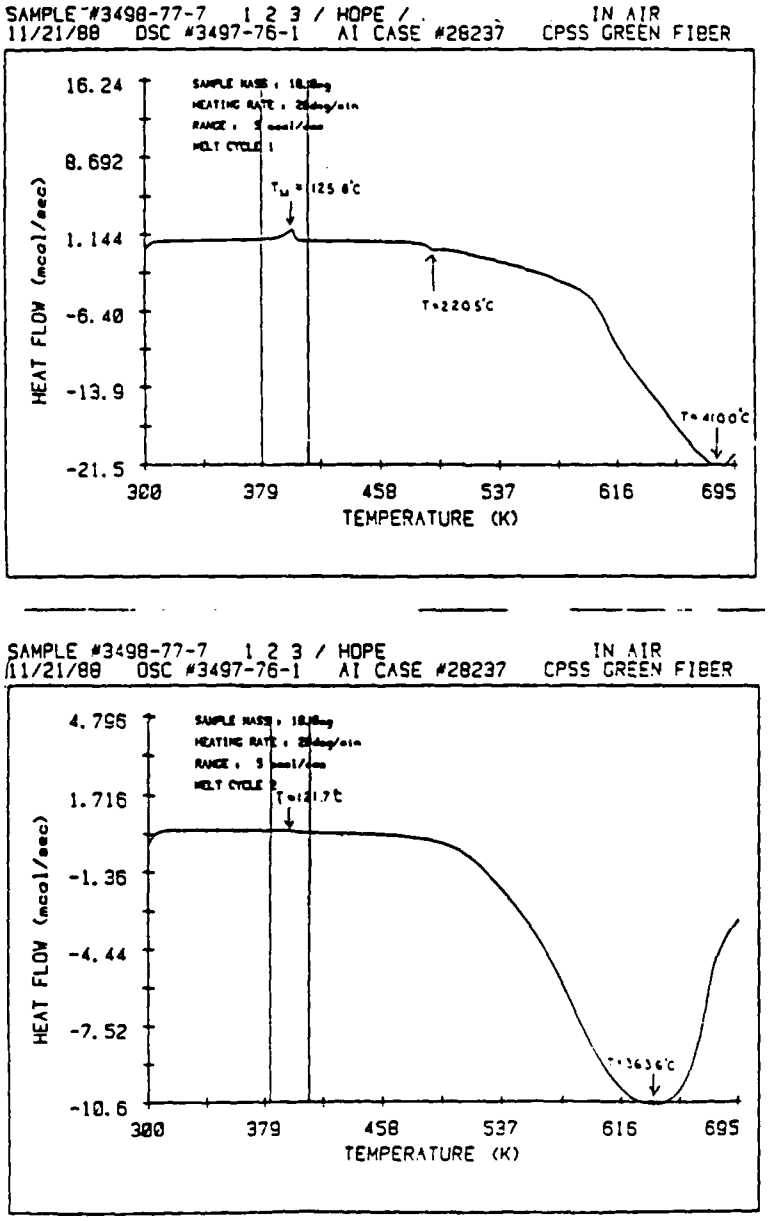

Figure 2.2.5(A): Thermal Analysis of $YBa_2Cu_3O_{7-x}$ Green Fiber With HDPE Blend
Above: First Heating Cycle in Air
Below: Second Heating Cycle in Air

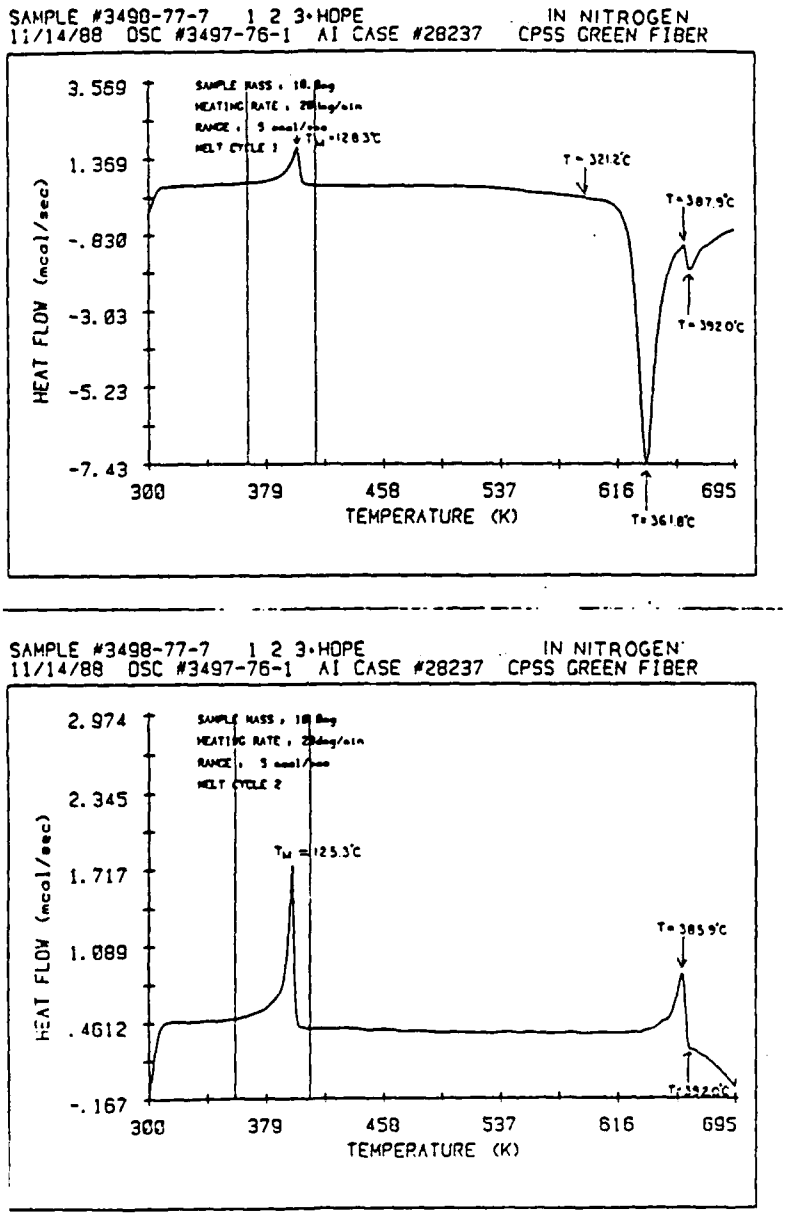

Figure 2.2.5(B): Thermal Analysis of $YBa_2Cu_3O_{7-x}$ Green Fiber With HDPE Blend
Above: First Heating Cycle in Nitrogen
Below: Second Heating Cycle in Nitrogen

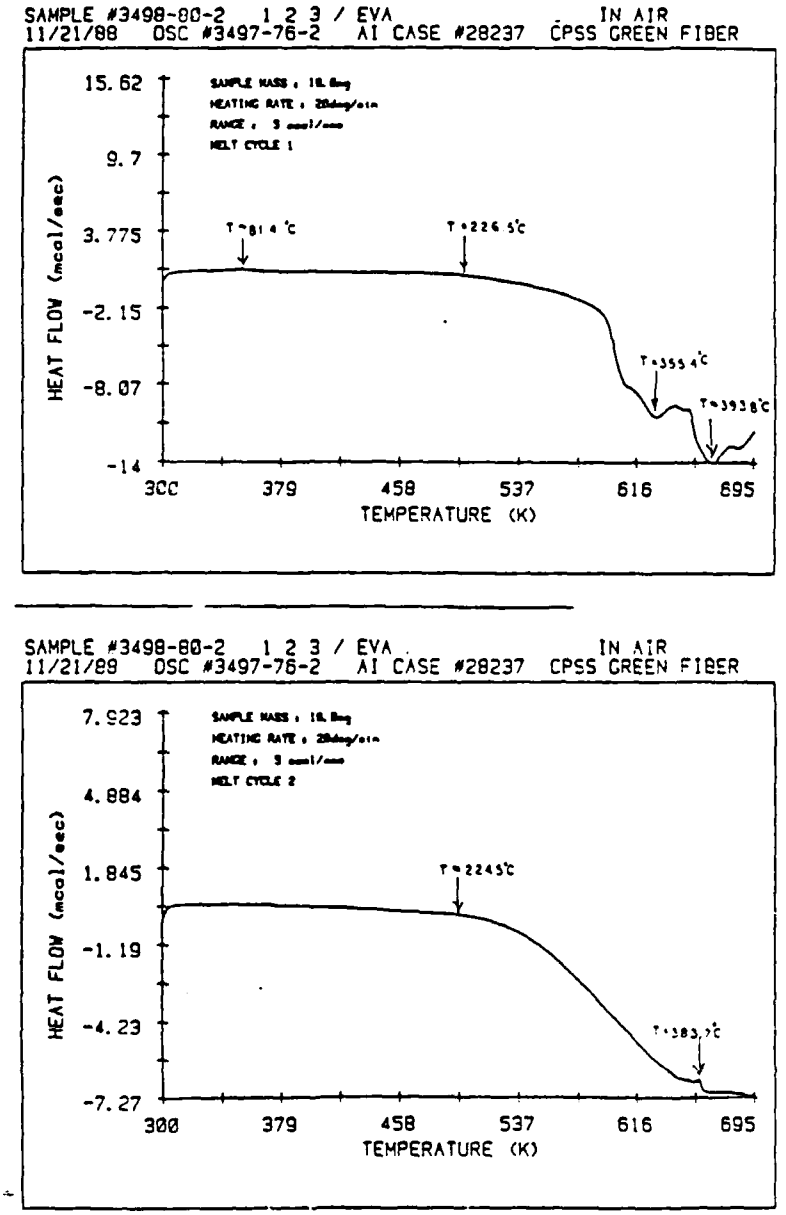

Figure 2.2.6(A): Thermal Analysis of $YBa_2Cu_3O_{7-x}$ Green Fiber With EVA Blend
Above: First Heating Cycle in Air
Below: Second Heating Cycle in Air

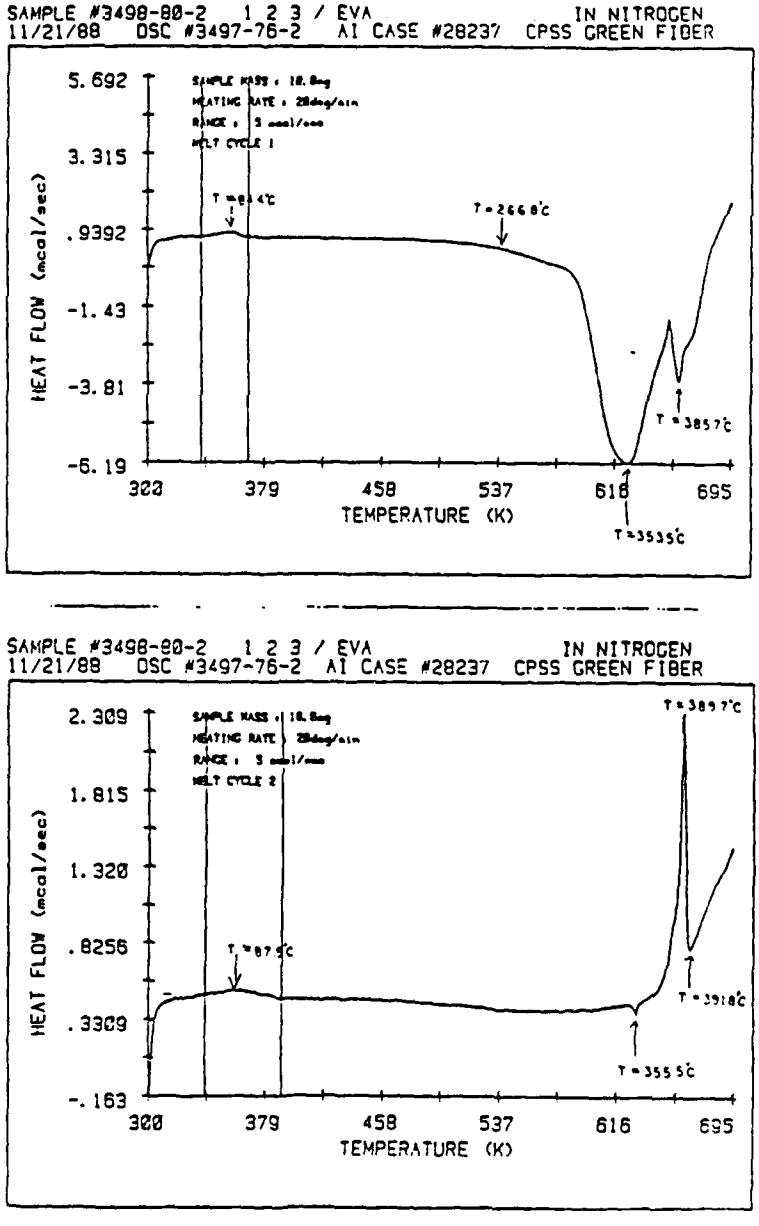

Figure 2.2.6(B): Thermal Analysis of $YBa_2Cu_3O_{7-x}$ Green Fiber With EVA Blend
Above: First Heating Cycle in Nitrogen
Below: Second Heating Cycle in Nitrogen

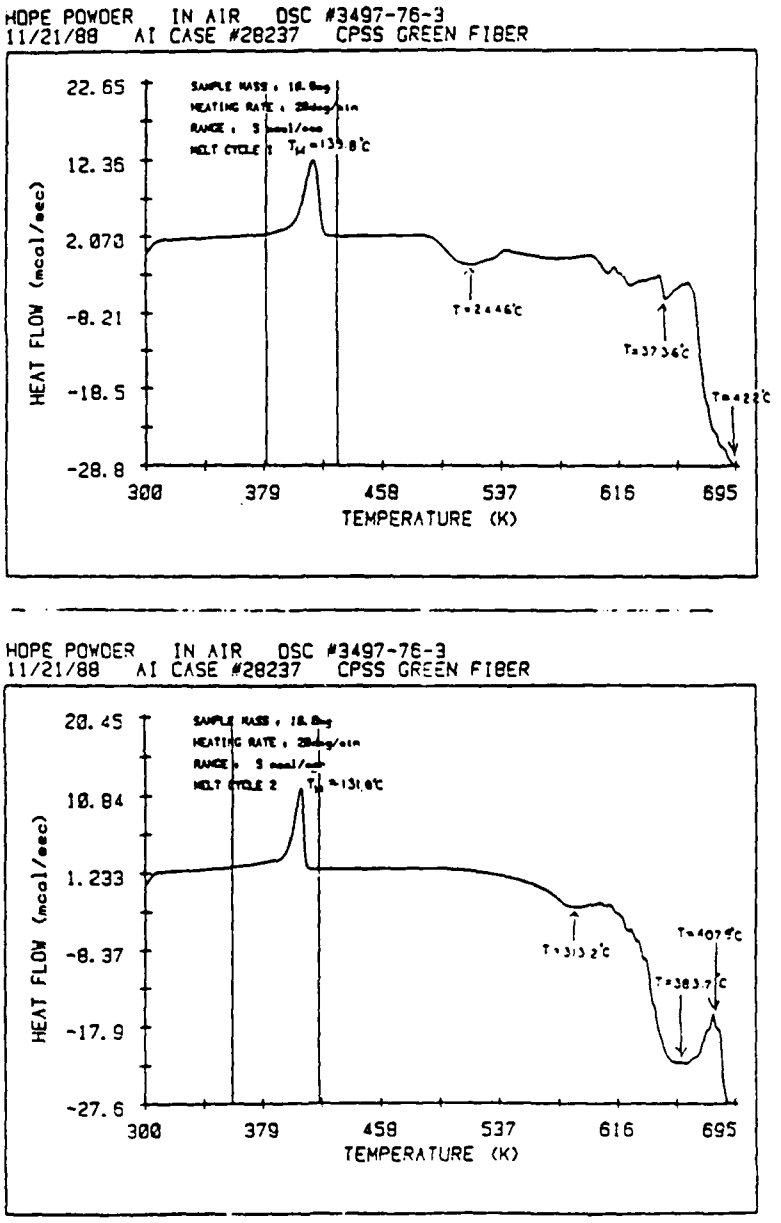

Figure 2.2.7(A): Thermal Analysis of HDPE Polymer
Above: First Heating Cycle in Air
Below: Second Heating Cycle in Air

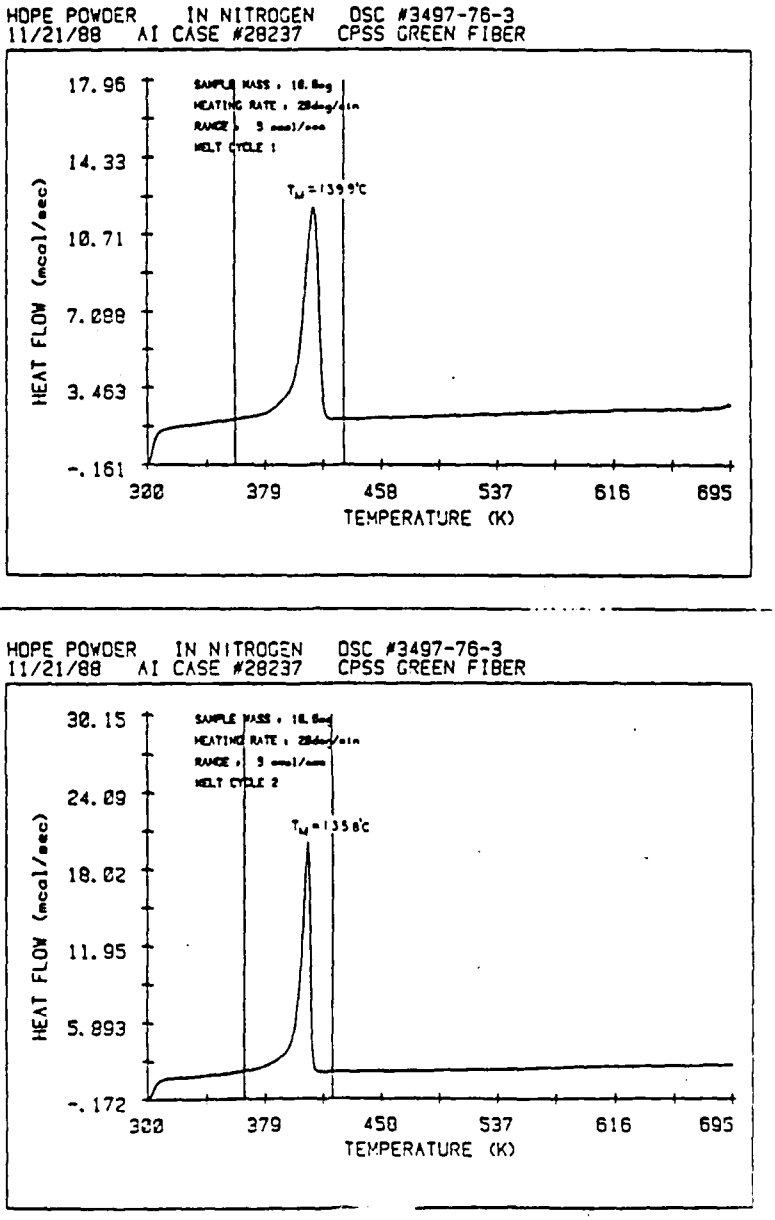

Figure 2.2.7(B): Thermal Analysis of HDPE Polymer
Above: First Heating Cycle in Nitrogen
Below: Second Heating Cycle in Nitrogen

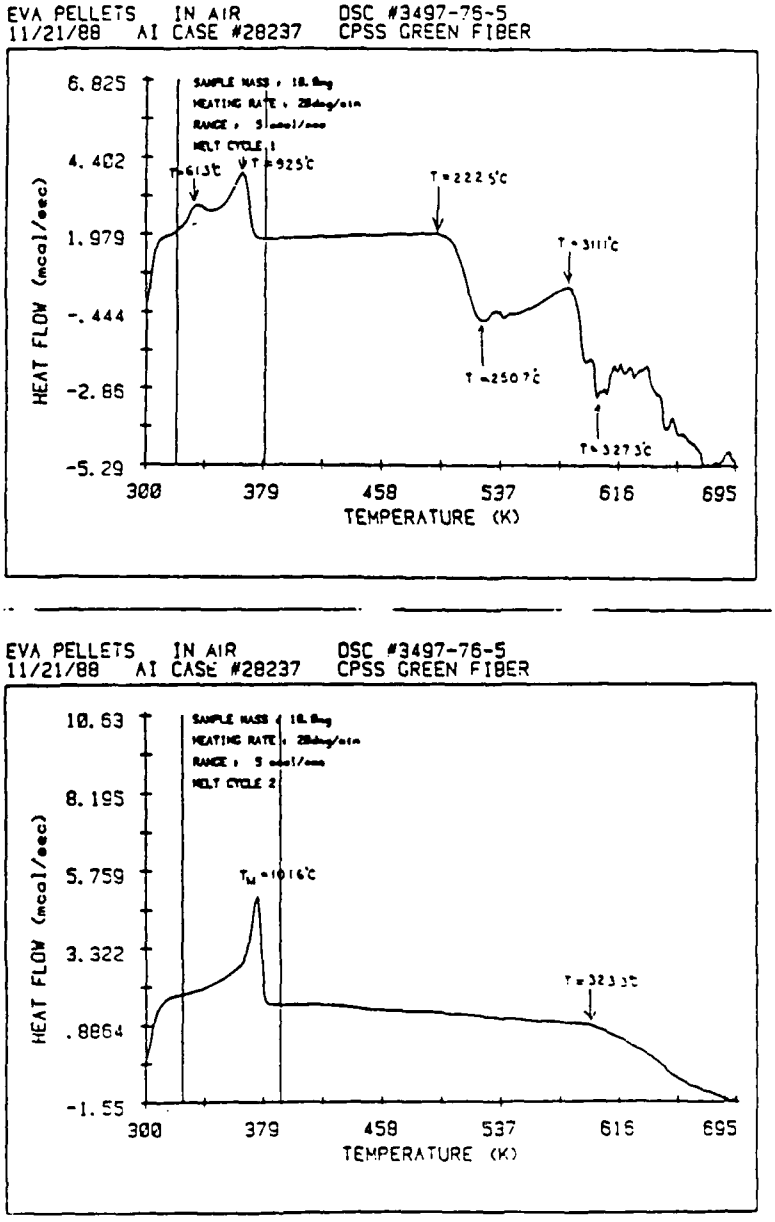

Figure 2.2.8(A): Thermal Analysis of EVA Polymer
Above: First Heating Cycle in Air
Below: Second Heating Cycle in Air

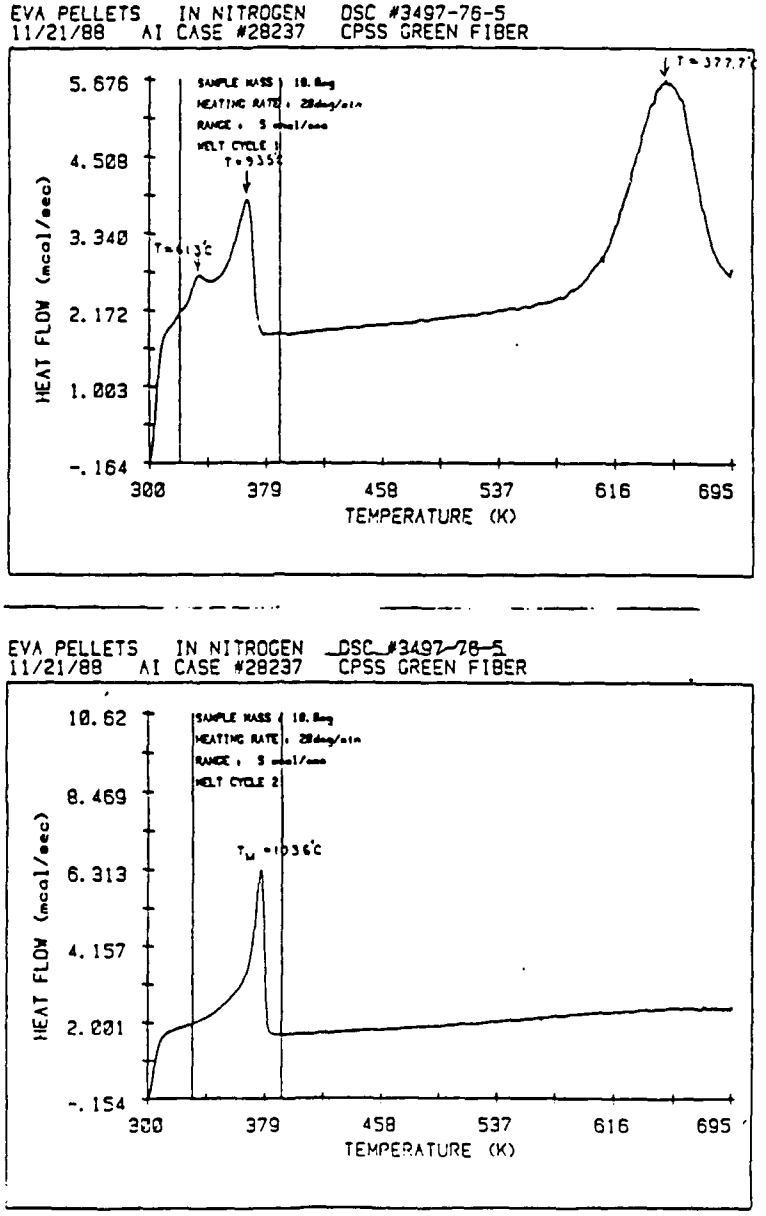

Figure 2.2.8(B): Thermal Analysis of EVA Polymer
Above: First Heating Cycle in Nitrogen
Below: Second Heating Cycle in Nitrogen

exotherm observed on first heat is due to the oxidation of ethylene and vinyl acetate by CuO. On first heat in nitrogen a second exotherm is observed at 386°C due to the oxidation of stearic acid processing aid with CuO in the $YBa_2Cu_3O_{7-x}$ powder.

In order to compare the effect of ethylene glycol processing aid on $YBa_2Cu_3O_{7-x}$ with that observed for stearic acid containing powder, a DSC of $YBa_2Cu_3O_{7-x}$ ceramic with 0.5 wt% ethylene glycol processing aid, Figure 2.2.9, was taken. Note that the heat flow scale on this DSC is smaller than that for Figure 2.2.4 of $YBa_2Cu_3O_{7-x}$ powder with 2 wt% stearic acid processing aid. The largest exotherm for this sample occurs at 219°C in air. The magnitude of this exotherm is small in comparison to that seen for stearic acid containing powder. It appears from this DSC that the ethylene glycol is oxidized by oxygen in air to form CO_2 and H_2O. The second heat shows a broad endotherm in air. In nitrogen a broad exotherm is observed on second heat.

The DSC for the fibers with $YBa_2Cu_3O_{7-x}$/ethylene glycol containing powder in HDPE is shown in Figure 2.2.10. The presence of ethylene glycol in this powder has little effect in facilitating the oxidation of ethylene monomer by CuO in the $YBa_2Cu_3O_{7-x}$ ceramic, as seen in the stearic acid containing sample. The DSC in air shows oxidation of ethylene monomer in this sample to be caused primarily by oxygen from air.

The DSC for the fibers from ethylene glycol containing $YBa_2Cu_3O_{7-x}$ in EVA is shown in Figure 2.2.11. This DSC in both air and nitrogen looks similar to the DSC of the stearic acid containing $YBa_2Cu_3O_{7-x}$/EVA sample. In this sample it appears that CuO is active as an oxidizing agent for the EVA polymer.

If one compares the molecular units in HDPE, EVA, stearic acid, and ethylene glycol as shown in Figure 2.2.12 one sees that in both EVA and stearic

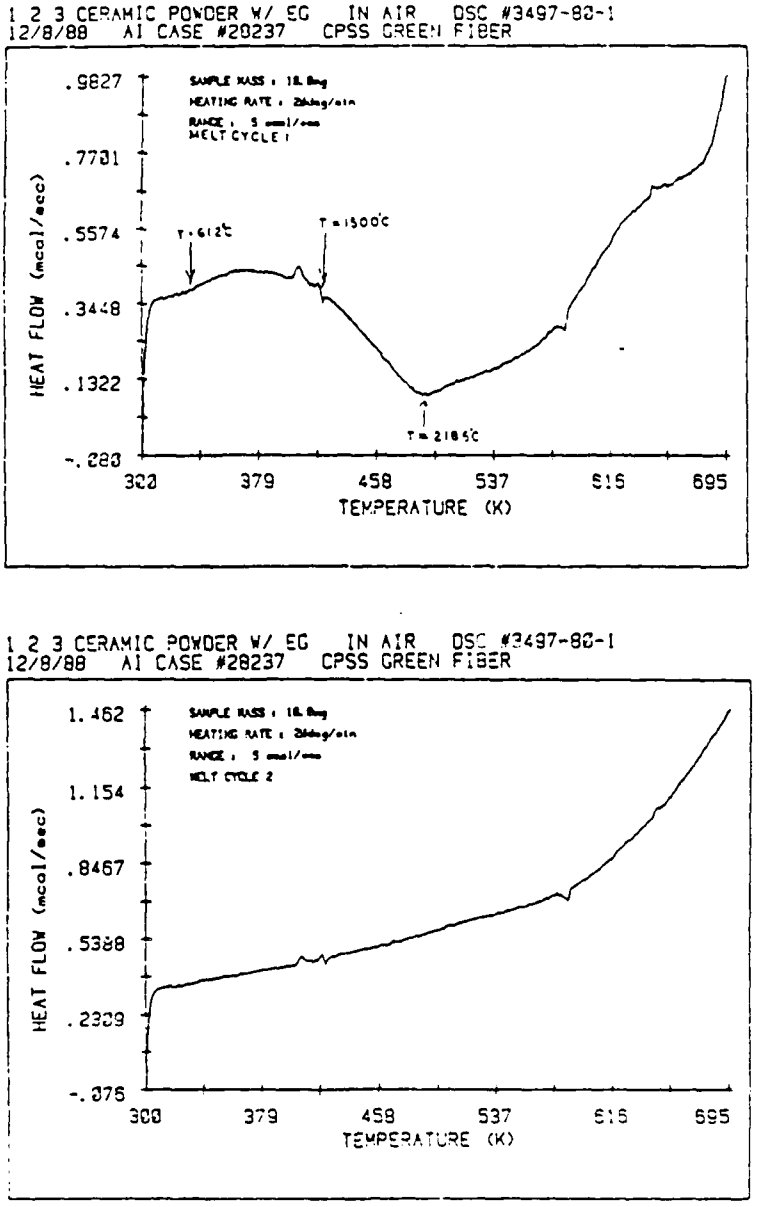

Figure 2.2.9(A): Thermal Analysis of $YBa_2Cu_3O_{7-x}$ Powder With 0.5 wt% Ethylene Glycol
Above: First Heating Cycle in Air
Below: Second Heating Cycle in Air

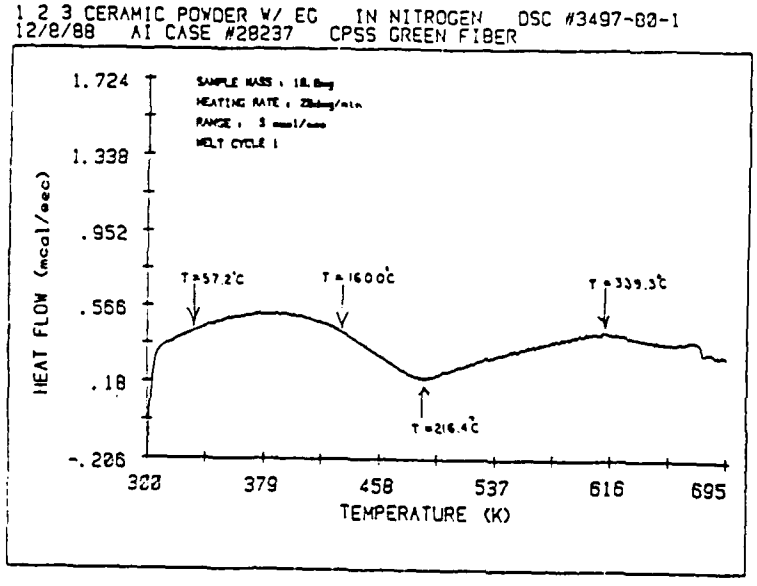

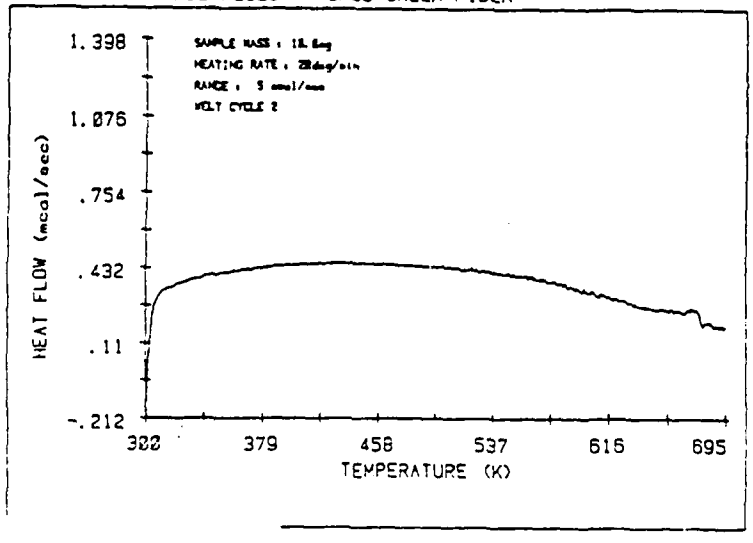

Figure 2.2.9(B): Thermal Analysis of $YBa_2Cu_3O_{7-x}$ Powder
With 0.5 wt% Ethylene Glycol
Above: First Heating Cycle in Nitrogen
Below: Second Heating Cycle in Nitrogen

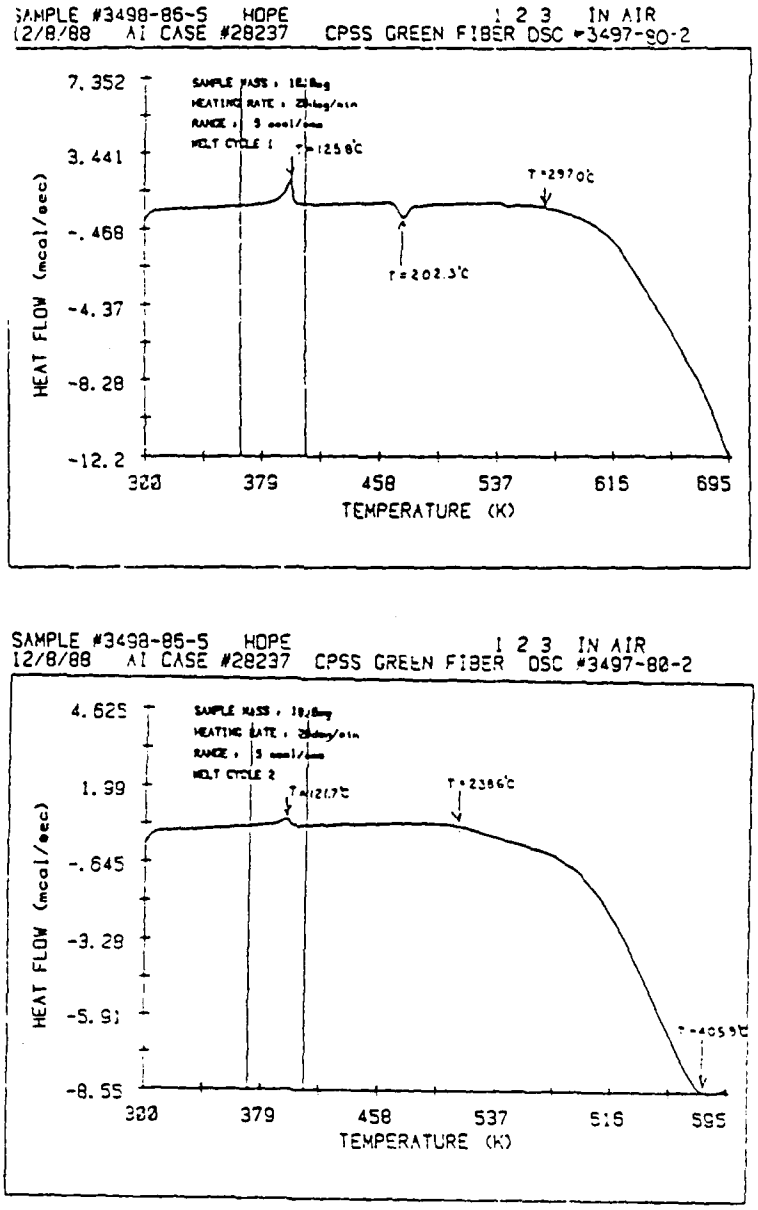

Figure 2.2.10(A): Thermal Analysis of Ethylene Glycol Milled-$YBa_2Cu_3O_{7-x}$ Green Fiber With HDPE Blend
Above: First Heating Cycle in Air
Below: Second Heating Cycle in Air

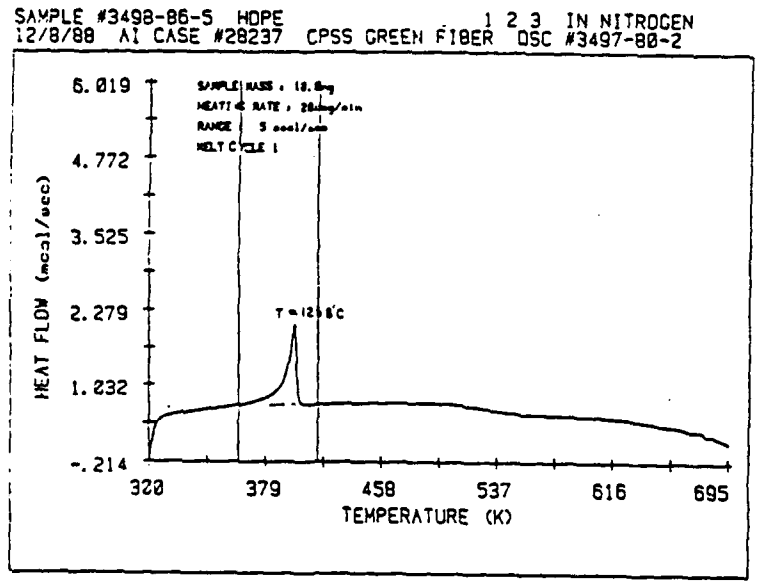

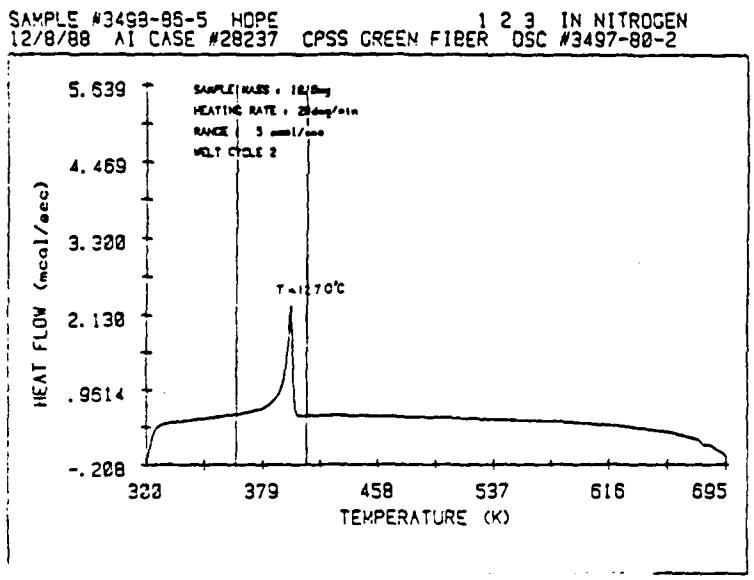

Figure 2.2.10(B): Thermal Analysis of Ethylene Glycol Milled-$YBa_2Cu_3O_{7-x}$ Green Fiber With HDPE Blend
Above: First Heating Cycle in Nitrogen
Below: Second Heating Cycle in Nitrogen

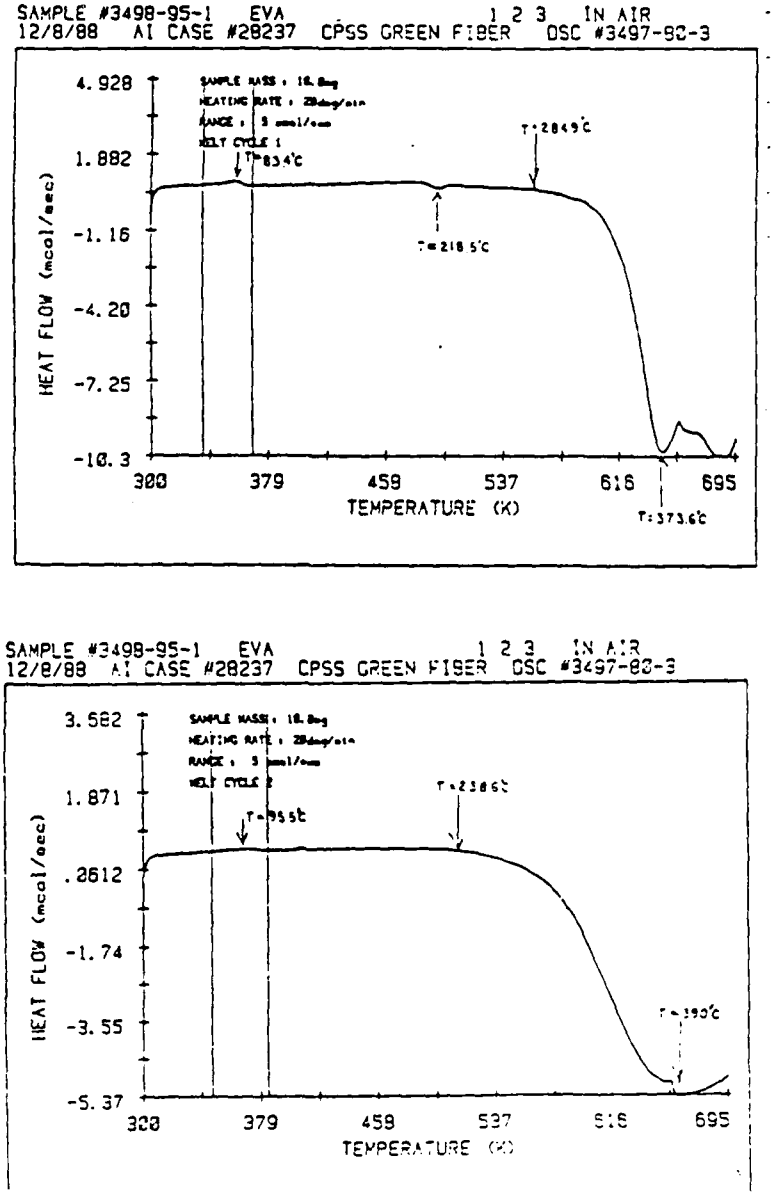

Figure 2.2.11(A): Thermal Analysis of Ethylene Glycol Milled-$YBa_2Cu_3O_{7-x}$ Green Fiber With EVA Blend
Above: First Heating Cycle in Air
Below: Second Heating Cycle in Air

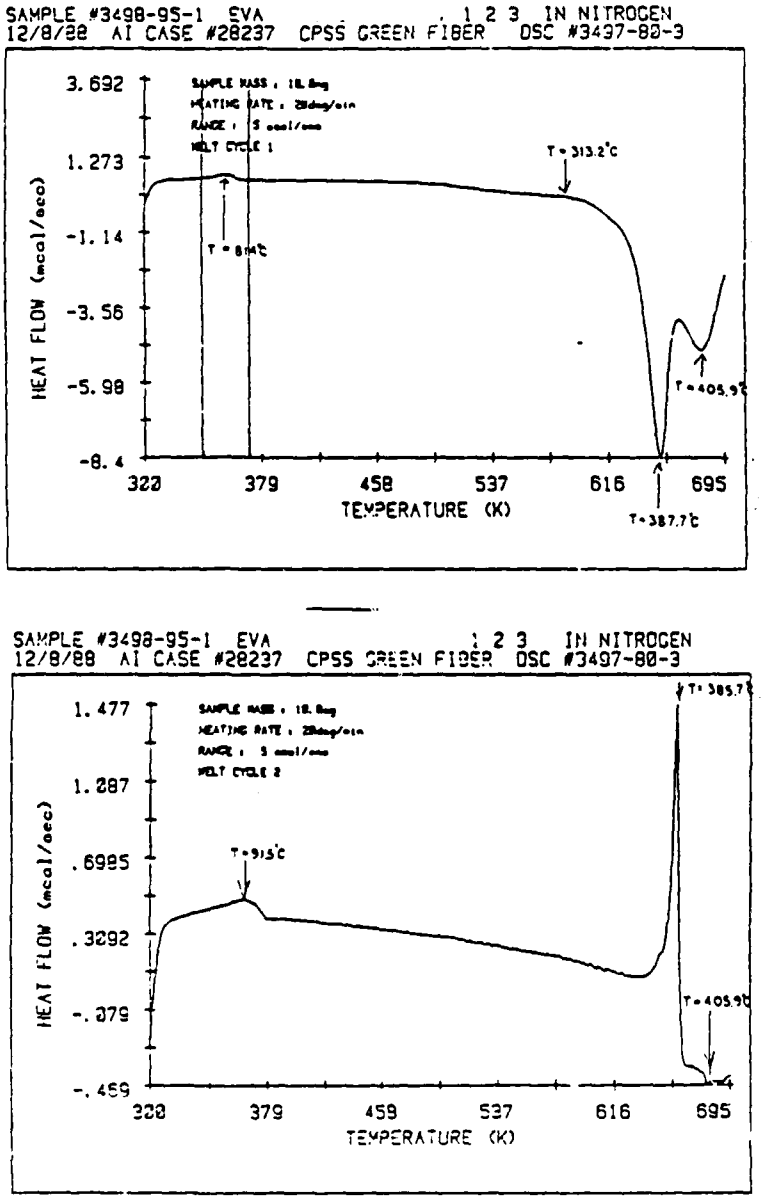

Figure 2.2.11(B): Thermal Analysis of Ethylene Glycol Milled-$YBa_2Cu_3O_{7-x}$ Green Fiber With EVA Blend
Above: First Heating Cycle in Nitrogen
Below: Second Heating Cycle in Nitrogen

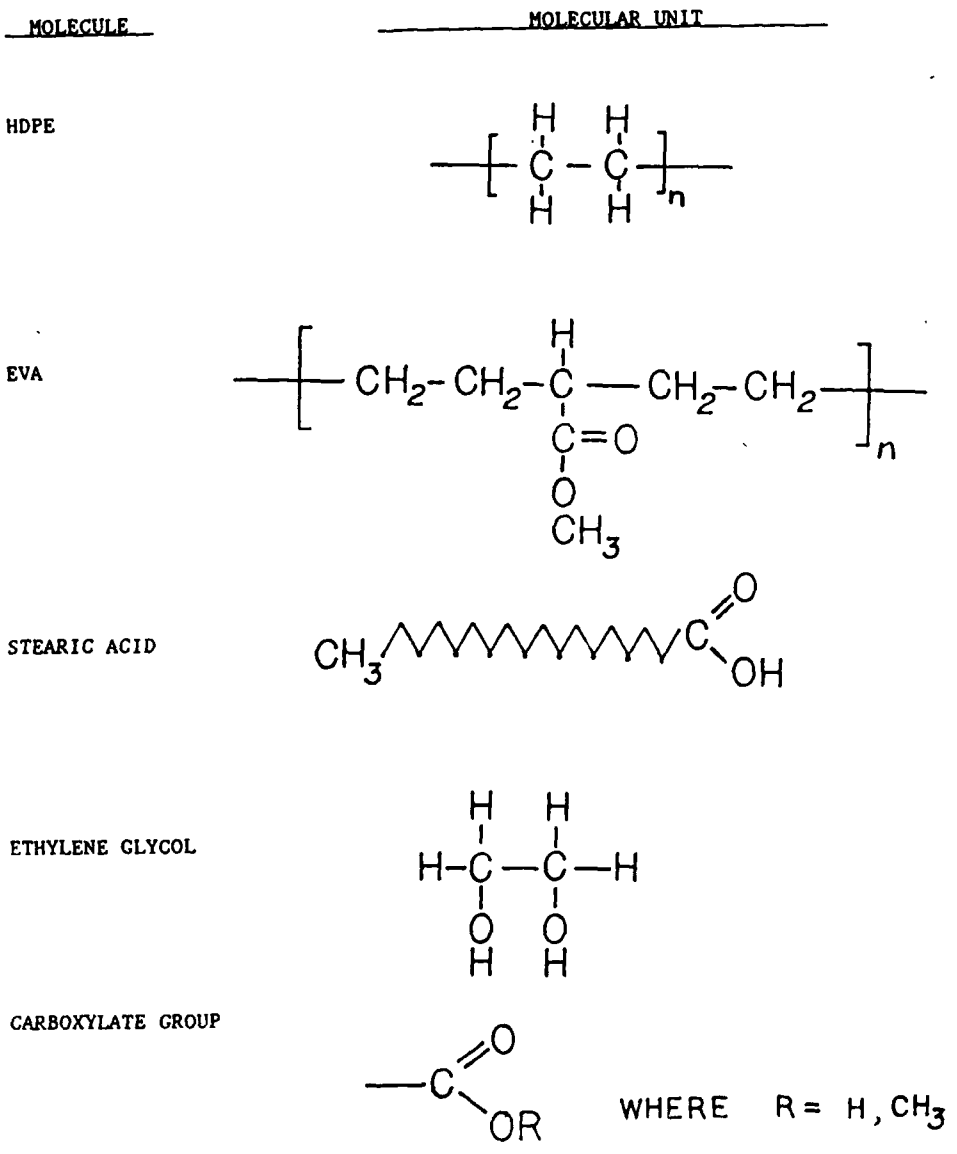

Figure 2.2.12: Molecular units of HDPE, EVA, Stearic Acid and Ethylene Glycol

acid there is a carboxylate chelating group with pi-electron delocalization between oxygen atoms which is known to have the correct bond angle to chelate to copper ions. Ethylene glycol has hydroxyl groups without the proper bond angle and pi-electron delocalization to form a good coordination bond to copper ions. It appears from this DSC study that molecules possessing carboxylate chelating groups facilitate the reaction of CuO from $YBa_2Cu_3O_{7-x}$ during thermal cycling. The CuO is more readily available to act as an oxidizing agent for the organic material. Stearic acid is particularly reactive with $YBa_2Cu_3O_{7-x}$.

2.2.4.4 X-Ray diffraction and carbon residue of fibers after binder burnout

These binder burnout observations caused great concern that the $YBa_2Cu_3O_{7-x}$ fibers could be degraded during the initial heating in the zone sintering process. Since the binder burst studies discussed previously did not exactly reproduce the thermal history during zone sintering, actual fibers from the zone sintering burnout process were examined. A set of experiments investigated the phase purity of the $YBa_2Cu_3O_{7-x}$ in the fibers during the heat treatment procedure. In the first series, fibers were dry spun with the usual acrylic carrier polymer system from the stearic acid milled, 5 wt% CuO doped $YBa_2Cu_3O_{7-x}$ powder. These were given the normal preheat used for zone sintering, which involves a 4°C/min. ramp to 500°C in a nitrogen-purged box furnace, followed by a 1 hour hold in air. An XRD pattern of the fibers at this point revealed that a major fraction of the $YBa_2Cu_3O_{7-x}$ was converted to $BaCO_3$, Y_2O_3, and CuO. Analysis[1] of the burnt-out fibers showed a carbon content of 2.68 wt%. It is not known if this carbon is char from binder residue, or tied up as barium

[1]Carbon analyses were done by the "Leco" combustion technique at Galbraith Laboratories, Inc.

carbonate from powder decomposition. (Note that if all barium from the $YBa_2Cu_3O_{7-x}$ reacted to form barium carbonate, the expected analysis would be 3.22 wt% carbon.)

These fibers were sintered at 935°C for six passes. An XRD pattern of the sintered filaments showed only very small amounts of barium cuprate, demonstrating that the $YBa_2Cu_3O_{7-x}$ phase reforms during the brief sintering process. The sintered fibers had a total carbon content of 0.18 wt%. This is essentially the same as the carbon content in the original as-calcined $YBa_2Cu_3O_{7-x}$ powder.

Faster heating during the binder burnout process decreases the extent of the phase decomposition in fibers made from stearic acid-milled powder. After a 16°C/min. ramp to 500°C in nitrogen followed by a 20-minute 500°C hold in air, a considerably smaller amount of the $YBa_2Cu_3O_{7-x}$ had degraded to form minor quantities of $BaCO_3$, $BaCuO_2$, and CuO.

Similar tests using ethylene glycol-milled $YBa_2Cu_3O_{7-x}$ powder showed much less decomposition than the stearic acid milled powder. Fibers were prepared from this powder by dry spinning. After the 4°C/min. ramp to 500°C in nitrogen and one hour soak in air at 500°C, only a small amount of barium carbonate contamination is seen in an XRD pattern of the fibers. After sintering at 993°C (six passes), small amounts of barium cuprate, 211, and CuO were detectable. In conclusion, some phase decomposition is seen in dry spun fibers exposed to the typical preheat procedure used for zone sintering. Stearic acid milling aid greatly exacerbates the decomposition of $YBa_2Cu_3O_{7-x}$. However, the $YBa_2Cu_3O_{7-x}$ phase is recovered after zone sintering. Carbon pickup occurs in stearic acid-milled powder after the 500°C preheat, but most of the carbon is removed during zone sintering.

2.2.3 Organic Additive Effects in Pressed Pellets

A related study of reactions between $YBa_2Cu_3O_{7-x}$ and organic additives was conducted using pressed pellets. This was motivated by the observations on fibers reported in the previous sections, and by a number of anomalous failures in attempts to sinter simple pressed pellets made from milled powder. We found that pellets made from powder which had been dry milled tended to ignite when heated in air.[2] After some experimentation, it was determined that a highly exothermic reaction occurred at temperatures around 150 to 200°C. The reaction typically initiated at the edge of a sample, and rapidly spread as a distinct combustion front through the specimen, generating smoke and acrid fumes. The specimens were severely degraded. Figure 2.2.13 shows what was once a round pellet. The reaction initiated on the left and propagated to the right. The pellet bloated and distorted to oval shape, as the combustion front caused the part to exfoliate. Other specimens were more dramatic, sometimes exfoliating into a greatly distended stack of nearly uniform flakes. After this reaction, the $YBa_2Cu_3O_{7-x}$ is partially decomposed to form barium carbonate, barium cuprate, yttria, cupric oxide and cuprous oxide.

This was examined in more detail in a series of 990°C sintering trials, using a number of different conditions during initial heating. No attempt was made to optimize the sintering of the pellets, since their purpose was merely to observe reaction that took place upon heating the $YBa_2Cu_3O_{7-x}$/additive combinations. The specimens were made from nearly phase pure $YBa_2Cu_3O_{7-x}$ powders prepared by three milling methods: A) dry milled using stearic acid as a milling

---

[2]Similar reactions were observed in YBCO pellets made from powder dry vibromilled with sorbitan trioleate, and with pellets made from calcium cuprate and barium cuprate powders dry vibromilled with stearic acid.

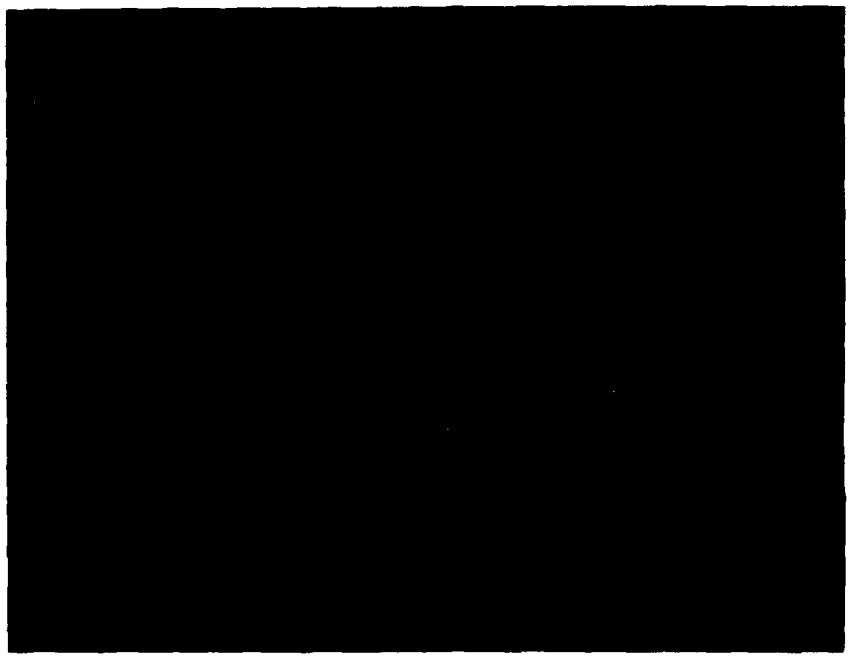

Figure 2.2.13: Exfoliated Pellet of Stearic Acid-Milled $YBa_2Cu_3O_{7-x}$ Powder

aid; B) dry milled using ethylene glycol as a milling aid; and C) jet milled, with no additive. These powders all had an average particle size of about 2.5 microns. Pellets were made from either 2.20 grams of powder (small pellets) or 7.00 grams (large pellets), and were pressed using a half inch diameter die at #10,000 psi. Also included were pieces cast from slip made by redispersing the stearic acid-milled powder in cyclohexane, using EMCOL CC-55[3] as a dispersant.

At the time we believed that the problem could be avoided by heating in air very slowly, or by conducting the initial heating in an oxygen-lean environment created by blowing nitrogen into the box furnace. The results appear in Table 2.2.7, showing which conditions lead to exfoliated pellets, and which produced sound sintered pellets. Notice that the organic-free jet milled $YBa_2Cu_3O_{7-x}$ always produced sound pellets. Powder dry milled with ethylene glycol also yielded sound pellets. In contrast, the cast specimens, produced from stearic acid-milled powder redispersed with EMCOL, always exfoliated. The small dry pressed stearic acid pellets survived if slowly heated, but exfoliated if heated more rapidly. The larger stearic acid pellets all exfoliated. The fact that the nitrogen-rich atmosphere failed to prevent the reaction suggests that the oxidant for the combustion is copper oxide from the solid, rather than atmospheric oxygen. The dependance on the specimen size indicates that this reaction is not inevitable, but depends upon transport.

A second set of experiments was conducted to determine if other types of organic materials also reacted with copper oxide in a similar fashion. Several different $YBa_2Cu_3O_{7-x}$ powders were used; these included jet milled $YBa_2Cu_3O_{7-x}$, an ethylene glycol-milled tetragonal $YBa_2Cu_3O_{7-x}$, a CuO-doped

---

[3]A polypropoxy quaternary ammonium acetate cationic surfactant from Witco Chemical Corporation.

TABLE 2.2.7

SINTERING CONDITIONS LEADING TO SOUND PELLETS OR EXFOLIATED PELLETS

INITIAL HEATING CONDITIONS

	PELLET MASS 2 GRAMS			PELLET MASS 7 GRAMS
POWDER TYPE	1°C/min N_2	1°C/min air	5°C/min air	1°C/min N_2
stearic acid dry milled	sound	sound	exfol.	exfol.
ethylene glycol dry milled	sound	sound	sound	sound
jet milled	sound	sound	sound	sound
stearic acid dry milled, redispersed EMCOL CC-55	exfol.	exfol.	exfol.	exfol.

$YBa_2Cu_3O_{7-x}$, and pure copper oxide powder. Pellets were prepared by dry pressing. The pellets were exposed to 2 wt% additive by wetting the pellets with drops of toluene solutions of oleic acid, stearic acid, sorbitan trioleate, and EMCOL CC-55. The specimens were heated to 990°C in air at 5°C/minute.

The tetragonal pellets doped with oleic acid, stearic acid, and sorbitan trioleate ignited and exfoliated. All other combinations survived. Several inferences can be drawn from this experiment. First, oleic acid and oleate also can react with the copper oxide in $YBa_2Cu_3O_{7-x}$, so these fatty acids are similar to stearic acid. Secondly, the jet-milled and ethylene glycol-milled orthorhombic $YBa_2Cu_3O_{7-x}$ survived exposure to a stearic acid solution, although orthorhombic $YBa_2Cu_3O_{7-x}$ milled with stearic acid always reacts. This suggests that the exposure during milling, when the stearic acid interacts with freshly exposed surface, promotes the reaction during heating. Thirdly, only the tetragonal $YBa_2Cu_3O_{7-x}$ powder reacted in this experiment. This powder was prepared in the usual manner, but cooled from the calcination temperature in nitrogen to maintain the tetragonal reduced state, and dry vibromilled with ethylene glycol in the usual way. The fact that the orthorhombic pellets survived while the otherwise identical tetragonal pellets exfoliated, suggests that the CuO/organic reaction rate is fast enough in the tetragonal pellets to cause ignition. Ignition is an extreme case of autocatalysis, so this data suggests that the tetragonal $YBa_2Cu_3O_{7-x}$ host phase is a more potent catalyst for the CuO/organic reaction than its orthorhombic intercalation compound.

In summary, stearic acid and similar materials can react with the copper oxide in $YBa_2Cu_3O_{7-x}$ with an exothermic reaction. Under certain circumstances, the exothermic CuO/stearic acid reaction occurs fast enough to ignite, and the rapid combustion causes the exfoliation damage. Smaller samples

heated slowly do not ignite, suggesting that either the stearic acid evaporates benignly, or the reaction occurs slowly enough to avoid ignition. The tetragonal $YBa_2Cu_3O_{7-x}$ phase appears to be more reactive than the orthorhombic phase. The ignition reaction is specific to certain organic compounds, such as stearic acid, oleates, and ethylene vinyl acetate. Other compounds, such as polyethylene or ethylene glycol, while capable of reacting with the cuprate, do not cause ignition. These materials can be removed during binder burnout without damage.

2.3 Heat Treatment of Fibers

2.3.1 Introduction

Previous activities in the sintering area were primarily focussed on determining the effect of sintering conditions on the behavior of fibers with similar pre-sintering processing, chiefly dry spun fibers made with Rhône-Poulenc $YBa_2Cu_3O_{7-x}$ powder. During this quarter, the focus was changed to examine the effect of pre-sintering processing with certain constant sintering conditions. Particular attention was devoted to evaluating a wide variety of $YBa_2Cu_3O_{7-x}$ powders produced from alternate raw materials, calcination conditions, grinding conditions, and processing aids.

The experimental design for sintering and annealing is essentially a feedback loop, where a heat treatment/powder characteristic condition is chosen, a number of short filament specimens are prepared, and the microstructures and the transport critical currents are determined. The intent is to improve the microstructures of the sintered filaments and enhance critical current. At present characterization is accomplished primarily by examination of fracture surfaces and polished sections by SEM, and by optical metallography.

Other techniques are accomplished with outside collaboration. Professor Lagerlof of Case Western Reserve University is currently examining sintered filaments by various transmission electron microscopy (TEM) methods.

2.3.2 Sintering of $YBa_2Cu_3O_{7-\delta}$ Fibers

Experiments performed during the first two quarters of this contract are aimed at simulating the manufacturing heat treatment process of continuous lengths of fiber rapidly passing through a multi-zone furnace. To achieve this, short lengths (approximately 6 inches long) of green fiber and a simple existing laboratory furnace are being employed. The fibers are placed on an alumina substrate setter that is passed through the horizontal tube furnace at a controlled speed. The alumina substrate rests upon a low thermal mass sled made of rigid alumina fiberboard attached to a slender alumina push rod. The rod is attached to a motorized positioning-track apparatus that moves the sled in and out of the hot zone at controlled rates of between 4 and 150 cm/min. The hot zone of the peak temperature is 4 cm wide and fairly uniform between approximately linear 7°C/cm thermal gradients. Currently the thermocouple used to measure the sample temperatures in-situ rests on top of the substrate directly next to the fibers on the sled. A fine diameter type K thermocouple of a small thermal mass is now used in order to more closely match the temperature response time of the very thin fibers. Green fiber storage prior to sintering is in a dry-air atmosphere.

As the fibers are passed through the furnace, they are heated to the peak temperature[4] in 4 to 8 min, remain at peak temperature for 1 to 2 min, and then cool at the same rate they were heated. An example of a typical heating profile is shown in Figure 2.3.1. The minimum temperature between successive passes is always below 800°C, but varies depending on when the drive mechanism is reversed. After sintering, samples are annealed for oxygen intercalation in a separate furnace.

During this report period, emphasis was on determining the effect of processing and powder variables upon sintering. Variables that were examined included physical powder characteristics, phase purity, powder milling conditions, and additives, and green fiber formulation. Many of these variables were repeated for both stoichiometric $YBa_2Cu_3O_{7-x}$, and $YBa_2Cu_3O_{7-x}$ doped with 5 weight percent CuO as a sintering aid. In most cases we used a constant set of sintering variables, such as time in the hot zone, heating and cooling rates, number of passes, and peak sintering temperature. After sintering, most specimens received the same annealing conditions including time, peak and minimum temperatures, atmosphere, and heating and cooling rates.

All of the fibers examined this quarter were prepared from CPSS powders that were dry spun or melt spun into fibers. Most fibers were of 100-400 μm in diameter and 10-20 cm in length. These experimental fibers are larger than the 25-50 μm diameter filaments preferred for the composite wire, but are easier to

---

[4]Peak temperatures are quoted as the reading from the thermocouple traveling with the fiber specimens. The actual temperature of the fiber specimen is not necessarily the same as the thermocouple peak temperature, due to differences in the heat transfer conditions. The actual fiber temperature, qualitatively judged by progress of sintering, appears to depend on fiber diameter and emissivity (bare vs. Ag coated) in a manner consistent with radiative heat transfer to the fiber surface.

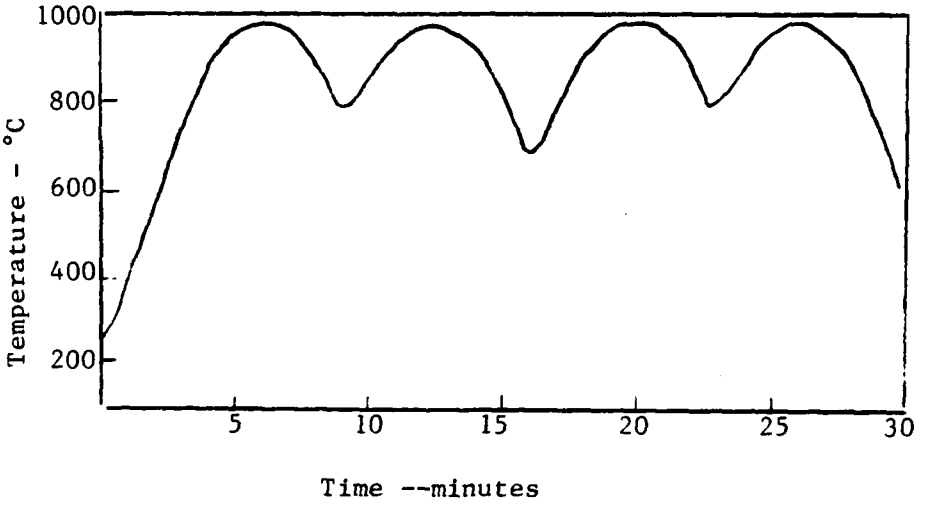

Figure 2.3.1: Typical Time-Temperature Profile for Zone Sintering

handle for metallographic analysis and bare filament electrical measurements.

We have previously determined that fine diameter green fibers can be directly sintered without a separate binder burnout step. However, in this case, we had a variety of types and sizes of fibers, some of which tended to combust if heated too rapidly in air. It was convenient to subject all of the fibers to an initial preheat for binder burnout in an oxygen-lean environment to prevent combustion. Fibers were heated to 500°C at a rate of 5-10°C/min in a nitrogen-purged box furnace and then cooled in air. Preheated fibers were stored at room temperature until needed for zone sintering experiments.

In previous work, some of the best results were obtained on samples heated to around 935°C (for copper oxide doped $YBa_2Cu_3O_{7-x}$ formulations) or 990°C (for stoichiometric $YBa_2Cu_3O_{7-x}$ formulations) with four, six or eight passes through the hot zone at a rate of approximately 5.5 cm/min, resulting in total sintering times of less that one half hour. These sets of conditions were used as a basis for further tests in this quarter, comparing sintered microstructures of filaments that were processed under several different conditions.

Oxygen intercalation was accomplished with a separate anneal, in which a batch of as-sintered filaments were loaded into a room temperature, closed tube furnace, heated to 450°C, held for two hours, then furnace-cooled. Of course the proposed manufacturing method requires continuous sintering, with oxygen intercalation occurring during a controlled anneal. For practical manufacturing, total residence time in the annealing section of the furnace must be less than an hour. Transformation kinetics data[5] for $YBa_2Cu_3O_{7-\delta}$ show a "nose"

---

[5]D. Shi and D.W. Capone, II, "Kinetic Processes of the Orthorhombic to Tetragonal Phase Transition," in High-Temperature Superconductors II, D.W. Capone, II, et al., eds., Materials Research Society, Pittsburgh, PA, 1988, pp. 175-178.

in the time-temperature-transformation (TTT) curve, indicating that isothermal anneals as short as 15 min might be adequate to oxidize the material into the superconducting orthorhombic state. Since the oxygen diffusion into the center of the filament is highly dependent on the sintered density of the filaments, critical current transport densities may not be truly optimized for a set of filaments that are all treated to the same intercalation conditions. The filaments that resulted with the best microstructures in this quarter will be used in the next quarter to determine empirically the minimum isothermal annealing time required for optimum oxygen intercalation.

2.3.3 Sintering Behavior of Dry Spun Fibers from Experimental Powders

A series of experiments were done using powders milled to median particle sizes in the submicron size range. The particle size was adjusted by wet vibromilling for extended times. Calcined $YBa_2Cu_3O_{7-x}$ from a single lot was dispersed in cyclohexane using sorbitan trioleate and vibromilled with zirconia media. Particle size distributions determined with a Horiba centrifugal sedimentation instrument are displayed in Table 2.3.1.

Dry spun fibers were prepared from these milled powders in the stoichiometric composition and 5 wt% CuO-doped composition. These fibers were zone sintered with six passes through the hot zone at the usual speed, followed by a two hour oxygen intercalation anneal at 450°C. Peak temperatures were 935°C for the CuO-doped powders and 993°C for the phase-pure powders. These temperatures were selected based on experience with the dry milled powders, which had a median particle size of about 2.5 microns. The microstructures of sintered fibers were examined by SEM and the densities were estimated with the point count

TABLE 2.3.1

PARTICLE SIZE OF $YBa_2Cu_3O_{7-x}$ POWDERS VIBROMILLED IN CYCLOHEXANE

Milling Time (hours)	Median Diameter (microns)	Size Range (microns)	Submicron Fraction
27	1.9	0.5-11	23%
70	0.94	0.5- 3	55%
143	0.65	0.5- 3	75%
168	--	--	--
242	--	--	--

Table 2.3.2

MICROSTRUCTURAL PARAMETERS FOR ZONE SINTERED
CuO-DOPED $YBa_2Cu_3O_{7-x}$ FIBERS AS A FUNCTION OF PARTICLE SIZE

Sample	Milling time (hours)	Median size (um)	Density (Percent)	Grain Size Range (um)	Pore Size Range (um)
27D	70	0.94	97.5	1 - 4	0.25- 1
20A	70	0.94	98	1 - 4	0.5 - 0.75
50D	143	0.65	97	0.5- 0.75	0.25- 0.75
27E	168	---	98	0.5- 1	0.2 - 1.0

TABLE 2.3.3

MICROSTRUCTURAL PARAMETERS FOR ZONE SINTERED
STOICHIOMETRIC $YBa_2Cu_3O_{7-x}$ FIBERS AS A FUNCTION OF PARTICLE SIZE

Sample	Milling time (hours)	Median size (um)	Density (Percent)	Grain Size Range (um)	Pore Size Range (um)
27B	27	1.9	92	2 - 4	0.75- 2
27C	70	0.94	99	2 - 7	not measured
46C	143	0.65	98	*	
46E	242	---	97	*	

* Large grains observed near the fiber surface with smaller grains in the fiber center, see text.

method from fracture surfaces. Grain and pore sizes were directly measured and reported as typical ranges.

The CuO-doped specimens all sintered to nearly full density at 935°C, with relatively fine grain sizes. Figures 2.3.2 and 2.3.3 show the fracture surfaces of specimens 27D and 50D. The densities and grain sizes for the individual specimens are listed in Table 2.3.2. Density and grain size do not correlate well with the starting particle size, probably because all specimens were essentially fully dense, and the grain size reflects the extent of grain growth. Lower sintering temperatures will be used to resolve the effect of particle size on microstructure development in the CuO-doped system.

The stoichiometric $YBa_2Cu_3O_{7-x}$ fibers also sintered to high density. Table 2.3.3 lists the densities and grain sizes. The fiber from the 27-hour milled powder reached 92% density, which is similar to the "standard" powders sintered at 993°C. This is not surprising since this powder had a median particle size of 1.9 microns, which is similar to the 2.5+/-0.5 micron median size of the standard powders. The fracture surface of this filament is shown in Figure 2.3.4

The 70-hour powder, with 0.94 micron median particle size, achieved full density with grains ranging between 2 and 7 microns. Figure 2.3.5 shows the fracture surface of this high density specimen., Unlike the previous specimen, which had about 8% porosity, this dense filament displayed no evidence of a Meissner effect, indicating that the 2 hour oxygen intercalation anneal was insufficient for this dense specimen.

The fibers from the powder milled for 143 and 242 hours were dramatically overfired at 993°C. These results were confirmed by repeating this experiment. These fibers developed a peculiar microstructure illustrated by the

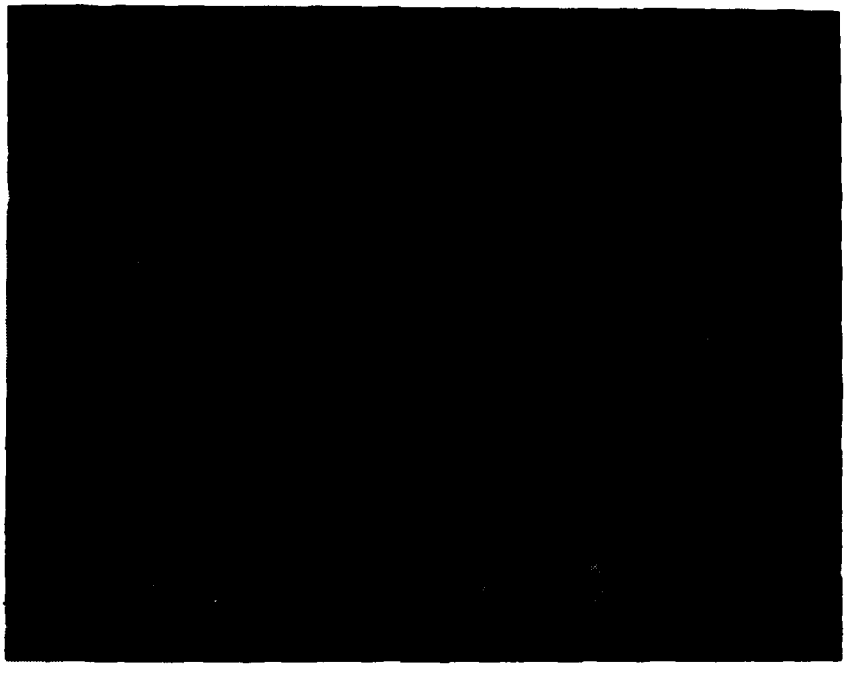

Figure 2.3.2: Fracture Surface of CuO-doped Experimental Powder Milled for 70 Hours Sintered at 935°C for Six Passes. Specimen 27D

Figure 2.3.3: Fracture Surface of CuO-doped Experimental Powder Milled for 143 Hours Sintered at 935°C for Six Passes. Specimen 50D

Figure 2.3.4: Fracture Surface of Stoichiometric Experimental Powder Milled for 27 Hours Sintered at 993°C for Six Passes. Specimen 27D

Figure 2.3.5: Fracture Surface of Stoichiometric Experimental Powder Milled for 70 Hours Sintered at 993°C for Six Passes. Specimen 27C

polished section in Figure 2.3.6. The core of the filament was porous, but the filaments had a thick outer shell of extensively recrystallized grains. In the large-grained outer shell a significant amount of second phase is visible. This is probably the remnant of a peritectic liquid developed at the 993°C peak sintering temperature. In this case the large size of the second phase regions, and the fact that these specimens took a good polish, makes them visible in the optical microscope. We have not yet been able to observe this phase in SEM due to contrast problems. It is possible that this phase is also present in other specimens, but has not been obvious due to poor contrast conditions.

Other experimental powders were examined in this period. Dry spun fibers were prepared from tetragonal $YBa_2Cu_3O_{7-x}$ powder. This powder was made in the usual way, but cooled in nitrogen to preserve the tetragonal state. Dry milling for 92 hours with ethylene glycol produced a powder with a median size of 3.0 microns. After sintering for six passes at 993°C these specimens were still very porous, as illustrated in Figure 2.3.7. Density can be roughly estimated as 75%. This is consistent with the larger particle size of this powder after milling.

Platy particle shapes are needed to induce grain alignment in the green fibers, which is expected to lead to a highly textured fired microstructure. Two promising powders were evaluated in the form of fibers. One method used the substitution of barium hydroxide for the barium carbonate, which appears to promote a more platy habit in the calcined material. Dry milling with ethylene glycol for 104 hours produced a powder with a median size of 3.7 microns. Unfortunately, the milled powder did not appear to be platy. Dry spun fibers were sintered with the usual 993°C, six pass schedule. These fibers did not appear to be textured, but were unusually dense for such a large particle

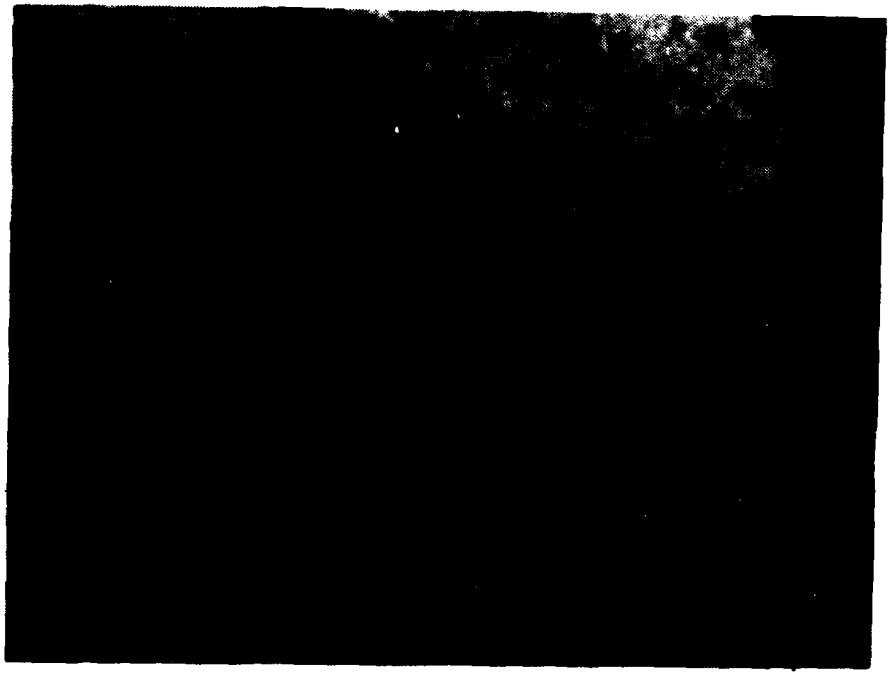

Figure 2.3.6: Polished Section Surface of Stoichiometric Experimental Powder Milled for 143 Hours Sintered at 993°C for Six Passes. Specimen 46C

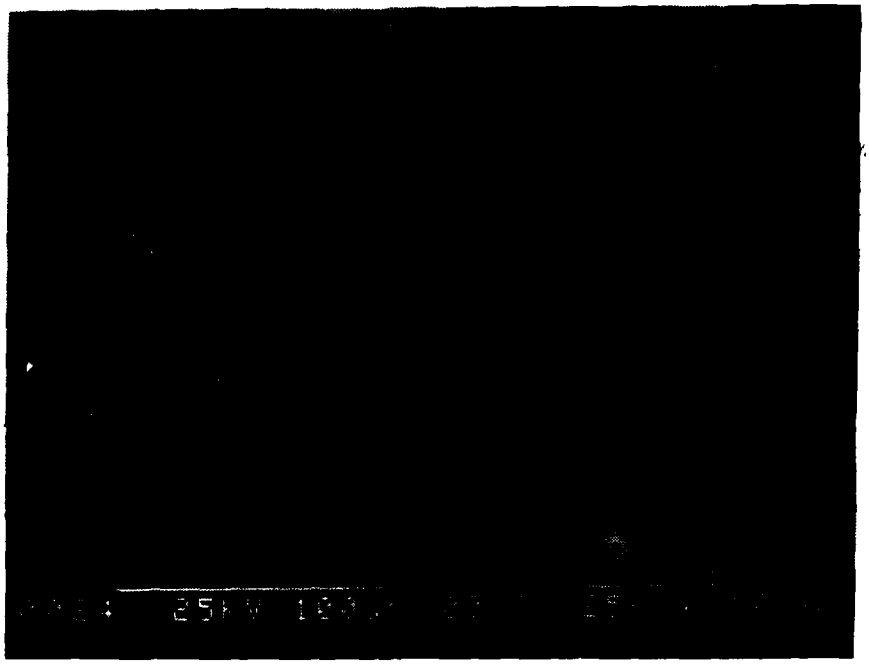

Figure 2.3.7: Fracture Surface of Filament Prepared With Tetragonal YBCO Powder After Sintering for Six Passes at 993°C Peak Temperature

size. Figure 2.3.8 shows the fracture surface, which indicates about a 99% density with grain sizes ranging up to 3-5 microns. Another experiment aimed at platy particles involved $YBa_2Cu_3O_{7-x}$ calcined in the presence of a potassium carbonate dopant. As reported by Murugaraj et.al.,[6] this produces quite platy grains in the calcined material. Milling for 104 hours produced a 5.5 micron powder. Dry spun fibers sintered at 993°C are shown in Figure 2.3.9. These specimens were 98% dense and had very large platy grains, 10 micron and greater in length. Both of these systems produced fibers with good Meissner evidence.

2.3.4 Sintering of Melt Spun $YBa_2Cu_3O_{7-x}$ Fibers

Characterizing melt spun fibers was a high priority which received attention as soon as spools of melt spun fibers were available. Five different types of $YBa_2Cu_3O_{7-x}$ fibers have been examined to date. These include HDPE-based fibers, with the stoichiometric and CuO-excess compositions. The first fibers were made with the stearic acid-milled powder before we were aware of its shortcomings (although in spite of these problems the sintered filaments were the best we have ever made). A second series of fibers were made with ethylene glycol-milled powder. These had good drawability, so fibers were available with diameters varying from 13.5 mils to 4 mils. The finer fibers were made by post-drawing. For example, the 4-mil diameter fibers were post-drawn cold from a spool of spin-drawn 7.5-mil fiber. Finally, $YBa_2Cu_3O_{7-x}$ fibers prepared with EVA carrier polymer were sintered.

---

[6]P. Murugaraj, J. Maier, and A. Rabenan, "Preparation of Highly Oriented Polycrystalline $YBa_{2-y}Cu_3O_x$ Superconductors," Solid State Comm. 66(7), 735-738 (1988).

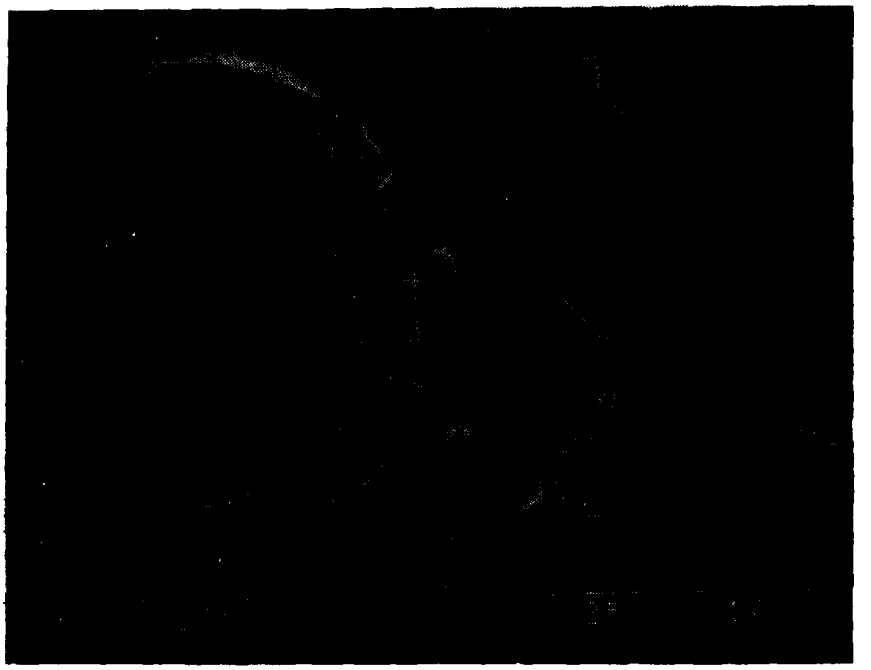

Figure 2.3.8: Fracture Surface of Filament Prepared With YBCO Powder Made With Barium Hydroxide After Sintering for Six Passes at 993°C Peak Temperature

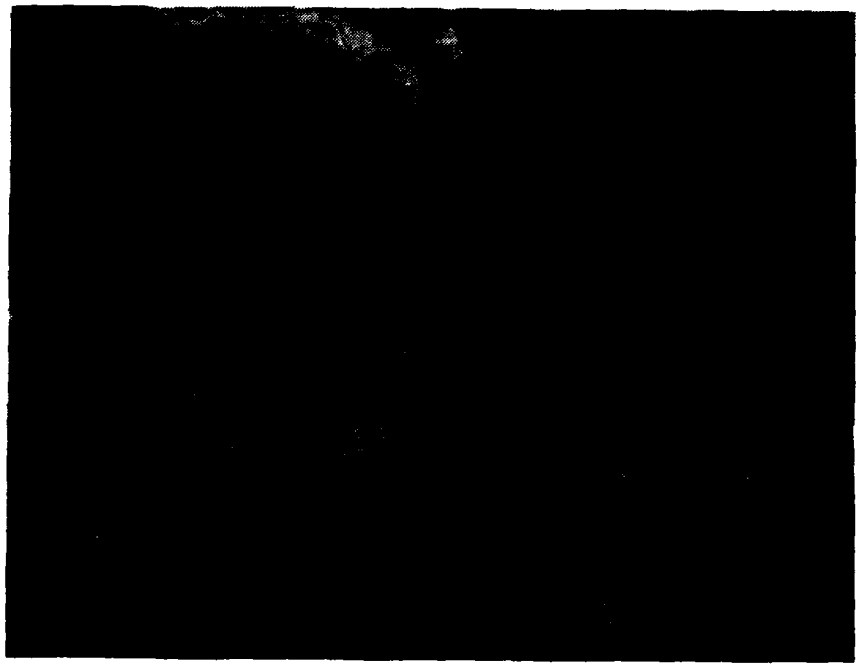

Figure 2.3.9: Fracture Surface of Filament Prepared With YBCO Powder Doped With Potassium Carbonate After Sintering for Six Passes at 993°C Peak Temperature

A number of sintering experiments were conducted on melt spun HDPE fibers loaded with 50 vol% ethylene glycol-milled stoichiometric $YBa_2Cu_3O_{7-x}$. The median particle size of this powder was relatively coarse, 3.7 microns, and only 10 wt% was finer than one micron. Consequently, the sintered density after the usual six passes at 993°C produced a comparatively low density around 85% theoretical. The grain size range was 2 to 10 microns. A fracture surface of this filament appears in Figure 2.3.10. The low sintered density is related to the large particle size in this particular powder batch, and should not be considered characteristic of melt spun fiber. Since the sintered filaments had open porosity, they displayed a good Meissner effect in liquid nitrogen.

Whether the green fibers were spin-drawn or post-drawn seemed to have little effect on the sintered microstructures. However, the post drawn fibers suffered a remarkable axial shrinkage upon initial heating to about 100°C. The fibers decreased in length by more than 50%, while diameters increased until they were about equal to the spin-drawn diameters. For example, a spin-drawn 340-micron diameter green fiber sintered to give a 300-micron filament, reflecting ordinary sintering shrinkage. A post-drawn 150-micron green fiber, however, became a 175-micron diameter sintered filament, with the increase in diameter occurring during initial heating. Essentially all of the elongation created during the post drawing was relaxed in a memory effect. The cold post-draw operation creates significant alignment in the polyethylene chains, which is frozen into the molecular structure of the polymer. Upon heating to near the polymer melting point the polymer relaxes to a more random orientation distribution, which causes the shrinkage. Clearly, a simple cold-drawn operation will not be an effective way to reduce fiber diameters.

Figure 2.3.10: Fracture Surface of a Melt-Spun HDPE Based Fiber Prepared From Ethylene Glycol-Milled Stoichiometric $YBa_2Cu_3O_{7-x}$ Powder, Sintered for Six Passes at 993°C

The green fiber solids loading is a compromise between low loadings for better spinning and high loadings for better sintering. We hoped that the drawability could be improved without sacrificing sintering by reducing the solids content. A spool of HDPE fiber was prepared with the ethylene glycol-milled powder at 40 vol% solids. Unfortunately, the drawability was no better, and the fiber could not retain its shape upon heating past the polymer melting point.

Fibers melt spun with EVA as the carrier polymer and ethylene glycol-milled $YBa_2Cu_3O_{7-x}$ were particularly flexible and elastic. During sintering, these had poorer shape retention than the HDPE fibers, and developed noticeable flat spots where they laid on the substrates. The sintering behavior of these fibers was otherwise the same as the same powder in the HDPE carrier. Experiments reported in Section 2.2 showed that EVA could be very reactive with $YBa_2Cu_3O_{7-x}$. In spite of this, the sintered filament from the EVA system appeared quite normal, and had no evidence of a second phase visible by optical metallography. The filaments had indications of a strong Meissner effect.

A number of HDPE-based fibers were prepared from the 2.7-micron $YBa_2Cu_3O_{7-x}$ powder milled with stearic acid. This powder was made with the CuO-excess composition, and so was sintered at 935°C. The microstructure of these filaments had a 90% dense matrix with grains ranging between 1 and 7 microns, typical of the CuO-excess composition. Although these were made with stearic acid, the filaments appeared to be of good quality, displaying a strong Meissner effect and a transport critical current about 800 A/cm^2. Figure 2.3.11 shows the typical microstructure of a fracture surface. The low magnification view in Figure 2.3.11 also illustrates a peculiar hole found in the center of the fiber. It runs continuously down the axis of the fiber. This hole was seen in

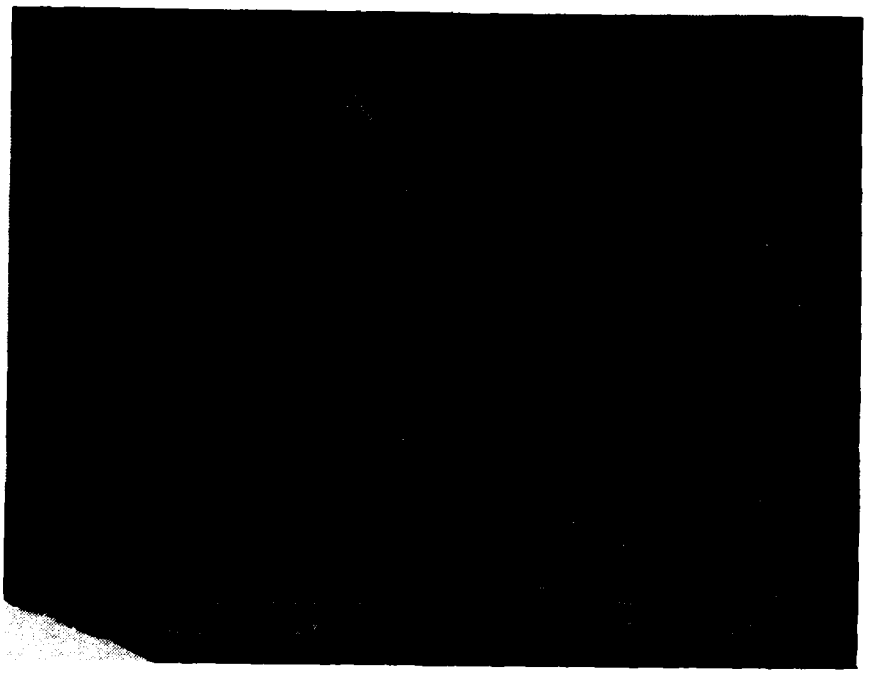

Figure 2.3.11: Fracture Surface of a Melt-Spun HDPE-Based Fiber Prepared From Stearic Acid-Milled Copper Oxide Excess $YBa_2Cu_3O_{7-x}$ Powder, Sintered for Six Passes at 935°C

every sintered melt spun fiber from powder milled with stearic acid. Nothing like this seemed to occur with other $YBa_2Cu_3O_{7-x}$ powders. The hole forms in the early heating stage between 350 and 390°C, before most of the polymer is removed. We suspect that the center hole is associated with the poor wetting between $YBa_2Cu_3O_{7-x}$ and polyethylene in the presence of stearic acid.

2.3.5 Jet-Milled $YBa_2Cu_3O_{7-x}$ Powder

Jet milling has been evaluated as an attractive means of grinding the calcined $YBa_2Cu_3O_{7-x}$. By the end of this quarter, we were nearly finished with a preliminary evaluation of jet milling. The jet-milled powder appears to be equivalent or superior to the ball-milled powder in sintering behavior. It requires no milling aid, which is an advantage since milling aids have been found to have unwelcome effects in fiber spinning and sintering. The jet-milled $YBa_2Cu_3O_{7-x}$ tend to be much more platy, which should lead to grain orientation in the spun fiber. At the end of this quarter, a jet mill was obtained and was being installed. We anticipate that we will shift entirely to jet milled powder by the next quarter.

2.3.6 Continuous Laboratory Scale Sintering Furnace

An appropriate laboratory furnace for sintering ceramic fiber in a continuous mode has been identified. The unit selected is an infrared belt furnace, manufactured by Radiant Technology Corporation (RTC A-306X). This furnace is capable of very rapid heating and cooling rates to precise temperatures with zone controlled atmospheres (limited to contamination of 5 ppm), so that an inert gas can be used in the binder burnout section, an air atmosphere in the sintering zone, followed by an oxygen-rich atmosphere for annealing during

cooling. A belt type furnace is appropriate for fiber sintering. The fibers can be supported by and carried on the belt through the operation without applying tension to the delicate filaments. This unit has adjustable belt speeds such that the total time of the heat treatment can be easily controlled. Current work at CPSS has emphasized multiple zone sintering which requires a furnace with a number of independently controlled zones. This particular model provides three zones.

The RTc A306-X radiant furnace uses quartz lamps as the heat source. As the name implies, the primary mode of heat transfer is radiation. With the view factors appropriate for radiation to a fine filament in a wide radiant cavity, the fibers should be heated very rapidly and uniformly.

Delivery of this unit is expected in the first week of January. Zone sintering and oxygen annealing development will be transferred to this furnace at that time. A green fiber payout spool will be fitted at the entrance to permit continuous sintering. At the exit the continuous sintered filament will be collected in half-meter lengths for evaluation and use in the development of the cladding module. When the cladding module is ready, it will be fitted at the exit to complete the lab scale continuous sintering and cladding facility. This facility is expected to be adequate for manufacturing small quantities of experimental ribbon conductor, and will be a test bed for development of the pilot scale facility in the following year.

2.4 Filament Cladding and Wire Fabrication

2.4.1 Introduction

The major activities in cladding were directed at the mechanical bonding of filaments to copper strips by solder reflow methods. As described

in the previous report, a key feature of this technique is producing $YBa2Cu_3O_{7-x}$ filaments with silver alloy-treated surfaces, which can be bonded to copper with solder. Much attention was devoted to further development of the silver treatment and the co-firing of the $YBa_2Cu_3O_{7-x}$ with the silver alloy. The design concept for the cladding machine was further developed, and components for the surrogate cladding line were obtained or are being evaluated. Alternative cladding methods, involving deposition of metals by electrochemical methods or MOCVD, were explored with external collaborators. Filaments with metal surface deposits were obtained for evaluation during this quarter.

The coating process for green fiber was further developed. With the availability of continuous melt spun green $YBa_2Cu_3O_{7-x}$ fibers, it was possible to develop procedures to silver coat green fiber continuously. Figure 2.4.1 shows a spool of silvered $YBa_2Cu_3O_{7-x}$ green fiber. A series of experiments was directed at defining the best size and shape of the silver particles in the coating. New coating formulations were tested using flaky silver particles which gave superior surface coverage even with rather thin coatings.

It was reported in the last quarterly report that use of silver in the surface treatment puts a limit on the sintering temperature for the cofire operation. Use of silver-palladium alloy in place of silver would stretch the limit higher. Silver-palladium alloys are usually available as a mechanical mixture or a chemically co-precipitated powder. Both of these are not true metallurgical alloys, and may give rise to some local melting of silver rich alloys. Handy & Harman, the suppliers of these powders, was requested to make a true metallurgical alloy of silver and palladium with 15 wt% palladium. They were able to supply such powder with specific surface area 4.21 sq.m./g. True

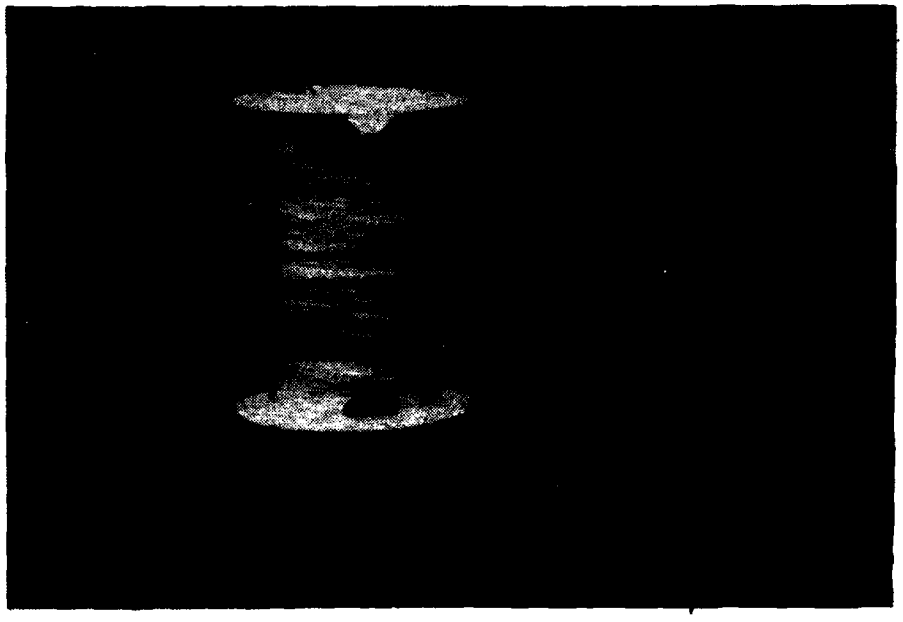

Figure 2.4.1: Spool of Silver Coated $YBa_2Cu_3O_{7-x}$ Green Fiber

alloying was verified using x-ray diffraction. A number of green fibers were coated with this alloy and evaluated for sintering and electrical properties.

2.4.2 Sintering of Coated Fibers

Microstructure - In the last quarter, it was shown that it is possible to cofire a silver coating with $YBa_2Cu_3O_{7-x}$. The resultant coating is very adherent. In this quarter, the green fibers, dry spun and melt spun, were coated with silver dopes made from flaky and equiaxed particles. The heat treatment conditions for sintering and oxygen annealing are given in Table 2.4.1 for the equiaxed and flaky silver particle coatings, and Table 2.4.2 for the Ag-Pd alloy coatings.

Defining the sintering conditions for the silver coated fibers is a complex procedure. The zone sintering process involves rather rapid heating and cooling, with little or no isothermal periods. With bare fibers, sintering temperature is defined by the peak temperature read from a thermocouple travelling with the specimens (see Section 2.3). The actual fiber temperature may be different, as it is determined largely by radiative heat transfer conditions. The silver coated fibers experience a different thermal history than bare fibers exposed to the same peak temperature, largely as a consequence of the slower radiative heat transfer due to the lower emissivity of the silver, compared to $YBa_2Cu_3O_{7-x}$. This introduces considerable ambiguity. "Temperature" reported in this section is again the reading of the travelling thermocouple. It should not be taken as the actual fiber temperature.

A silver coating puts a limit on the time at temperatures higher than 930°C. Therefore silver coating was used on fibers containing excess CuO which could be sintered at a lower temperature. The fiber can pass through six

TABLE 2.4.1

SUPERCONDUCTING PROPERTIES OF COFIRED Ag COATED YBCO FIBERS

SAMPLE	GREEN FIBER	COATING	SINTERING TREATMENT	OXYGEN ANNEAL	MEISSNER EFFECT	ELECTRICAL PROPERTIES
00779	00123 DRY SPUN RP YBCO + CuO	00738/EQ	950°C FOR 15 min	OVERNIGHT, AIR 525°C	NONE	NRT
00785	00123 DRY SPUN RP YBCO + CuO	00738/EQ	500 - 900°C IN AIR, 900 - 950°C IN N_2, 950°C, 15min, N_2	OVERNIGHT, AIR 525°C	NONE	NRT
00794	00123 DRY SPUN RP YBCO + CuO	00738/EQ	920°C, 15min, AIR 950°C, 15min, N_2	OVERNIGHT, AIR 525°C	NONE	NRT
01006	00128A DRY SPUN RP YBCO + CuO	00738/EQ	927°C PEAK, 12 PASSES, 5.5 cm/min	525°C, 30min, O_2	GOOD	J_c = 60 A/sq.cm
01039	00123 DRY SPUN RP YBCO + CuO	00738/EQ	927°C PEAK, 12 PASSES, 5.9 cm/min	525°C, 30min, O_2	GOOD	
01072	00931 DRY SPUN RP YBCO + CuO	00738/EQ	938°C PEAK, 6 PASSES, 5.5 cm/min	475°C, 30min, O_2	GOOD	
02237-1	00940 DRY SPUN RP YBCO + CuO	02236/FQ	933°C PEAK, 4 PASSES, 5.5 cm/min	450°C, 2 HR, O_2	GOOD	
02237-2	3498-84-1 MELT SPUN YBCO + CuO IN HDPE	02236/EQ	933°C PEAK, 4 PASSES, 5.5 cm/min	450°C, 2 HR, O_2	GOOD	

NRT - NO RESISTIVE TRANSITION
EQ - EQUIAXED PARTICLES
FL - FLAKEY PARTICLES

TABLE 2.4.1 (CONTINUED)

SUPERCONDUCTING PROPERTIES OF COFIRED Ag COATED YBCO FIBERS

SAMPLE	GREEN FIBER	COATING	SINTERING TREATMENT	OXYGEN ANNEAL	MEISSNER EFFECT	ELECTRICAL PROPERTIES
01091	00931 DRY SPUN RP YBCO + CuO	FLAKE	935°C PEAK, 4 PASSES 5.5 cm/min	470°C, 1 HR, O_2	GOOD	
02204	00940 DRY SPUN RP YBCO + CuO	FLAKE	935°C PEAK, 4 PASSES 5.5 cm/min	470°C, 1 HR, O_2	NONE	NRT
02205	00940 DRY SPUN RP YBCO + CuO	FLAKE	927°C PEAK, 12 PASSES 5.5 cm/min	470°C, 1 HR, O_2	NONE	NRT
02223	00940 DRY SPUN RP YBCO + CuO	FLAKE	935°C PEAK, 12 PASSES 5.5 cm/min	544°C, 3 HRS, O_2	VERY WEAK	
02245-1	3498-84-1 MELT SPUN YBCO + CuO IN HDPE	FLAKE	933°C PEAK, 4 PASSES 5.5 cm/min	450°C, 8 HRS, O_2	FAIR	
02245-2	00940 DRY SPUN RP YBCO + CuO	FLAKE	933°C PEAK, 4 PASSES 5.5 cm/min	450°C, 8 HRS, O_2	FAIR	

NRT - NO RESISTIVE TRANSITION

TABLE 2.4.2

SUPERCONDUCTING PROPERTIES OF COFIRED Ag/Pd COATED YBCO FIBERS

SAMPLE	GREEN FIBER	COATING	SINTERING TREATMENT	OXYGEN ANNEAL	MEISSNER EFFECT	ELECTRICAL PROPERTIES
01038	00931 DRY SPUN RF YBCO + CuO	00954/CP	960°C PEAK, 8 PASSES 5.4 cm/min	525°C, 30min, O_2	WEAK	
01046- 1,2,3	00931 DRY SPUN RF YBCO + CuO	00954/CP	957°C PEAK, 8 PASSES 5.5 cm/min	525°C, 30min, O_2	WEAK	
01054	00931 DRY SPUN RF YBCO + CuO	00955/CP	960°C, 30min, ATR	480°C, 30min, O_2	NONE	NRT
02232-1	00940 DRY SPUN RF YBCO + CuO	02153/CP	993°C PEAK, 6 PASSES 5.5 cm/min	450°C, 2 HR, O_2	WEAK	
02232-2	00940 DRY SPUN RF YBCO + CuO	02154/PA	933°C PEAK, 6 PASSES 5.5 cm/min	450°C, 2 HR, O_2	WEAK	
02232-3	3498-77-7 7mil diam. MELT SPUN YBCO IN HDPE	02153/CP	993oC PEAK, 6 PASSES 5.5 cm/min	450°C, 2 HR, O_2	WEAK	
02232-4	3498-77-7 7mil diam. MELT SPUN YBCO IN HDPE	02154/PA	993°C PEAK, 6 PASSES 5.5 cm/min	450°C, 2 HR, O_2	WEAK	
02232-3L	3498-77-7 7mil diam. MELT SPUN YBCO IN HDPE	02153/CP	993°C PEAK, 6 PASSES 5.5 cm/min	450°C, 8 HRS, O_2	GOOD	
02232-4L	3498-77-7 7mil diam. MELT SPUN YBCO IN HDPE	02154/PA	993°C PEAK, 6 PASSES 5.5 cm/min	450°C, 8 HRS, O_2	GOOD	

NRT = NO RESISTIVE TRANSITION

CP = COPRECIPITATED SILVER-PALLADIUM POWDER

PA = PREALLOYED SILVER-PALLADIUM POWDER

times through a heated zone with a peak temperature of 935°C before melting due to Ag-Ag_2O eutectic. The coated fibers processed with 935°C peak temperature and four passes develop a more porous microstructure compared to bare fibers. Figure 2.4.2 shows the fracture surfaces of coated and bare filaments. However, such a difference in the microstructure is not apparent for filaments sintered at 930°C peak temperature and 12 passes. Figure 2.4.3 shows the fracture surfaces of Ag-coated and bare filaments sintered at 930°C and 12 passes. The green fiber used for all four sintered filaments was dry spun PMMA based fiber with Rhône-Poulenc $YBa_2Cu_3O_{7-x}$ powder. The coated melt spun filaments also show a porous microstructure. It is clear that the sintering treatment and perhaps the binder burnout schedule will have to be modified in order to get fully dense sintered microstructures from coated fibers.

Melt spun fibers containing pure $YBa_2Cu_3O_{7-x}$ were coated with Ag-Pd slurries made from co-precipitated and pre-alloyed powders. The coatings did not melt at a peak temperature as high as 993°C. The filaments were found to stick to the alumina substrate at a few points. This sticking is perhaps due to local sintering of silver-palladium to the substrate. Preliminary experiments show that there was no major difference in sticking behavior of co-precipitated and pre-alloyed powders. Co-precipitated powders are readily available and are cheaper than the pre-alloyed powders. The question of which Ag-Pd powder is better will be answered during the next quarter.

Filaments coated with equiaxed silver particles show good superconducting properties. However, the filaments coated with flaky silver particles behave differently when given the same 2 hour oxygen annealing treatment as the bare filaments, the coated filaments showed very weak or no Meissner effect. However, when the time for oxygen anneal was increased to 8 hours a fair to good

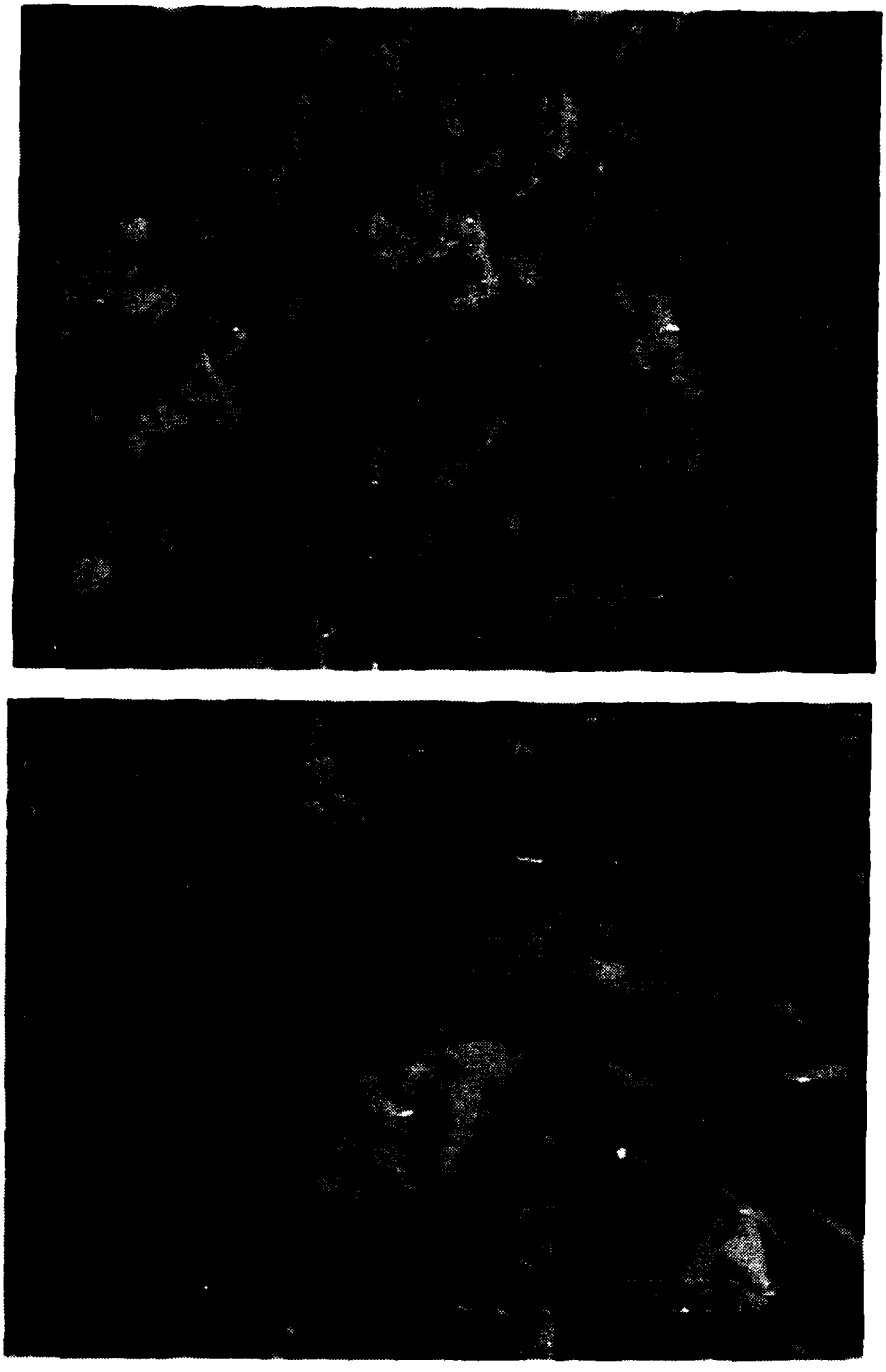

Figure 2.4.2: Fracture Surfaces Filaments Sintered for 12 Passes at 935°C A) Silver Coated B) Bare Fiber

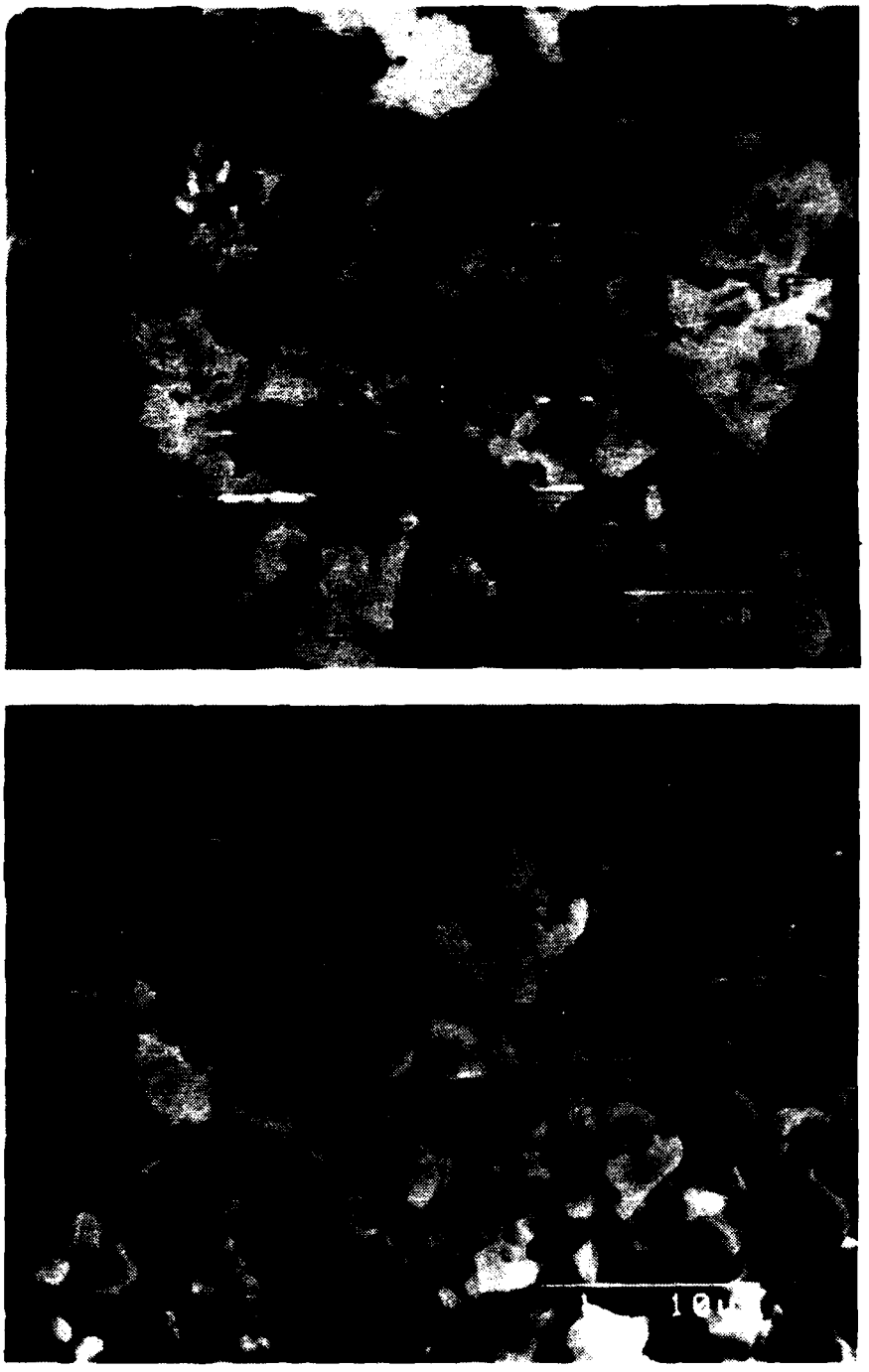

Figure 2.4.3: Fracture Surfaces of Filaments Sintered for 12 Passes at 930°C A) Silver Coated B) Bare Fiber

Meissner effect was observed. This phenomenon can be explained in terms of the morphology the hermiticity of the sintered coating of the silver particles. The equiaxed particle coating sintered to give in a very porous surface which allows easy oxygen diffusion. The flaky particles almost hermetically seal the surface, making oxygen diffusion much slower. Figure 2.4.4 shows the surfaces of these two coatings. The thickness and permeability of the silver coatings need to be tailored to fit the desired oxygen annealing kinetics. For rapid oxygen annealing, a porous silver coating is preferable.

2.4.3 Cladding

During last quarter samples of composite conductors were made by reflowing the solder in a 95% N_2 + 5% H_2 atmosphere. It was noticed that the molten solder would flow away through the open ends of the composite making the wetting of filaments difficult. Composite samples were made with a copper channel which could be sealed after placing the solder strips and the filaments inside it. Figure 2.4.5 shows the cross-section of such a composite. The wetting of the silver clad filament by the solder is very good; no large voids can be seen in the solder. Similar experiments were tried using a N_2 atmosphere instead of forming gas, and similar results were obtained. No oxidation of the solder or copper was observed. However, experiments to reflow in air did not succeed; both solder and the copper oxidized.

Cladding unit for surrogate fiber - The copper channel required for the cladding line is not available commercially. It is best to form it in line from the copper foil using a rolling mill. The copper foil required for the cladding line has been purchased. Oxygen free C10200 copper with soft anneal was chosen since that grade of copper does not undergo embrittlement after heat

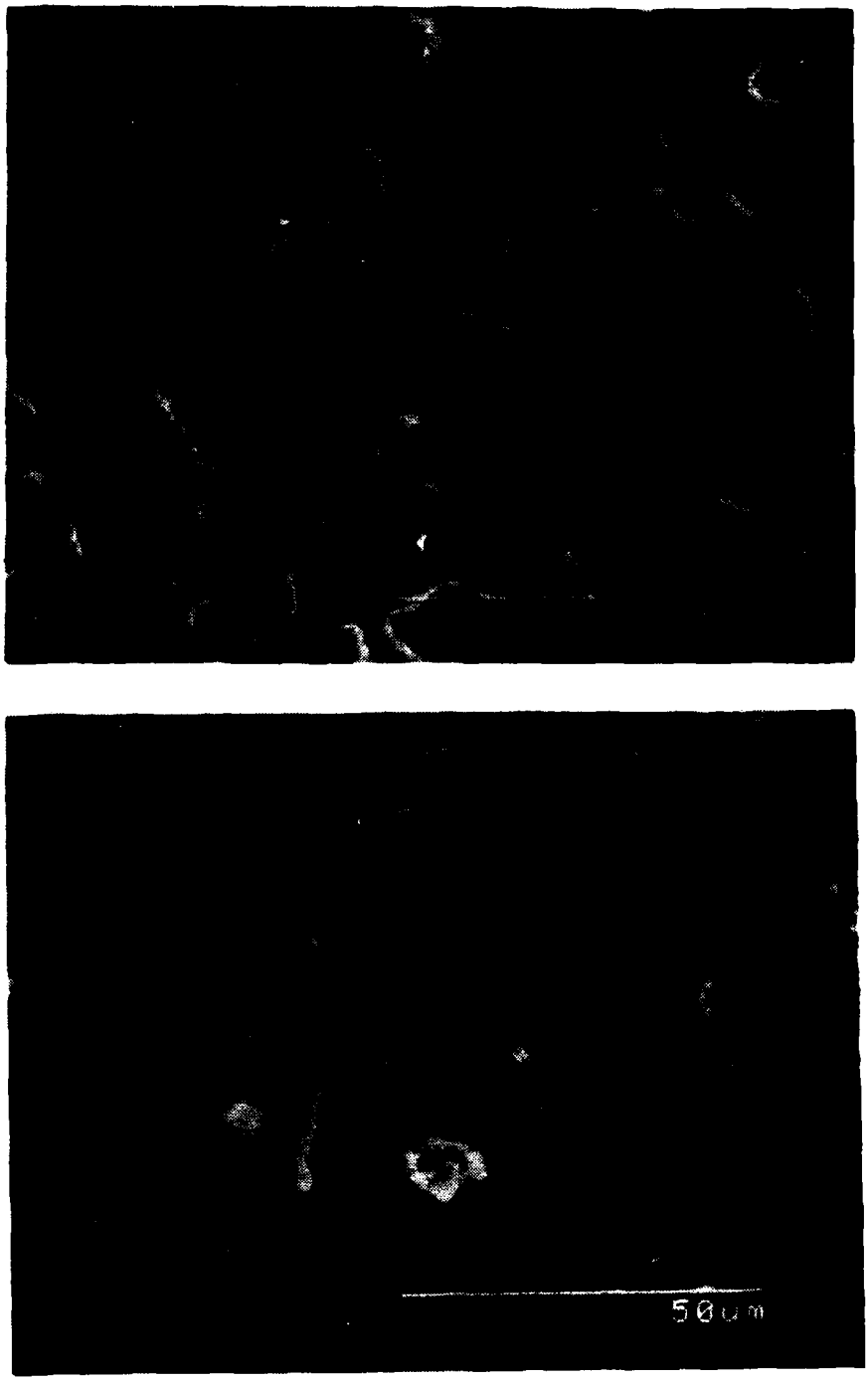

Figure 2.4.4: Comparison of the Ag Coatings From Equiaxed (above) and Flakey Particles (below)

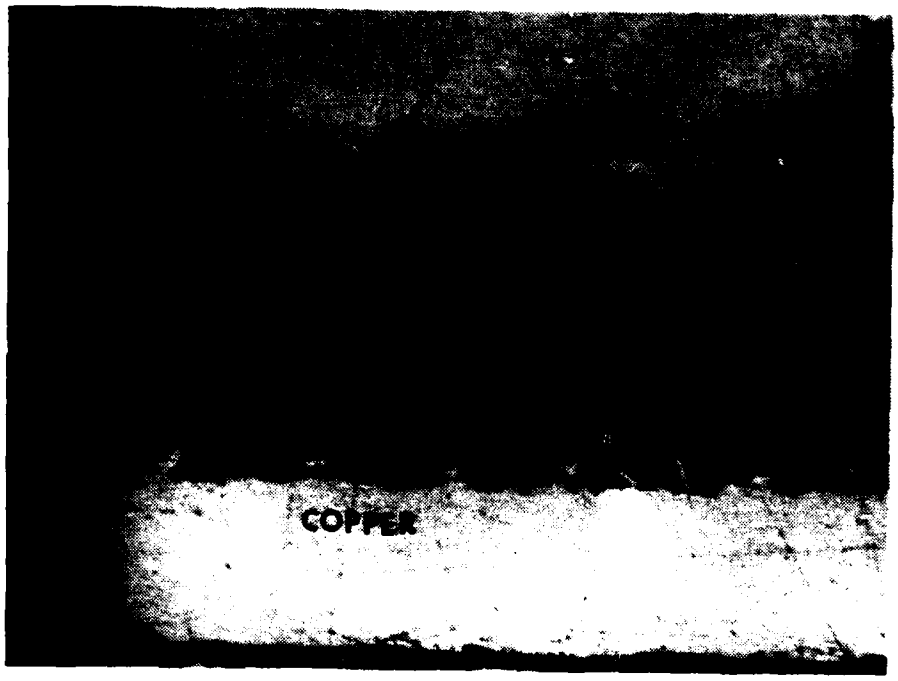

Figure 2.4.5: Cross Section of Prototype Composite Fabricated With the Solder Reflow Method

treatment above 375°C. Solder overlayed copper strip has been ordered with expected delivery in mid-February.

There are two possibilities for constructing the reflow unit that will be part of this cladding unit. It can either be constructed from scratch using heating elements, temperature controllers, etc., or it can be constructed through modification of a furnace. Hot platen reflow furnaces are especially attractive from the point of view of cost and time. Two such furnaces, MCT/Browne 6820™ and Falcon Five from Sikama, were evaluated. Both of the furnaces have a nitrogen hood for protection from oxidation. The experiment consisted of sending a composite made of copper and solder through the furnace and watching the reflow. The belt speed in the MCT/Browne furnace could be slowed down to 5 cm/min., the desired speed for cladding operation, and the solder did reflow. The nitrogen hood was not adequate, resulting in the oxidation of the solder and the copper. The Sikama furnace was not able to reflow the solder at its lowest speed, 15 cm/min. The manufacturer is confident that at slower speeds, reflow should be possible. Further experiments are planned.

2.4.4 MOCVD of aluminum on superconducting filaments

Dr. Ward Stevens of Advanced Technology Materials, New Milford, CT, undertook an exploratory project to produce aluminum claddings on sintered $YBa_2Cu_3O_{7-x}$ filaments using metallorganic chemical vapor deposition (MOCVD). This section is based on a report prepared by Dr. Stevens. The superconducting filaments were sintered from dry spun fibers made from Rhône-Poulenc powders provided by CPSS. The electrical characterization was performed at CPSS. The primary objective was to obtain aluminum coatings about 1 mil thick in several

minutes residence time, without degrading the superconducting properties of the $YBa_2Cu_3O_{7-x}$. Deposition temperatures were to be kept as low as practical.

Two aluminum MOCVD reagents were utilized for deposition, triisobutylaluminum and triethylaluminum, with the bulk of the work employing the former. Several modifications of the MOCVD process were examined including hot-wall and cold-wall deposition, as well as novel methods proprietary to Advanced Technology Materials. With limited experimentation in each method, cold-wall reactors yielded the best coating, a smooth, dense conformal coating. Other techniques produced coatings that had nodular or sooty morphologies. Observations of cold wall reactor deposits suggest that 1 micron thick coatings can be grown within minutes. The aim of the ATM study was to determine the feasibility of depositing aluminum via MOCVD onto short lengths of superconducting filaments by various methods and to determine the viability of this approach.

The majority of the investigations utilized TIBAL (triisobutylaluminum) as the aluminum source reagent. This decision was based on cost, deposition experience, temperature of deposition, and pyrophoricity. In quantity, TIBAL is a low cost chemical. In a quantity of 0.2 gallons the cost is $13/pound, while in tank car quantities, the cost is about $2/pound. On a metals basis, these costs are $100 and $15/pound of aluminum, respectively. Triisobutylaluminum has been recognized as a source reagent for aluminum deposition since the early 1960's. Several patents and technical papers describe the CVD process and its use in structural, wear, and microelectronic applications. Although there are a number of modifications to the process, including low pressure deposition, "catalysts" gases, and carrier gases, deposition is carried out at temperatures between 220 and 270°C in an inert atmosphere.

Isobutylene is used as a carrier to avoid the decomposition of the TIBAL into diisobutylaluminum hydride:

$$[(CH_3)_2CH\text{-}CH_2]_3Al = [(CH_3)_2CH\text{-}CH_2]_3AlH + (CH_3)_2C = CH_2$$

This reaction occurs at temperatures between 100 and 150°C, but is reversible in the presence of excess isobutylene. At about 220°C diisobutylaluminum hydride thermally decomposes to form aluminum:

$$[(CH_3)_2CH\text{-}CH_2]_3Al \rightarrow Al + 3/2\ H_2 + 2[(CH_3)_2C = CH_2]$$

Hot-wall depositions of aluminum were carried out in the reactor consisting of a Pyrex™ glass tube with O-ring sealing end caps which permitted the introduction and exhaust of process gases. Purified (mol-sieves/Ridox™) nitrogen was used to purge the reactor prior to the introduction of TIBAL. To avoid the premature decomposition of the TIBAL into diisobutylaluminum hydride, isobutylene was used as the carrier gas to transport the aluminum source into the reactor. Nitrogen was used as a diluent. To provide for a sufficient concentration of the reagent in the gas stream, the reagent, transfer tubing, and reactor were held at approximately 100 and 70°C in two separate experiments. At these temperatures TIBAL has a vapor pressure of about 15 and 4 torr, respectively. Various literature references report the optimum deposition temperature for the substrate for TIBAL to be between 220 and 270°C. Depositions were carried out at about 250°C.

A quartz lamp was used to heat a graphite susceptor in the cold wall reactor in a set-up nearly identical to the hot-wall reactor with the exception of the heat source.

Deposition of aluminum in a hot-wall reactor is mechanically the easiest method for obtaining aluminum films. However, at atmospheric pressure this technique suffers from problems of gas phase nucleation and soot formation.

Small aluminum particles formed in the gas phase result in nodular or sooty growth. Reducing the concentration of organometallic or reducing the pressure of deposition are means of controlling the amount of gas phase nucleation.

Run times for the hot-wall depositions were two hours in both of the above examples. In the reduced concentration run a glass fiber was included along with the superconducting filaments. As seen in Figure 2.4.6, the growth morphology is much more coarse, perhaps an indication of fewer nucleation sites during the initial stages of growth. The deposit thickness on the glass filament is approximately 40 microns while the deposit on the superconductors was on the average 20 microns. The differences in thickness may be due to differences in the growth modes and their relative densities.

By just heating the substrate, as in a cold-wall reactor, gas phase nucleation can also be controlled. Reagent enters the deposition chamber and composes directly on the substrate. In this fashion, very smooth coatings of aluminum were deposited on the superconducting filaments (Figure 2.4.7). However, the thickness of these deposits was limited to about 1 micron. Observation of the growing surface suggested that these films grew within about 20 minutes, after which no additional growth appeared to occur. These results require verification by parametric experiment. If this were the case, nucleation aids might be employed to sustain reasonable growth rates.

In conclusion, conformal, dense aluminum deposits could be applied to superconducting filaments by MOCVD using triisobutylaluminum via hot-wall and cold-wall deposition schemes. Thin, one micron, hermetic coatings could be applied within minutes and may be useful as a starting point for alternate metal deposition processes, CVD or others.

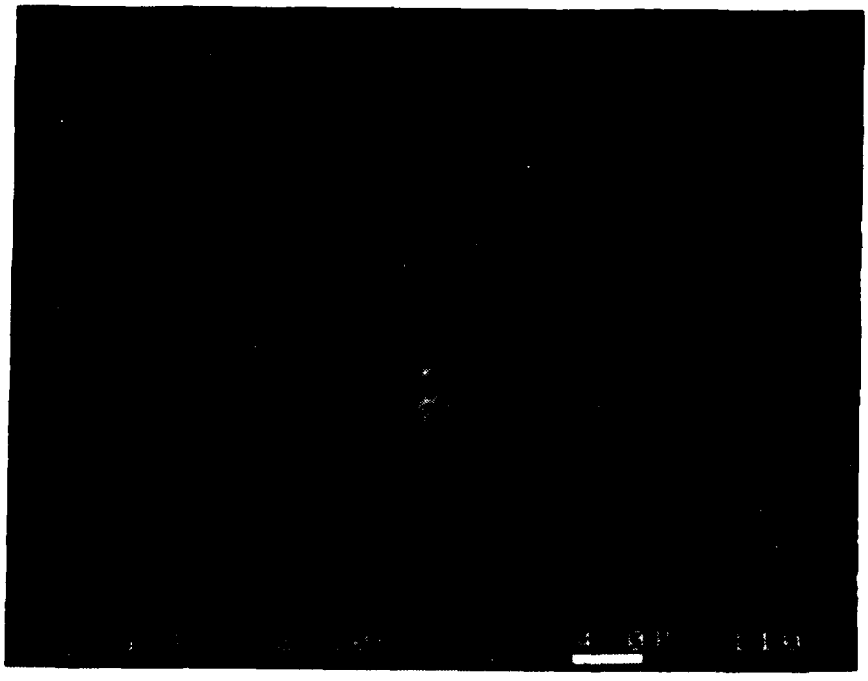

Figure 2.4.6: Morphology of MOCVD Aluminum Deposit on $YBa_2Cu_3O_{7-x}$ Filament Produced at ATM in a Hot Wall Reactor

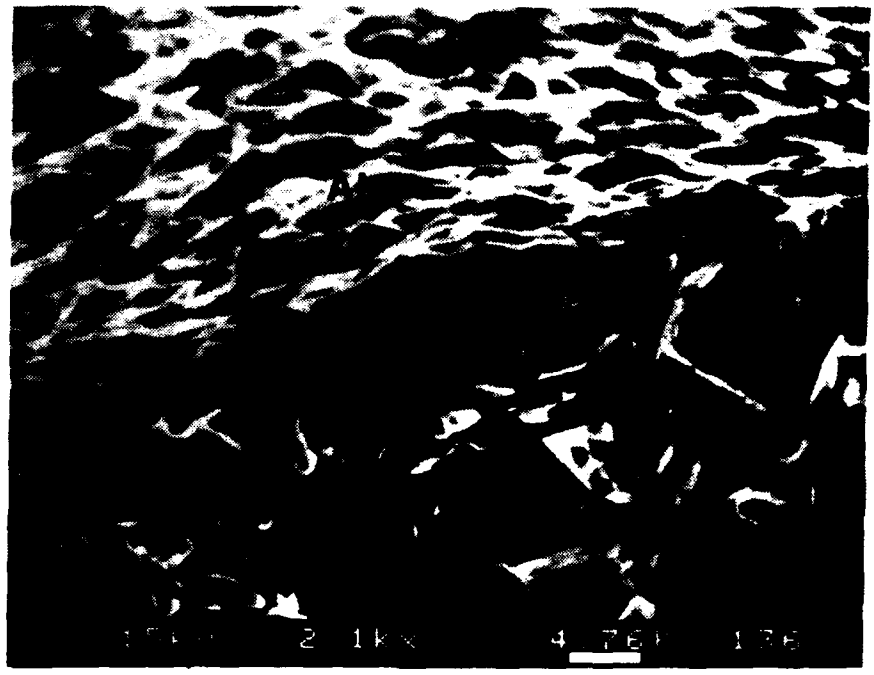

Figure 2.4.7: MOCVD Aluminum Deposit on $YBa_2Cu_3O_{7-x}$ Filament Produced at ATM in a Cold Wall Reactor

Only the filament processed in the cold-wall reactor exhibited Meissner effect. An attempt was made to measure the transition temperature of this filament. However, the measuring current passed through the metal only and no transition was observed. This could be due to an insulating layer of alumina at the filament-aluminum interface. More details are given in the section on electromagnetic characteristics.

2.4.5 The electrodeposition of an aluminum-manganese metallic glass from molten salts

This work was performed by Dr. Gery Stafford of the Institute for Materials Science and Engineering at the National Institute of Standards and Technology, as part of the collaboration with Dr. David Lashmore. The superconducting filaments were sintered dry spun fibers made from Rhône-Poulenc powder at CPS Superconductor Corporation. This section of the report is prepared from the report written by Dr. Stafford.

Aluminum and some of its alloys can be electrodeposited from molten salt electrolytes. The electroactive species in eutectic (2:1 mole ratio) $AlCl_3$:NaCl melts is $Al_2Cl_7^-$ and is present at concentrations approaching 3.5 M. Its reaction occurs by the following

$$4\ Al_2Cl_7^- + 3\ e^- \rightarrow Al + 7\ AlCl_4^-$$

The reduction of $AlCl_4^-$ occurs at potentials more negative than required for $Al_2Cl_7^-$ reduction, and becomes prominent as the acidity ($AlCl_3$ content) of the melt is reduced. The kinetics for the aluminum deposition reaction are quite fast, and one has little electrochemical control over deposit morphology which is generally nodular and quite often dendritic. Efforts to obtain bright aluminum deposits from chloroaluminate electrolytes have included studies of

deposition onto various substrates, use of AC superposition and the addition of water, organics and metal chlorides. The most remarkable improvement has been seen with the addition of small amounts of $MnCl_2$. In this study aluminum deposit was attempted onto superconducting filaments from a $MnCl_2$ doped $2AlCl_3$:NaCl electrolyte.

All melts were at the eutectic composition, 2:1 mole ratio $AlCl_3$:NaCl. The powders were thoroughly mixed in a dry box before being transferred to the cell. The temperature of the mixture was increased to 150°C and the resultant melt was pre-electrolyzed for 48 hours using a platinum screen working electrode held at a potential of +0.01 volt with respect to the aluminum wire in the same electrolyte. The desired amount of $MnCl_2$ was then added. The melt temperature for all experiments was 175°C. Potential control was maintained with a PAR Model 363 Potentiostat/Galvanostat and a PAR Model 175 Universal Programmer. The counter and reference electrodes were 2 mm aluminum wire.

The $YBa_2Cu_3O_{7-x}$ filament was lowered into the molten salt electrolyte while at a potential of +0.1 volt with respect to an Al wire. This cathodically protects the filament until it reaches thermal equilibrium. At this potential, a cathodic current of 20-40 μA was generally observed. This current level is very low and indicates that the system is relatively stable. A rest potential of +1.856 v vs. Al was observed, indicating that the $YBa_2Cu_3O_{7-x}$ is quite resistant to anodic reactions in this electrolyte.

Deposits were obtained using DC as well as pulsed deposition. The best deposits were obtained using a pulsed deposition (10 msec - 3 v/Al; 110 msec - 1 v/Al) and with 1.9 wt% $MnCl_2$. Figure 2.4.8 shows the structure of the deposit. Estimated thickness of this deposit is 4.7 μm and the estimated composition is 31 wt% Mn (from standardless semi-quantitative analysis in EDS)

Figure 2.4.8: Electrodeposited Aluminum-Manganese Alloy on a $YBa_2Cu_3O_{7-x}$ Filament Produced at NIST

and rest aluminum. Based on the estimated deposit concentration, it should be entirely amorphous.

The aluminum plated filaments gave indications of a strong Meissner effect by the "float" method used at CPSS. Actual magnetic measurements of the Meissner fraction are being done at NIST. Unfortunately, these wires had no resistive transition. Apparently the aluminum coating is separated from the superconducting core by a resistive barrier. This suggests that aluminum alloys are too reactive to directly deposit on $YBa_2Cu_3O_{7-x}$.

2.4.6 Electrodes Deposition from Aqueous Solution

Professor Stanley Bruckenstein of the State University of New York-Buffalo succeeded in depositing copper directly onto some of our sintered $YBa_2Cu_3O_{7-x}$ filaments with an aqueous electroless method. Unfortunately, the filaments were no longer superconducting. This work is in a very preliminary stage, and is being pursued further.

2.5 Electric and Magnetic Characteristics

This section describes the changes made in techniques for electrical and magnetic characterization as well as the characteristics of a number of different filaments. The method of making electrical contact to the filament was improved, as was the accuracy and responsiveness of the Jc and T_c testing routines. Preliminary results on attempts to clad $YBa2Cu_3O_{7-x}$ filaments with CVD-aluminum and electrolytic copper resulted in no measurable T_c, due either to degradation of the filament or the presence of an electrical barrier between the filament and the cladding. Efforts to clad filaments using the silver coated fiber technique were more successful. Bare filaments melt spun from CPSS powder

were also measured, showing higher Tc and lower normal state resistivity than filaments dry spun from Rhône-Poulenc powder. Jc tests show roughly comparable results for old and new filaments.

2.5.1 Contact resistance

A study of the effect of varying contact material and processing technique on the surface resistance, ρ ■($\Omega \bullet cm^2$), of electrical contacts[7] to bare $YBa2Cu_3O_{7-x}$ filaments was initiated. The purpose was to reduce contact resistance sufficiently to allow higher current to be passed through the filaments without inducing Joule heating at the contact pads. Tests were performed on filaments which were dry spun from Rhône-Poulenc $YBa_2Cu_3O_{7-x}$ powder. Filaments were stored in a vacuum desiccator immediately after sintering. Electrical contact to the filaments was made by sputtering a silver contact pad onto the filament, connecting a wire to the pad using silver epoxy, and annealing the filaments for two hours in oxygen at 450°C followed by a furnace cool. Silver epoxy was chosen because it is applied at low temperature, contains silver, has a high mechanical integrity, and makes a reliably low resistance connection to silver coated copper wire. A variety of silver inks, paints, pastes, and epoxies were tested for their ability to make good contact to silver coated copper wire, prior to the selection of silver epoxy. Annealing the electroded filament in oxygen serves to further intercalate oxygen into the specimen and to improve the contract between the silver electrode and the filament, presumably by diffusion

---

[7]Contact resistivities are the product of contact resistance and contact area. Contact resistivities less than 10 micro ohm-cm^2 are needed for transport of the critical current measurements, according to J.W. Ekin, et al., Proceedings of the International Meeting on Advanced Materials, Vol. 6, Materials Research Society, (1988).

of Ag into the surface.

Surface resistance was measured by cooling the superconducting filament to 77K, measuring the two-point resistance across the contact/filament/-contact system, and dividing by two. The contact area was taken to be the area of the sputtered silver pad ($0.12cm^2$). Table 2.5.1 shows the surface resistance of a number of identically processed filaments. The values scatter around 10 x 10^{-5} $\Omega \bullet cm^2$, which are low enough for reliable measurements. The variance in the contact resistance is assumed to be due to differences in the surface microstructures of the filaments. These values represent a 2-3 order of magnitude improvement over the contact resistance of similar samples which had silver epoxy applied after the oxygen anneal. It was not possible to directly measure the effect of the oxygen anneal on these filaments since the filaments were not superconducting prior to annealing. Work is underway to measure the effect by annealing a set of filaments, making electrical contact, measuring contact resistance, annealing again, and measuring contact resistance again. This same technique was used to make contact to filaments melt spun from phase-pure CPSS powder, resulting in a less dramatic improvement in contact resistance. Work is underway to optimize the technique, particularly the oxygen anneal, for these filaments.

2.5.2 Critical Temperature Measurement Technique

The computerized data acquisition system described in the first quarterly report is now in operation and undergoing continual refinement and development. The instrumentation is as previously described but the algorithms for data acquisition have been modified as various shortcomings in the original

Table 2.5.1

CONTACT RESISTANCE OF $YBa_2Cu_3O_{7-x}$ FILAMENTS
USING EPO-TEK H20S SILVER EPOXY

Filament	Contact Resistance ($\Omega \cdot cm^2$)
019065C	2.0×10^{-5}
019065B1	26.9×10^{-5}
019065B2	22.9×10^{-5}
019065G	8.4×10^{-5}

software have been exposed. Initially the excitation from the current source was to have been a 5 Hz 10mA square wave. This has been modified to a 1.12 Hz 1.0 mA square wave. The frequency was reduced by lengthening the plateaus of the waveform to 440 ms each. This was done to permit an averaging routine to be inserted into the T_c algorithm. Each data point consists of a temperature read immediately prior to acquiring the filament voltage and the filament voltage, which is the sum of the averages of three positive and three negative voltage readings, divided by two. Data can be acquired as frequently as one data point every 3.3 seconds. Temperature control is sufficient to permit very slow ramping of temperature over this time period. The amplitude of the source current was reduced in order to insure that the measured voltage is the result of a superconducting/normal phase transformation and not of flux flow. This is at the expense of an order of magnitude in resistivity detectability. For a typical CPSS filament we can be certain that what we are calling zero resistivity is no more than $10^{-7}\mu\Omega$-cm. As the need to avoid flux flow becomes less stringent, we can easily enhance sensitivity to resistivity.

Figure 2.5.1 shows the resistive transition for sample 01153B2, a filament produced from Rhône-Poulenc powder in August 1988. This transition was the first one monitored using the algorithm described above. Temperature control and measurement were achieved using our original technique, that is the temperature was monitored with a 0.005" type K thermocouple placed adjacent to the filament and the filament was immersed in liquid nitrogen then fixed at a point immediately above the liquid surface. One cannot be certain that the temperatures recorded using this method accurately reflect the filament temperature, thus comment on the measured Tc until more reliable data is

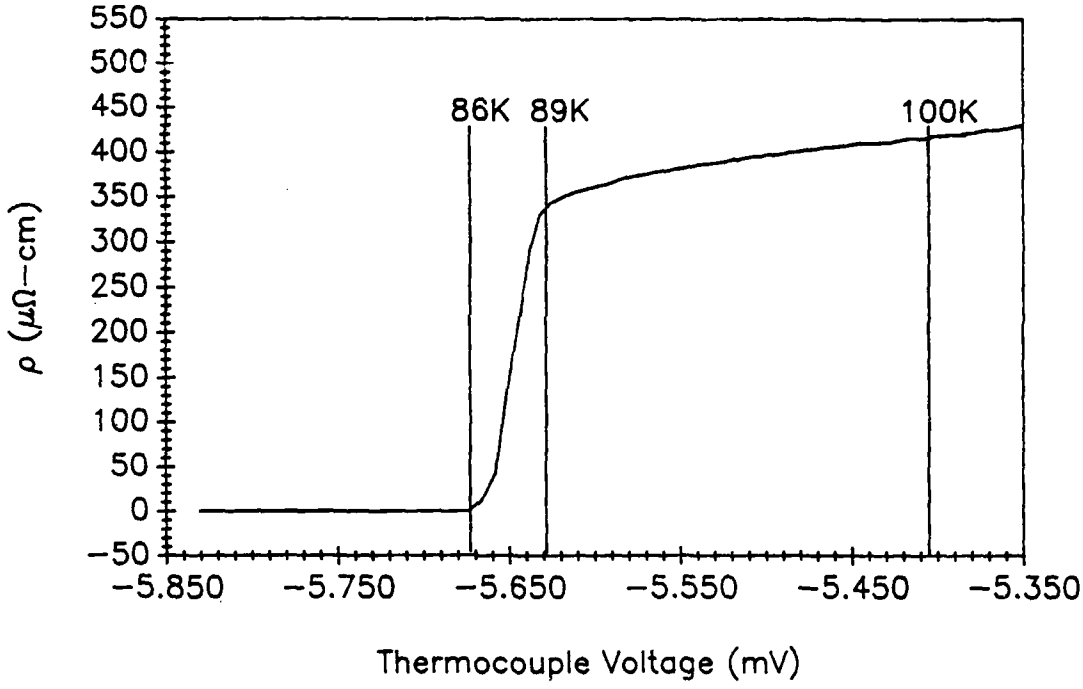

Figure 2.5.1: Resistive Transition of Filament 01153B2. Temperature Monitored With a Thermocouple, Transport Voltage Separated From Thermal Voltage Using Square Wave Algorithm.

presented later in this discussion. The important point to note is that the algorithm has successfully eliminated thermal voltages.

This same filament was tested again using the liquid nitrogen cryostat and Lake Shore 805 temperature controller with a silicon diode thermometer. This data is shown in Figure 2.5.2. The onset of resistance occurs at 85.7 K, in essential agreement with Figure 2.5.1. The Tc for this filament is lower than had been estimated previously (90 K) using data collected on a two-channel chart recorder from a thermocouple and a Keithley 181 nanovoltmeter. The probable causes of the error are the slow response of the 181 voltmeter and the difficulty in collecting one data pair from two separate chart recorder traces. This lower transition temperature will have a significant effect on the Jc of filaments operating at 77 K, and suggests that close attention must be paid to Tc data when interpreting variations in Jc for different processing conditions. The presence of the anomalous 'humps' in the normal state portion of Figure 2.5.2 is the result of a thermal lag between the filament under test and the thermometer. The temperature in the cryostat sample chamber is controlled by heating the nitrogen vapor as it passes into the chamber from the liquid nitrogen bath in the cryostat. The thermal lag is most pronounced when the rate at which this vapor is heated is greatest. This occurs when the temperature set point has just been reset to a new value. These set points are 90 K, 95 K, 110 K, and 120 K. The correlation between the anomalies in the data and these set points is quite close. There are two choices available for eliminating this artifact. One is to insert a large number of setpoints into the scanning routine via the computer software, the other approach is to eliminate the source of the thermal lag. The second approach provides a much more satisfactory resolution to the problem and was the method selected. The

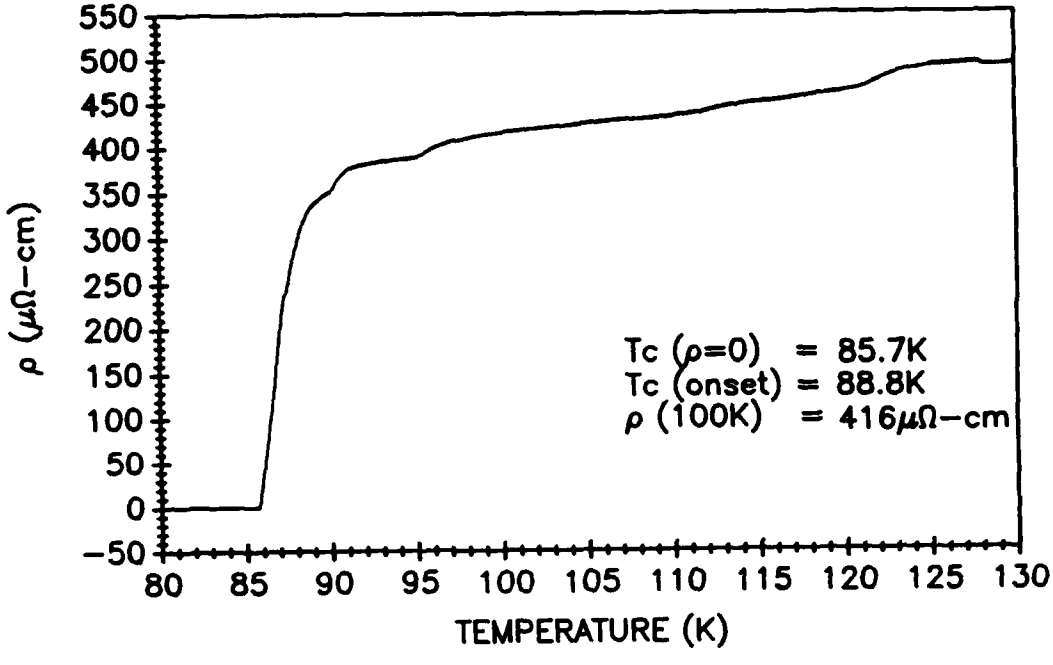

Figure 2.5.2: Resistive Transition for Filament 01153B2. Temperature Controlled Using Liquid Nitrogen Cryostat and Monitored With a Silicon Diode Thermometer

source of the thermal lag is the sample holder itself. Samples are mounted onto a 2" wide printed circuit card which is in turn thermally anchored to a 0.75" wide copper finger on the sample holder. The thermometer is also thermally anchored to the copper finger. Because the PC card is a thermal insulator, the filament is able to respond to changes in the temperature of the nitrogen vapor more quickly than the thermometer, and so the resistivity of the filament corresponds to a temperature higher than that measured by the thermometer. Placing the thermometer on the PC card reduced the thermal lag, but did not completely eliminate it. The presence of the copper finger is also the source of another problem with the Tc routine; i.e, the inordinately long amount of time required to heat the sample from 77 K to 300 K, typically about 4½ hours. The test duration was reduced to 1 hour by shortening the temperature scan to 77 K to 130 K and further reduced to 40 minutes by replacing the copper finger with a polyethylene one. Figure 2.5.3 shows two traces taken on filament 019092, a filament made during this quarter using CPSS phase pure powder. The copper finger was used for the solid curve, the polyethylene finger for the dashed curve. Though still present, the effect of the thermal lag is significantly reduced by using the polyethylene sample holder. During the next quarter the software will be modified to increase the number of temperature set points and thereby smooth out the nitrogen vapor heating profile. In addition, the effective scan time will be halved by further modifying the software to permit testing of two filaments simultaneously.

2.5.3 Critical Current Measurement Technique

All Jc measurements described in this report were taken at 77 K in self field, using the computer controlled data acquisition system. The testing

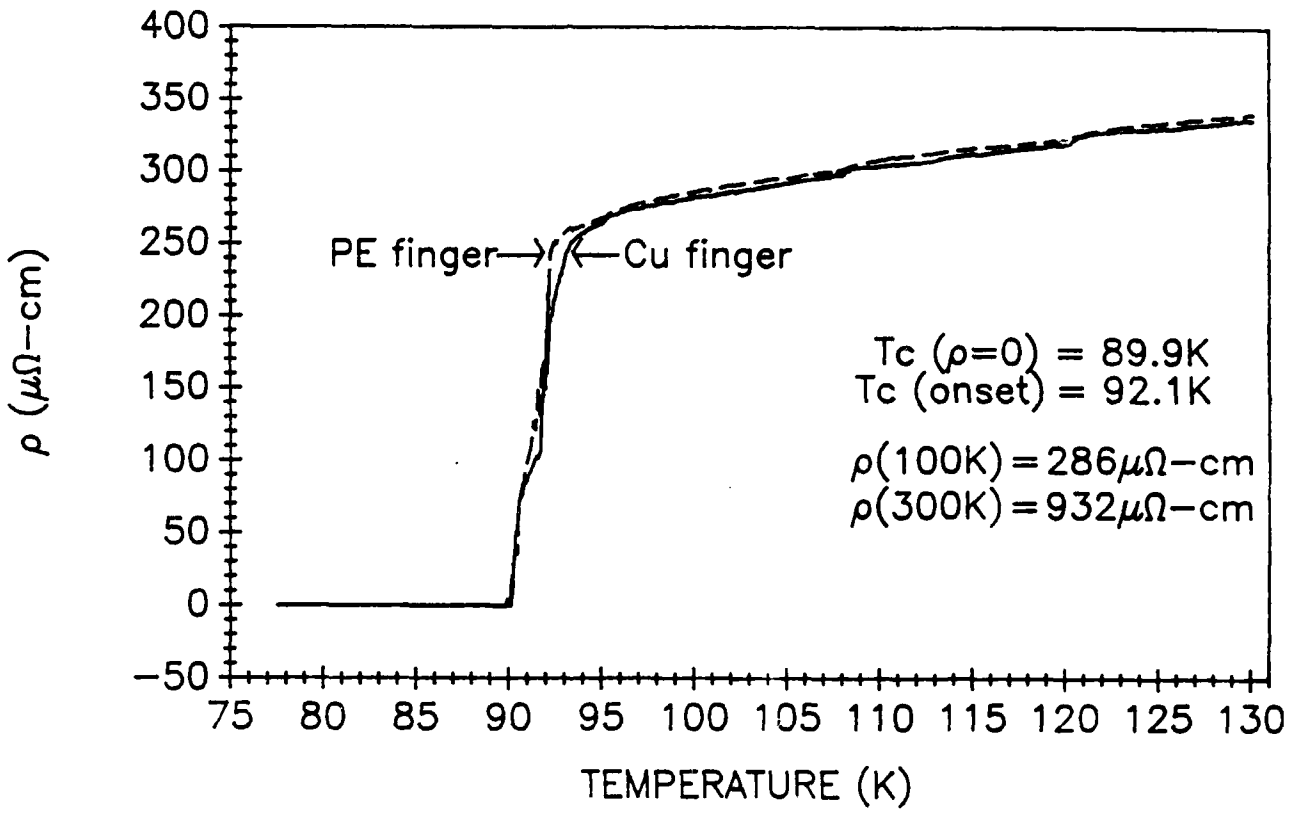

Figure 2.5.3: Resistive Transition Showing the Effect of Replacing the Copper Sample Holder With a Polyethylene Holder.

routine scans a 100 milliampere range of current in 1.0 milliamp steps to establish Jc. The correct range over which to test is determined by passing current through the sample until at least a 1.0 μV response is generated. The current is incremented in 25 mA steps until this response is detected. At this point the search is ended and the current source is programmed to generate a 100 mA scan of current centered about the point where the response was detected. Once the correct range for the test has been set up, the current source and the voltmeter are triggered to begin data acquisition. One voltage reading is collected in the middle of each current step, with the data being stored in the internal buffer of the voltmeter. This technique should allow data to be collected at 9 readings per second, the maximum reading rate of the voltmeter. It turns out that the maximum reading rate is somewhat less than that. Figure 2.5.4 shows data collected on sample 01153A2, a filament dry spun from Rhône-Poulenc powder. Four different scans were taken at four different reading rates. It is clear that a 0.4-second reading rate provides erroneous data, presumably due to the manner in which the voltmeter responds to a small voltage step.

Another important point to note about the data in Figure 2.5.4 is the step like nature of the V-I curve. The reason for these steps, which are several data points wide, is that the Keithley 196 meter automatically turns on an internal running average filter whenever the most sensitive voltage scale is used. This filter can only be disabled, but unfortunately an unacceptably noisy signal resulted. To solve this problem a short averaging routine was inserted into the software. The advantage of this averaging routine over the internal filter is that now it calculates a discreet average for readings within each individual current step. The number of readings required to gather data in this manner exceeds the capacity of the voltmeter's internal buffer, requiring

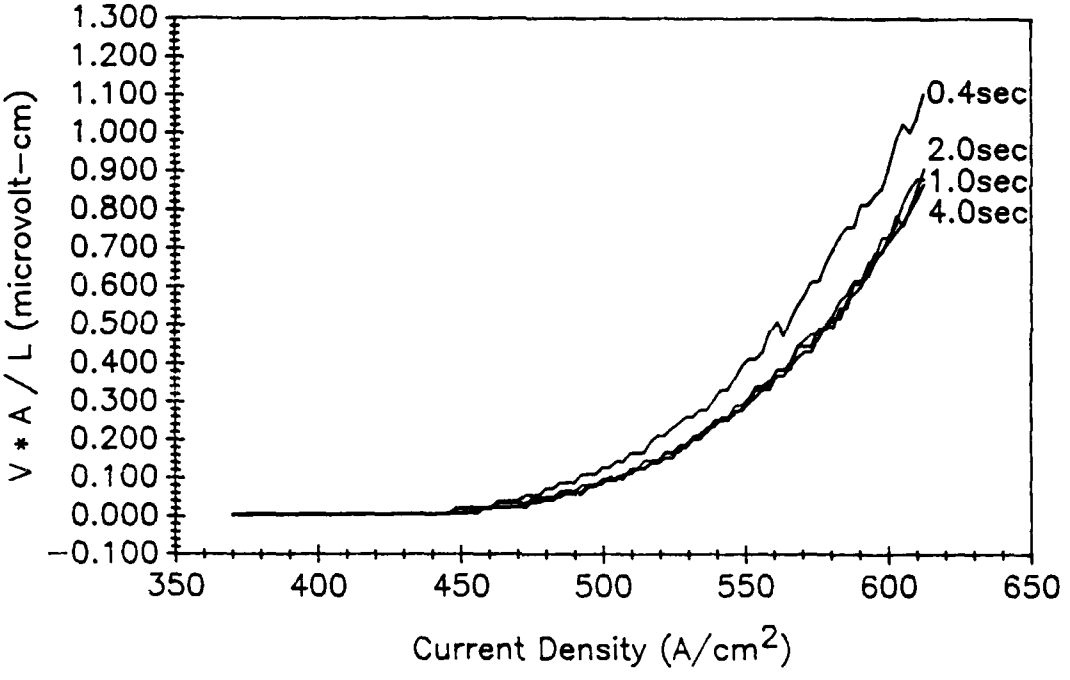

Figure 2.5.4: V-I Characteristics of Filament 01153A2 Taken Consecutively at Various Reading Rates. Jc is 50 Amps/cm^2.

readings to be collected directly from the voltmeter over the IEEE bus at the maximum rate of the bus line. Consequently, the current step dwell time must then be set to match the product of this new reading rate and the number of readings taken at each current step. This dwell time was empirically determined using the internal timer of the IEEE controller software. To guard against variations in the reading rate resulting in a particular voltage reading being assigned to the wrong current value, the first and last value of each group of voltages are discarded. At present 10 voltage readings per current step are taken, resulting in each data point being the average of 8 values. The appropriate current step dwell time for this setup turns out to be 2.105 seconds. Since the Keithley 228 current source cannot accept 1 msec resolution for inputs larger than 1.010 seconds, it was necessary to alternate dwell time between 2.10 and 2.11 seconds. Figure 2.5.5 shows the V-I characteristic for sample 019092, a filament melt spun from CPSS phase-pure powder. The two traces were taken consecutively on the same filament to test repeatability. The step like nature of Figure 2.5.4 is completely absent, and the data appears reasonably quiet. A closer examination of the data, however, reveals that a problem still exists. Figure 2.5.6 contains the same data as Figure 2.5.5, but is plotted on a log scale. It is clear from this plot that the noise level does interfere with the data at levels near the CPSS Jc criterion ($10^{-3}\mu$V-cm). In fact, one of the traces flattens out at a level exceeding the Jc criterion. This suggests that the zeroing routine which sets the baseline for the data at the beginning of data acquisition needs to average over a longer period of time. Since the time required to perform the Jc test is currently only 3½ minutes, it seems reasonable to double the number of readings per data point in an effort to quiet the data further. This would result in a total run time of 6.3 minutes.

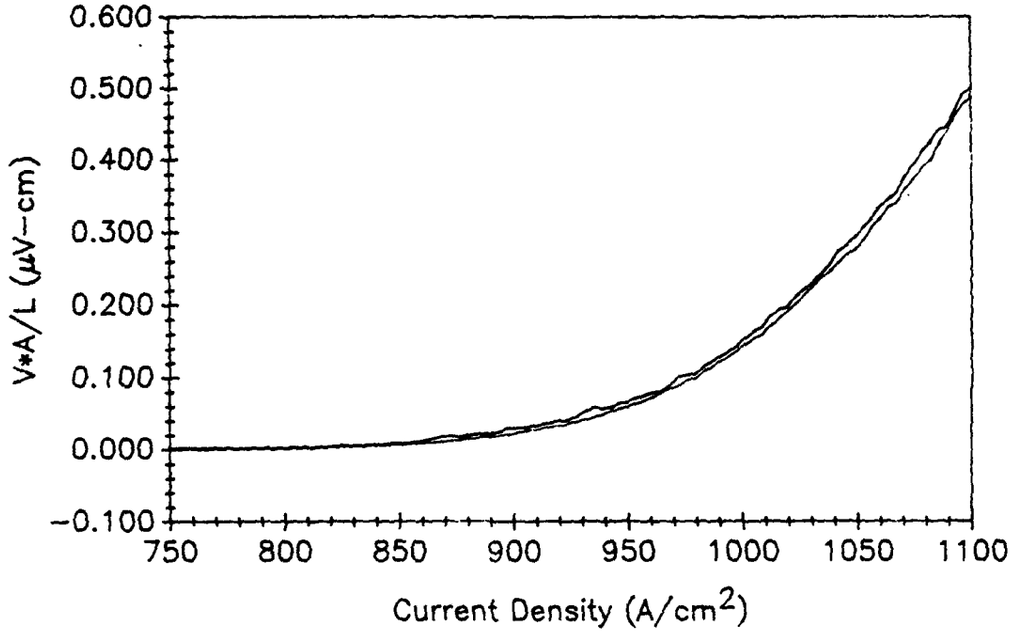

Figure 2.5.5: Two V-I Characteristics for Filament 019092, Taken Consecutively, Showing the Effect of Disabling the Voltmeter's Internal Filter and the Reproducibility of the Testing Routine. Jc is 800 Amps/cm^2.

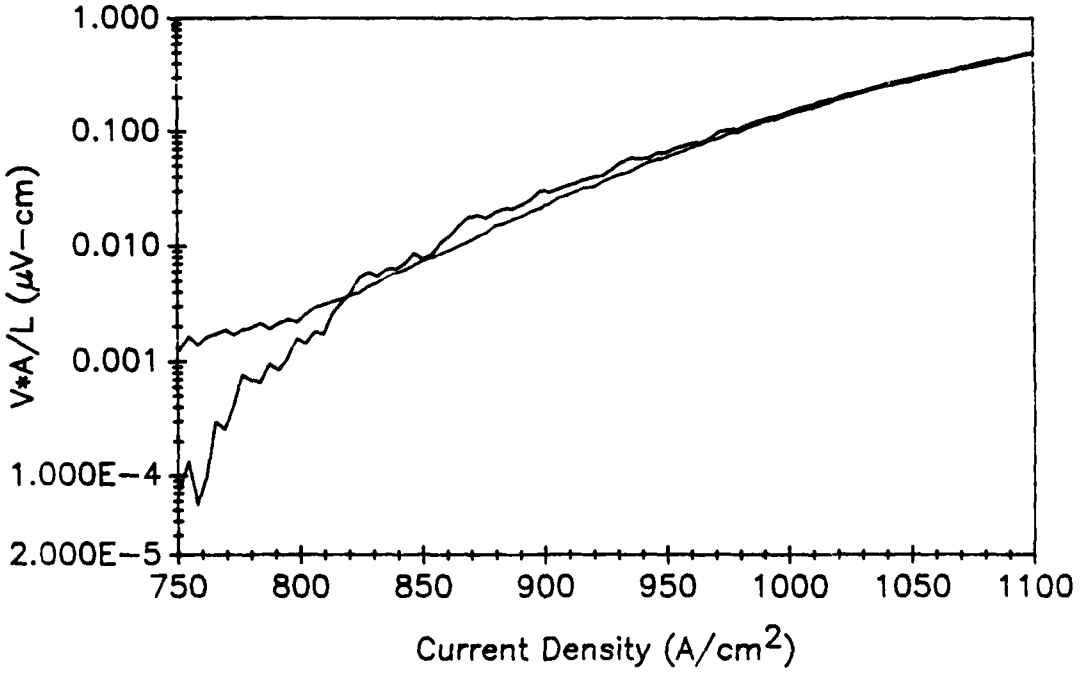

Figure 2.5.6: Two Log V-I Characteristics of Filament 019092, Taken Consecutively, Showing the Effect of Signal Noise on Data in the Vicinity of the Jc Criterion.

It is appropriate at this point to discuss the manner in which the current density data is presented. A simple reporting of the Jc value, even when the Jc criterion is completely specified, does not provide sufficient information for comparing data. The most careful way of presenting data for comparison would be to compare the entire V-I curve for each sample. Where this is not practical, it is common[8] to report the 'n-value' in addition to Jc and the Jc criterion. Superconductors are expected to approximately follow the voltage-current relationship,

$$V = Vo*(I/I_o)^n,$$

where I_o is a reference critical current at a voltage criterion of V_o, V and I are the instantaneous voltage and current respectively, and n reflects the shape of the curve. Larger n values refer to steeper transitions, with values for conventional superconductors typically ranging from 20 to 60. A routine for deriving n from the Jc data will be developed and inserted into the testing module in the next quarter so that the n-value of filament samples will become a routine part of the CPSS database.

2.5.4 Characteristics of filaments

Figure 2.5.7 shows T_c data for two bare filaments, both dry spun from Rhône-Poulenc excess copper oxide powder and exposed to identical heat treatments. The difference in the processing of these two filaments is that 19065D1 was subjected to a 1 hour 500°C O2 anneal after silver contact pads had been sputtered onto the surface while 19065I1 was annealed before sputtering.

---

[8]"Development of Standards for Superconductors", L.F. Goodrich, ed., Electromagnetic Technology Division, Center for Electronics and Electrical Engineering, National Engineering Laboratory, National Bureau of Standards, Boulder, CO, DOE Contract DE-AI01-76PR06010, Interim Report, February 1988.

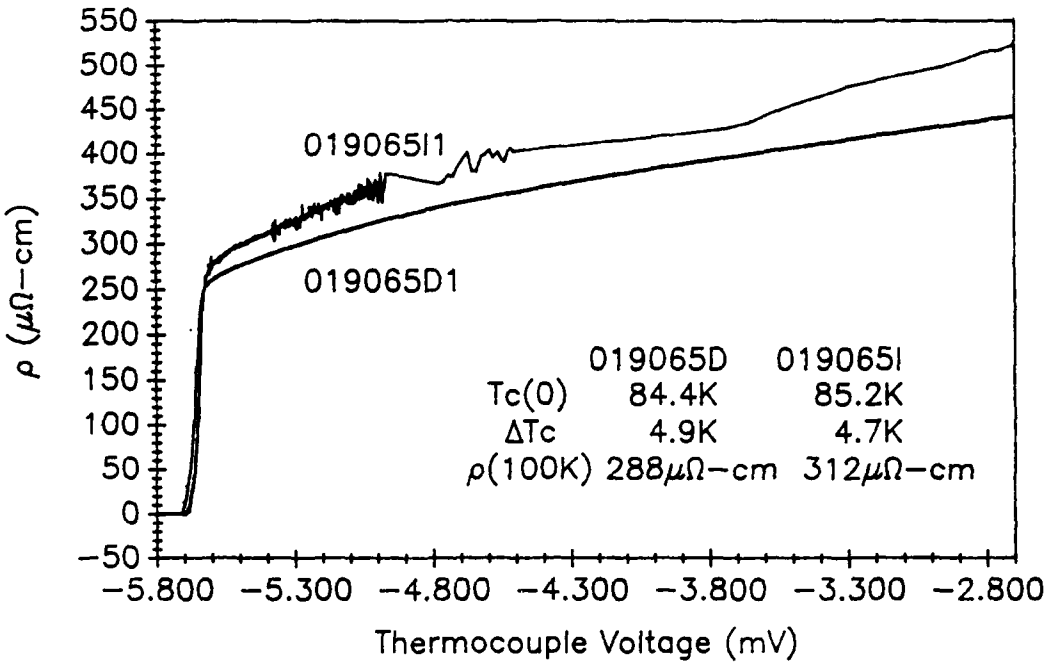

Figure 2.5.7: Resistivity vs. Temperature (expressed as thermocouple voltage) for Two Dry Spun Rhône-Poulenc Filaments, 02 Annealed before (19065I1) and After (19065D1) Silver Contact Pads Were Sputtered Onto Them.

Filament 19065I1 has a higher normal state resistivity and a higher T_c. This suggests that the silver has diffused into filament 19065D1 causing the lower resistivity. The difference in Tc is probably not significant. This data can be compared with that in Figure 2.5.3, the Tc for filament 019092, which shows significantly higher Tc and a ρ(100 K) essentially the same as that of the silver impregnated filament.

Figure 2.5.8 shows the Tc curve for a CPSS melt spun filament which has been clad with a Ag/Pd coating using the methods described in Section 2.4. The important points about this data are that this technique results in a cladding which makes low resistance contact with the filament and does not drastically degrade the performance of the superconductor. Since the presence of the cladding is expected to significantly alter the sintering kinetics of the fiber, it is not surprising that the sintering schedule needs to be re-optimized for clad fibers. The superconducting transition of the Ag/Pd clad filament is in marked contrast to the ρ(T) vs. T curves for filaments clad using two other methods. Figure 2.5.9 shows the temperature dependence of the resistivity for filaments clad with aluminum deposited by MOCVD and copper deposited by an electroless plating technique. The copper clad filament shows no resistive transition and has a resistance of about what one would expect for current travelling through a metal tube of 200 μm diameter. Either the deposition process has degraded the superconducting phase to the point where it is no longer superconducting, or the contact resistance between the coating and the filament is higher than the resistance along the coating. The aluminum clad filament has a similarly low normal state resistance, but shows what may be a partial superconducting transition. It may be that for this filament there is not a continuous aluminum path so that current must pass through the filament for a

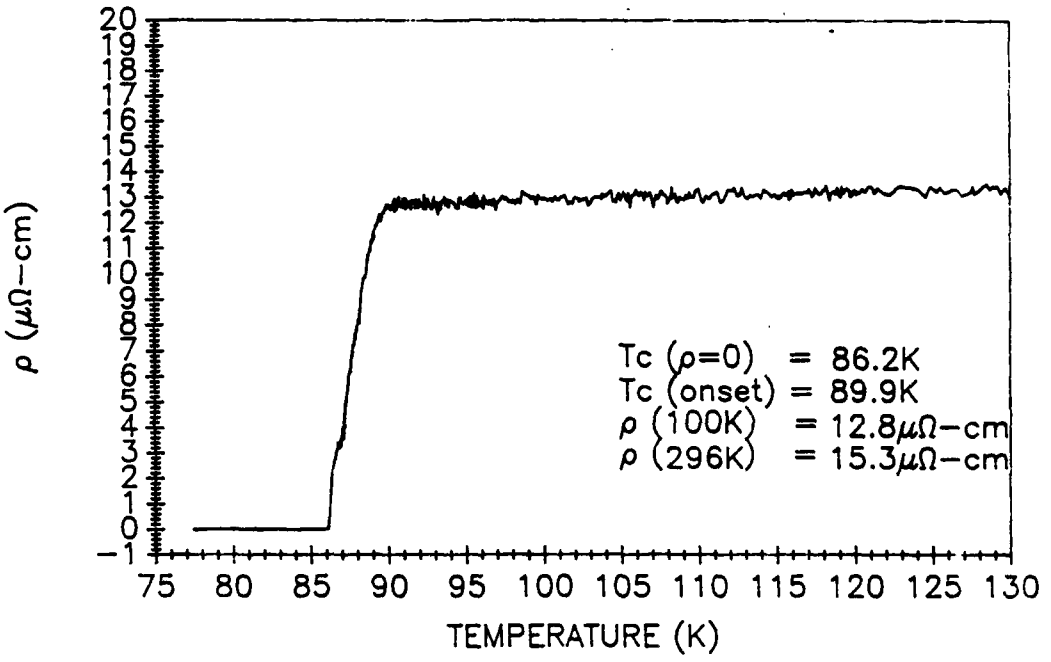

Figure 2.5.8 Resistivity vs. temperature for a Ag/Pd coated YBa_2Cu_3O7-x filament sintered at 993°C with six passes

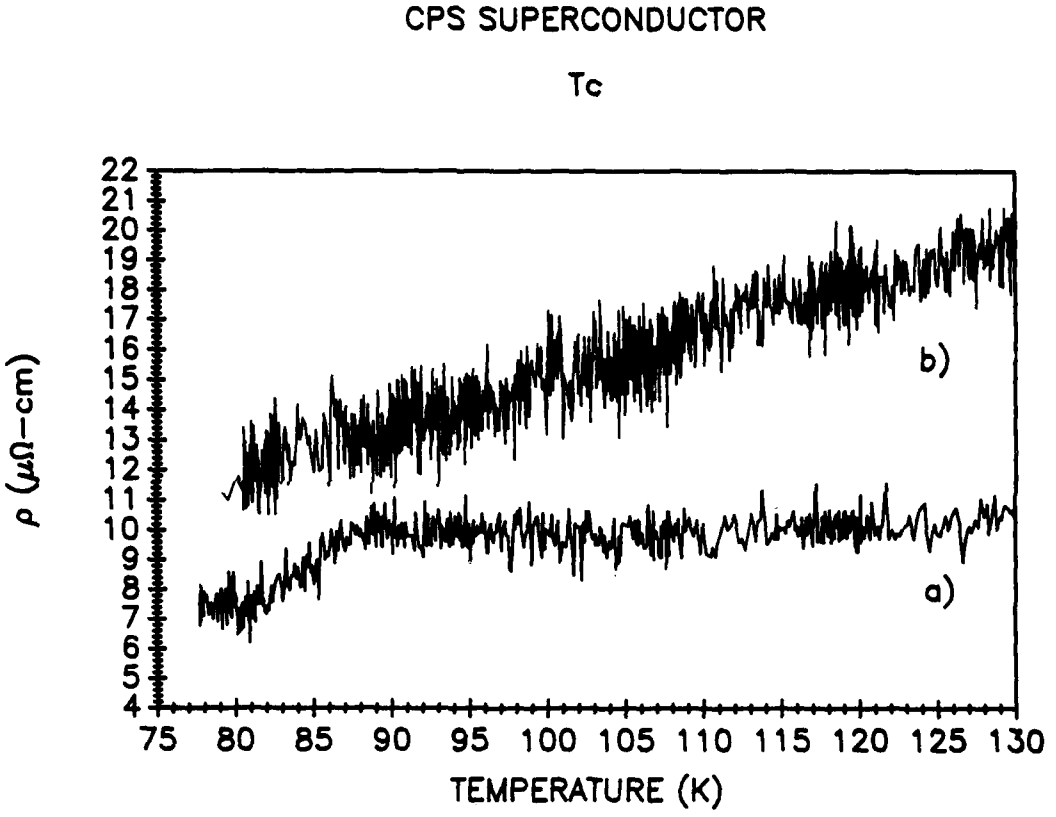

Figure 2.5.9: Resistance VS. Temperature for Filaments Clad With: A) Aluminum Using a Cold-Wall CVD Technique (ATM Corp.) and B) Copper Using Electroless Deposition (SUNY-Buffalo)

distance in spite of high contact resistance. It is important to note that both the aluminum and copper clad filaments showed only a weak Meissner effect prior to sending them out for coating. Better filaments have been sent to SUNY-Buffalo for electroless coating.

2.6 Summary

Substantial progress has been made in every step of the wire fabrication task. We can produce adequate quantities of an improved $YBa_2Cu_3O_{7-x}$ powder for our raw material. Strong, handlable $YBa_2Cu_3O_{7-x}$ green fiber is being continuously produced on spools, with diameters beginning to approach our targets. We have improved understanding of the binder burnout and sintering. By the end of this quarter, we were still sintering fibers in a batch mode, but are on the verge of continuous sintering. Continuous silver coated green fiber can be produced. We have made progress toward continuous cladding using the mechanical cladding concept.

An extensive powder optimization study was undertaken to provide an improved $YBa_2Cu_3O_{7-x}$ powder feedstock for the program. Eleven different powders, representing variations in calcination, raw materials, and milling conditions, were prepared and spun into fibers. Particle sizes varied from 0.69 to more than 3 microns. The study uncovered some deleterious effects of anticaking aids used in dry milling. Jet milling was identified as the preferred particle size reduction method, and has been adopted for future $YBa_2Cu_3O_{7-x}$ powder production.

The melt spinning process was successfully applied to $YBa_2Cu_3O_{7-x}$ powders at 50 vol% solids loadings. Spools of continuous fiber were produced with diameters ranging between 3 and 15 mils, depending upon drawing conditions. $YBa_2Cu_3O_{7-x}$ fibers were melt spun with several carrier polymer systems, including

high density polyethylene and ethylene vinylacetate. Evaluation of other carrier polymers continues. Spinning and drawing behavior was found to be sensitive to the milling aids used in powder preparation. The dry spinning process in now used only for small experimental powder lots.

The $YBa_2Cu_3O_{7-x}$ was found to be reactive with organic polymers and processing aids during binder burnout. These reactions were studied in detail. Under certain conditions the reaction can destroy the specimen, as the copper oxide in $YBa_2Cu_3O_{7-x}$ oxidizes the organic. The reaction of $YBa_2Cu_3O_{7-x}$ powders with stearic acid is particularly bad. Ethylene glycol milling aid is benign. In fibers, the carrier polymer can react with the $YBa_2Cu_3O_{7-x}$, especially under conditions of slow heating. Ethylene vinyl acetate is more reactive than polyethylene. Stearic acid exacerbates the reaction between the polymers and $YBa_2Cu_3O_{7-x}$. With fast heating, however, these reactions can be avoided, producing sintered filaments with no apparent degradation. Analysis of sintered fiber shows carbon levels at 0.18%, which is the same as the starting powder.

Work continued on the rapid zone sintering of $YBa_2Cu_3O_{7-x}$ fibers. The sintering of a variety of $YBa_2Cu_3O_{7-x}$ powders was examined in the form of dry spun fibers. This provided some data on the effect of particle size on the rapid zone sintering of $YBa_2Cu_3O_{7-x}$. Melt spun fibers sinter well, achieving a microstructure consistent with the particle size. Fibers from different carrier polymers sinter similarly, although EVA fibers have less shape retention than HDPE fibers.

The cladding work centered on mechanical cladding of silver treated filaments by solder bonding to copper strips. The silver treatment is now done continuously. The thin silver coating is co-fired with the $YBa_2Cu_3O_{7-x}$ fiber in the zone sintering operation. Silver-palladium alloy coatings were developed

further for higher sintering temperature. The solder reflow bonding process was further developed using small coupon specimens. Solder run-out during the reflow bonding was eliminated by using a channel shaped copper strip. The components for the continuous surrogate cladding module are still being evaluated, so the continuous cladding experiments have been delayed.

Alternate cladding methods were explored with outside collaborators. Aluminum deposits on $YBa_2Cu_3O_{7-x}$ filament surfaces were produced by MOCVD at ATM, but the superconductivity was degraded. Lashmore and Stafford at NIST deposited Al-Mn alloys on filaments by molten salt electrodeposition. The Meissner effect proved that superconductivity was retained, but no resistive transition was found by the transport method, due to a resistive layer between the $YBa_2Cu_3O_{7-x}$ substrate and the metal deposit. Electroless plated copper deposits were obtained on $YBa_2Cu_3O_{7-x}$ filaments at SUNY-Buffalo, but the superconductivity was degraded.

Electrical characterization work focused on improving measurement techniques for single filaments. An improved method was developed for making low resistance contacts, which reduced contact resistance of silver pads on $YBa_2Cu_3O_{7-x}$ filaments three orders of magnitude, down to as low as 20 micro ohm/cm^2. New software was written for computer controlled determination of critical current and resistive transition. Measurements were begun on electrical characterization of the sintered silver coated filaments.

SECTION 3

HIGH TEMPERATURE SUPERCONDUCTOR MOTOR DESIGN AND FABRICATION

KEITH HOEMANN, VERN KIEFFER, AND JERRY LLOYD

EMERSON MOTOR COMPANY

3.1 Program Initiation and Manpower

As mentioned in the previous quarterly report, Emerson elected not to start on the program until after receipt of a signed contract, which was obtained in early October,1988. The first activity was to assign a motor design engineer and a mechanical engineer to the project on a full time basis. Emerson did not have any engineers with the necessary qualifications, that could be made available on a full time basis, so our original intent was to go to the outside and hire the necessary personnel.

We engaged several placement services in March, 1988 to find some potential candidates, with the major emphasis being placed on getting a good qualified motor designer that is well versed in all types of electric motors. We identified three possible candidates for the position in the March - April time frame; but due to the delay of receiving a signed contract until October, two of the candidates were no longer available. The third candidate had just verbally accepted the position and planned on starting on November 21,1988, when he had a sudden severe illness in the family and had to back out of the job offer. We negotiated five weeks with a forth candidate; but could not mutually agree on a relocation package.

We have since found another candidate that has agreed to take the position and is scheduled to start with Emerson on February 6, 1989. His name is Alan D. Crapo. He obtained his M.S. in Electrical Engineering from Brigham Young University in 1978. He has a very strong background in electrical machines with 10 years of research and design experience at Westinghouse R&D, Inland Motor, and Seagate Technology.

We have also interviewed one mechanical engineer with an extensive background in superconductor technology; but he was not interested in the position

because he wanted to manage a group of researchers working on the program and not to physically do all the work himself. The engineer for this position needs to have expertise in cryogenics, bearing systems, and preferably some experience in superconductor materials.

3.2 Literature Research

The second activity was to begin a detailed literature search on superconductor motors and mechanical systems. This activity was initiated in two ways:

1. Engaged Tom Lipo of the University of Wisconson - Madison, to have one of his students begin the literature search and start collecting the pertinent articles for review by T. Lipo and the full time motor designer, when he becomes available. The student has completed the initial search on the data base available at the university, and is now in the process of reviewing and copying the papers.

2. Conducted a patent search on superconductor machines throughout the world and are in the process of obtaining copies of the patents for review. We have identified some 63 patents the pertain to motors that we will be reviewing. Many of the patents are from Japan and will need to be interpreted.

3.3 Application Study

In order to begin work in evaluating motor technologies that are potential candidates for HTSC wire, we engaged Tom Lipo of the University of Wisconson - Madison, to evaluate potential motor technologies and also design a homopolar machine as a basis for determining some of the properties that maybe necessary for the wire. We have also initiated a design study of a dc heteropolar machine at Emerson.

3.3.1 Homopolar Motor

The homopolar machine is the only electric motor that does not contain any time varying magnetic fields. All other machines are operated from alternating

power sources or have ac fields induced in them as a result of providing rotation to the machine. If we cannot develop a HTSC wire that will function in ac magnetic fields, then this will be the best motor design to evaluate HTSC wire in for our proof-of-principle motor.

The homopolar machine, commonly called the Faraday disc motor, was first built by Michael Faraday in 1831, and in its simplest form, consists of a conducting disc rotating in a magnetic field that is parallel to its axis of rotation.[1] (Figure 3.3.1). The magnetic field is generated by placing a coil of wire circumferential around the disc armature and energizing the coil with a dc current source. A dc current is also applied to the disc through a set of slip rings and brushes in such a way as to produce a current flow in the disc from the center to the outer edge. The magnetic flux and current in the disc are always at right angles to one another. Therefore per Fleming's rule, a force will be produced on the disc that is perpendicular to both the current vector and the flux vector, resulting in a torque on the disc (Figure 3.3.2).

$$T = B \times I \cdot r$$

Where T is the torque

B is flux density

I is current in disc

r is effective mean disc radius

One of the major problems of this type of machine is the current collection system. Since the armature E.M.F. of this machine tends to be very low, the armature current required is very high, leading to high currents through the brushes. A considerable amount of research needs to be done in this area if this type of machine is used as the initial motor.

Since the field winding of this type of machine can be easily isolated from the rotating disc, it is a very convenient design for a HTSC motor.

---

[1] J. R. Bumby, "Superconducting Rotating Electrical Machines",Clarendon Press, Oxford, 1983, pp. 34-38.

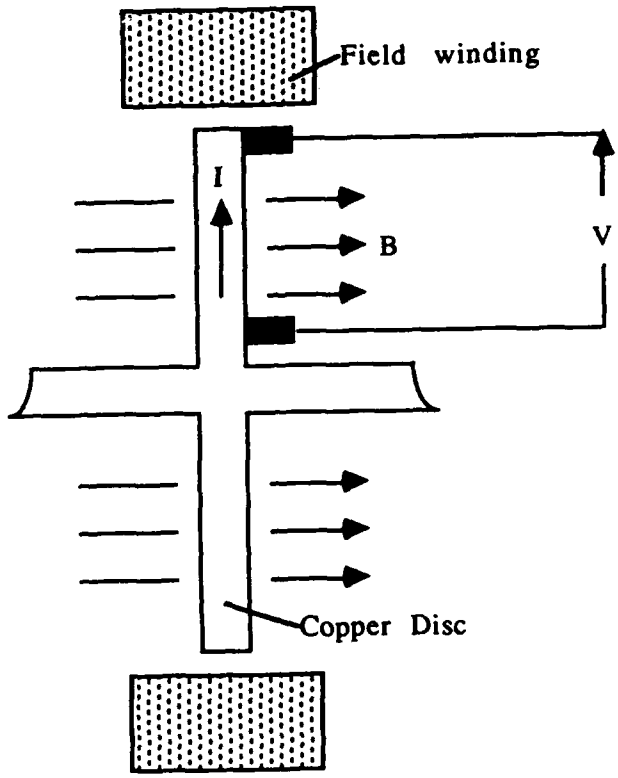

Figure 3.3.1 Side view of homopolar disc motor.

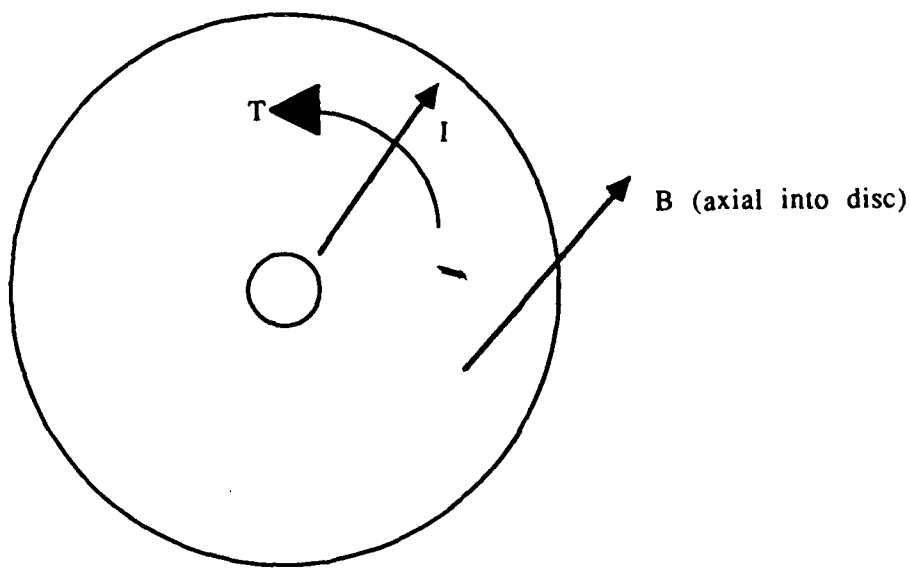

Figure 3.3.2 Axial view of disc.

In order to further evaluate this potential HTSC motor application, T. Lipo is designing a 10 hp homopolar disc motor with the following parameters:

B= 3 tesla (DC field only)

J_c= 10^5 A/cm^2

Output= 10 hp @ 1800 rpm

The results of this study will be reported on in the next quarterly report.

3.3.2 DC Heteropolar Machine

The main advantage to be gained in the application of HTSC wire to the heteropolar machine is primarily an increase in the magnetic loading which leads to a machine design with smaller volume than its conventional counterpart. In addition, the high magnetic loading can be achieved without the need of an iron magnet circuit, resulting in an increase in the power-to-weight ratio of between 3 to 5. The disadvantage of this type of machine for HTSC is it does contain time varying magnetic fields.

The basic performance equations for a cylindrical heteropolar machine with magnetic and electrical symmetry under steady-state conditions are:

Terminal Voltage $V_s = V_B + I_a \cdot r_a$

Back E.M.F. $V_B = (2 \cdot N \cdot P/\pi a)\ w_r \emptyset \approx K w_r \emptyset$

Torque / Amp $K_T = K \cdot \emptyset$

Output Power $P_o = V_B I_a = K_T I_a w_r$

Under most conditions, V_s, P_o, and w_r are given with I_a being determined by V_B and r_a. Since V_B will range between .8 and .9 (V_s) the main factor determining Power Output / Volume is N$\emptyset$. As $\emptyset$ is increased, N decreases and reduces in size for the same performance allowing higher power densities.

$\emptyset = B_g A_g$

Where: B_g = Flux density in air gap

A_g = Area of air gap

From the above equations, in order to increase Ø, one must increase B_g, A_g, or both. However, saturation characteristics of the steel or the fixed flux density of permanent magnets, limit B_g such that to obtain higher Ø for larger horsepower motors, one must typically increase A_g thereby increasing volume.

For example, a typical 10 hp ac motor would have a B_g of .63 Tesla, a wound field dc machine .75 - .85 Tesla, and a permanent magnet machine using high energy rare earth magnets almost 1.0 Tesla.

With a field winding using superconductors, and if a flux density of 3 tesla could be possible, it could reduce the air gap area to 1/3 of that with the highest energy magnets. Since this density is beyond steel saturation limits, an ironloss armature and field poles would further reduce the machine mass. The space factor for the armature would improve by as much as 20 percent. This could reduce the mass of the machine's active material by greater than 4 and the volume by 3.

Because of the elimination of the steel and the need for less area or fewer conductors, the motor inductance would be dramatically reduced, improving commutation and minimizing the size of com-poles used on higher horsepower dc machines.

With the significant reduction in the mass of the armature, the total moment of inertia, J_T , is reduced thereby reducing the mechanical time constant of the machine,

$$T_M = R_a J_T/(K_T V_B)$$

The decrease in inductance reduces the electrical time constant,

$$T_e = L/R$$

providing for a significant improvement in dynamic performance.

Under normal operating conditions, a small ac field will be superimposed on the dc field due to the armature reaction, winding distribution, and com-poles (if required). The superconductor will need to be stable at 10 to 20 percent of the dc field in order to be effective.

Current technology for superconductors is in the 77° K temperature range requiring special low temperature equipment and techniques that need to be

researched. While the active material mass, motor inertia, electrical and mechanical time constants can be reduced, the temperature requirements, along with shielding of the very high flux fields, may lead to a larger system than current dc motor technology.

A more detailed analysis of this machine will be completed during the next quarter.

3.4 Wire Properties for HTSC Motor

Mohamed A. Hilal of the University of Wisconson - Madison, Appilied Superconductivity Center was engaged as a consultant to study and report on physical properties, effect of the environment, test requirements, and test methods for HTSC.

One of the main concerns of using HTSC wire in electric machines is the effect the magnetic fields will have on the properties of the HTSC. Of most concern is the effect of time varying or ac magnetic fields, since all electric machines, except the homopolar machine, have some ac magnetic fields throughout the machine. If the HTSC cannot be made to operate in ac fields then this will eliminate practically all the motor technologies that are commonly used today, since homopolar motors are not now commercially produced in any volume nor are they a practical design.

The ac losses in a superconductor subjected to time varying magnetic fields are the result of hysteresis effects within the superconductor and eddy currents flowing in the normal matrix. The magnitude of these losses are a function of the diameter of the wire or filaments, the critical current density of the material and the twist pitch of the conductor. There has been a considerable amount of research conducted on this subject and M. Hilal is currently evaluating this information and will be reporting on these properties and how wires will need to be processed to function in ac magnetic fields. Some preliminary information indicates that we may need to develop a wire that is made up of multiple strands of HTSC wire with a filament diameter in the sub-micron range and a critical current density, $J_c > 10^5$ Amps/cm^2.

3.5 Winding Stresses on Wire

In order to determine the mechanical stresses the wire will encounter under various manufacturing process, a preliminary study was conducted on current winding practices.

There are five basic methods presently used to wind electric mechanics.

1) Manual coil placement or hand winding.
2) Pre-winding coils and mechanical coil insertion.
3) Skein wound coils.
4) In-slot-winding by needle winding machines.
5) Bobbin winding.

3.5.1 Manual Placement

The manual placing of coils into stators is currently only practiced in the manufacture of motors in very low volume batch work, for special motors and large formed coil machines. On small to medium sized machines, this involves winding the coils on winding forms which are designed to give the proper length of turn and approximate coil shape. These forms are placed on a continuous coil winding machine, which is basically a spindle drive with accessories to control turn count, winding speed, and tension on the wire. Depending on the type of motor being wound, these coils can be a simple circle or rectangular in shape. The radius that the wire is generally bent over is usually greater than 3 mm on the rectangular coils.

When wire is wound in order to form shaped winding elements, it should keep the shape purposely given to it once the winding tension is released from the wire. The shape should be maintained even when the coils are removed from the forms. The characteristic that allows this to happen is called the spring-back resilience of the wire and is a function of the wire hardness and tension on the wire during the coil wind process. Experience has shown that in order to produce coils with minimal spring-back, the wire tension needs to be controlled such that it is

65 to 85 percent of the yield strength of the wire. The yield strength of copper is about 8.4 kg/mm^2, so copper windings generally experience a winding force of 5.5 to 7.1 kg/mm^2 (7,000 to 10,000 psi).

Winding rectangular coils can also induce additional stress in the wire due to the irregular shape causing the speed that the wire is being pull from the source to pulsate in velocity. Depending on the winding speed, long-narrow forms can cause the wire to elongate as the wire completes the long span and starts the short span. This can impose forces on the wires in excess of 8.5 kg/mm_2 if the coil shape and winding speed are not well controlled.

The forces on the wire due to hand placement of the coils in the slots is very dependent on the individual doing the placement and the fullness of the slots. If the slots are above 60 percent full, it is not uncommon for the operator to use a hammer and slot knife to drive the wire to the bottom the the slots. However, this can be controlled with the proper instruction and design.

3.5.2 Coil Insertion Process

The second method, pre-winding coils and mechanical coil insertion, is the most widely used method in ac motors today. The forces the wires experience during the coil winding process are the same as above, however, the winding radii are usually a little greater, 5 mm minimum (Figure 3.5.2).

During the insertion process the coils are removed from the formers to a transfer tool (Figure 3.5.3). This transfer tool is then positioned onto the coil insertion tooling and the windings are transferred into their insertion slots over the insertion lamella or blades (Figure 3.5.4) The insertion lamella are designed to protect the wires as they are inserted into the stator slots (3.5.5). They are highly polished and plated with a hard chrome to reduce the winding forces. The wire generally experiences bending radii greater than 6 mm.

The insertion process is illustrated in Figure 3.5.6. In representation "A" the coils (4) are shown after they are transferred into the insertion tooling. The

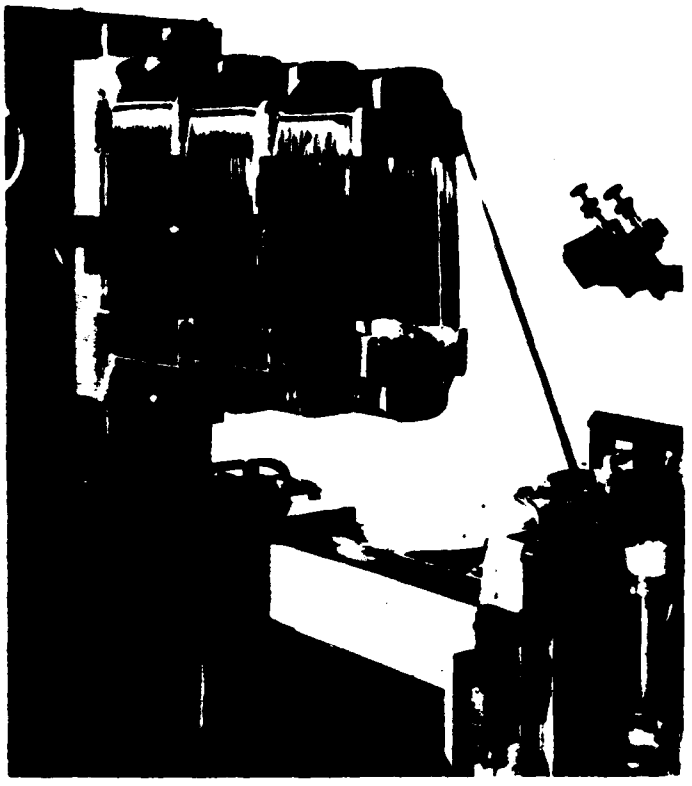

Figure 3.5.2 Coil former.

Figure 3.5.3 Coil transfer tool placed on former for coil removal.

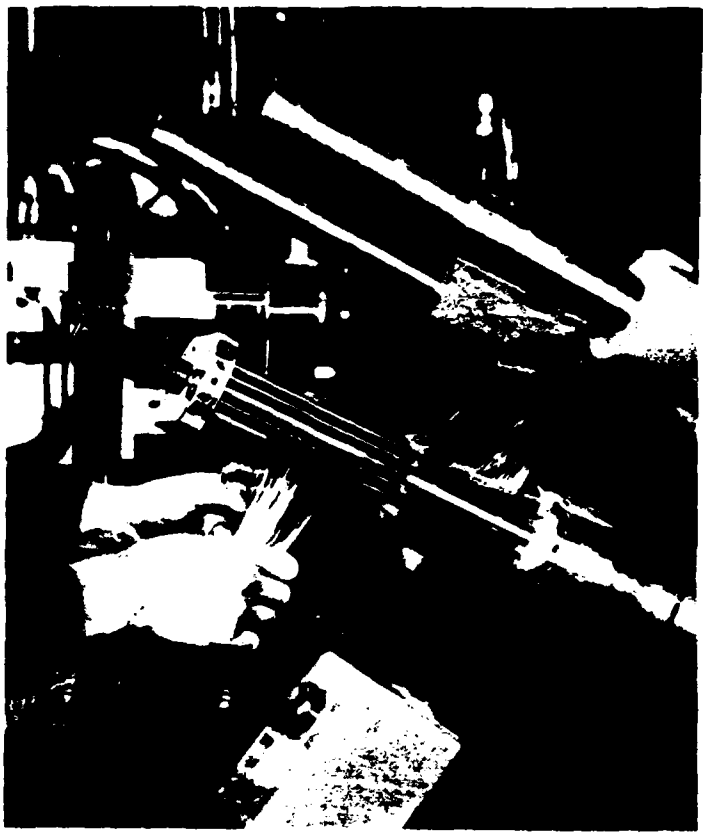

Figure 3.5.4 Coil transfer tool placed onto insertion tooling for coil transfer.

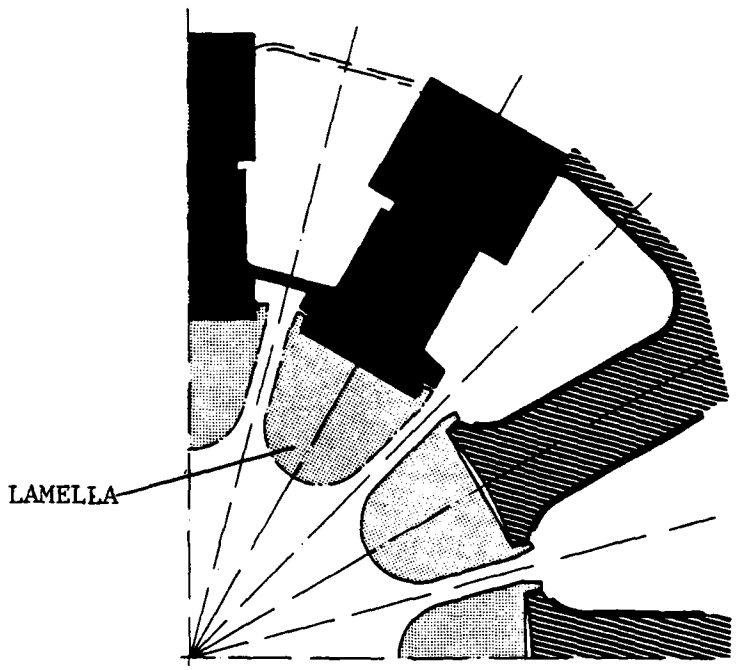

Figure 3.5.5 Top section view of insertion tooling.

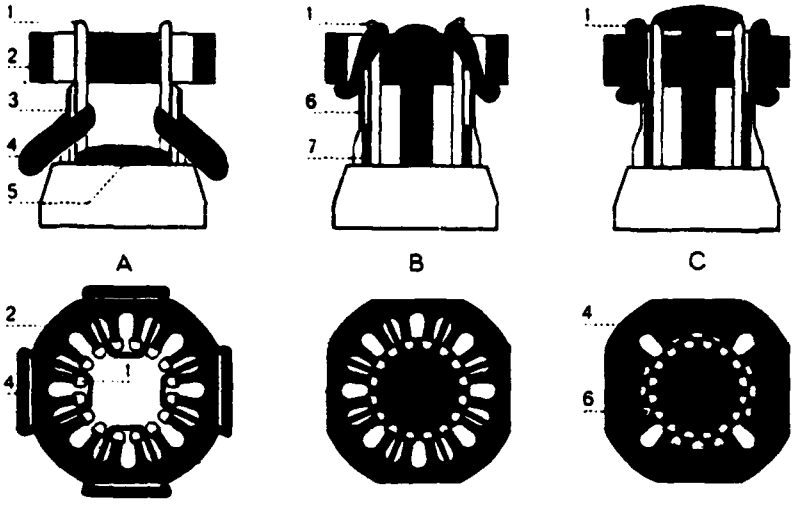

Figure 3.5.6 Coil transfer process.

stator (2) rests on the tooling and one can depict the insertion lamella (1), wedge guides (3) and the insertion star (5).

Representation "B" shows the insertion process shortly after its beginning. The insertion star (5) moves upward, pulls the coils (4) with it and places them into the stator slots. The wedge push rods (7) move the wedges (6) up and position them in the stator slots as closures.

Representation "C" demonstrates the completion of the insertion process. The insertion star retracts and the stator may be removed from the tooling.

During the insertion process, the column of wires are pushed up the insertion lamella with the insertion star. The entire force of inserting the wires is exerted on the bottom wire or wires in each column that is touching the insertion star. An inserting machine was equipped with a force transducer in order to measure this insertion force. Experiments were run on several sizes of motors, with varying wire sizes and slot fullness. Figure 3.5.7 is a graph of the typical force imposed on the insertion star. The stator represented in this graph was a NEMA 48-4 pole stator that had 12 coils being inserted into a 32 slot stator. The maximum force exerted on the star was 900 kg. Therefore, there was 37.5 kg of force exerted on the bottom wire of each coil.

The contact area of the insertion star to the wires is about 12 mm long by 0.7 mm wide. Hence, the force on the wire is about 4.5 kg/mm^2.

3.5.3 Skein Winding

In the previous processes the coils and poles were individually wound on the formers and inserted in the stator. The skein winding process generates all the coils and poles for an entire phase from a single large coil. A large round coil of predetermined diameter is wound with the number of turns of a single coil. This large coil is then placed in a forming machine that forms the coils in a serpentine fashion (Figure 3.5.8), to define the poles of the stator. These coils are then placed in the stator slots either by hand or with the coil insertion process.

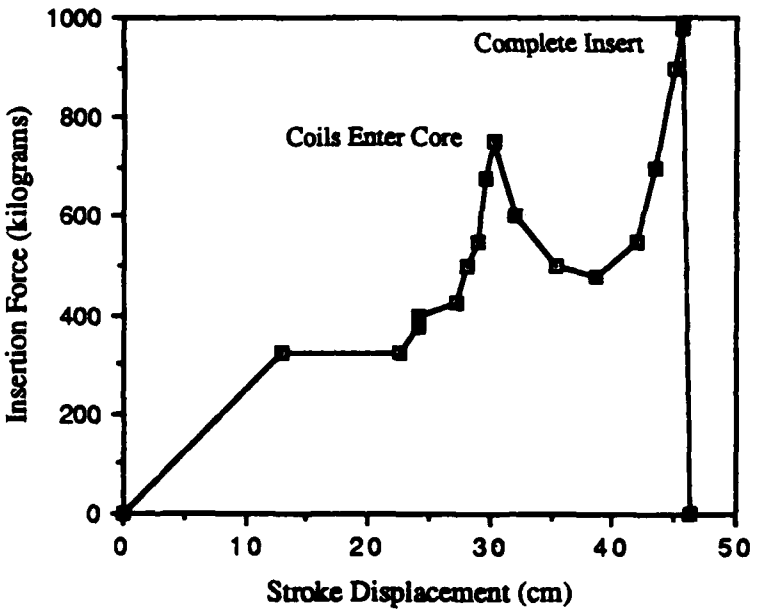

Figure 3.5.7 Insertion force on NEMA 48 - 4 pole.

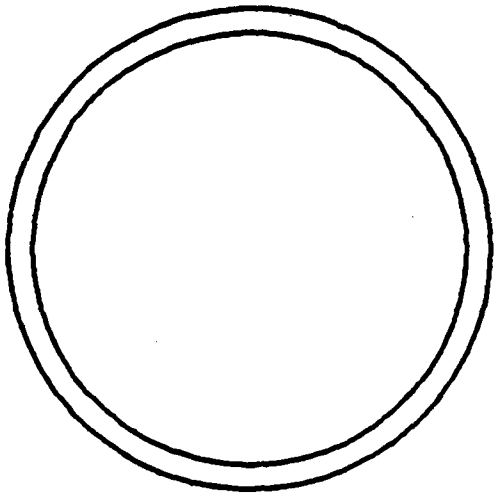

LARGE COIL
(A)

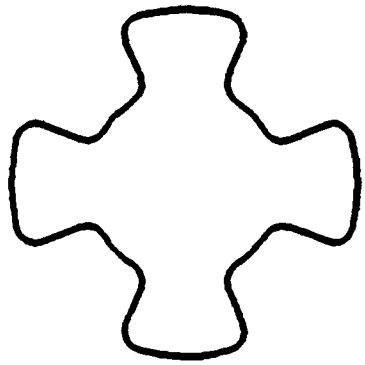

FORMED FOR INSERTION
(B)

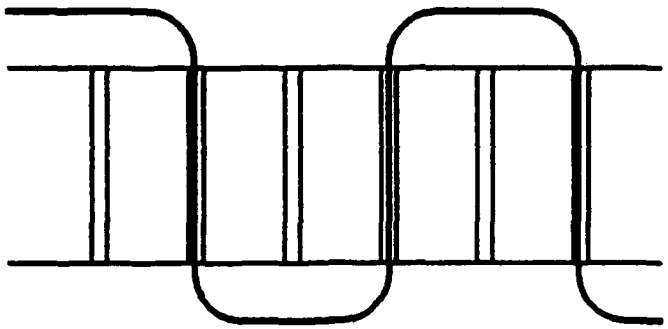

(C)

FIGURE 3.5.8 SKEIN WINDING PROCESS

The insertion forces on the wires are the same as the processes described above; however, the bending radii to wind and form the coils are greater than the pre-formed coils. Typical radii are usually greater than 10 mm.

3.5.4 Needle Winding

The in-slot winding by needle winding machines are used on salient pole motors and wound rotors or armatures. The basic process consists of threading the wire through the arm of a gun winder and out a winding needle. The winding needle is then traversed through the slots of the stator or armature as it winds the wire directly in place one turn at a time. Figure 3.5.9 is a drawing of a typical winding needle. The main disadvantage of this process is the small bending radii that the wire will experience as it leaves the winding needle which can be as small as 1 mm.

As in the other processes, the winding tension needs to be near the yield strength of copper, or the material being wound, so that the wires stay in place as the tension is removed. If this is not done, the coils will be very loose and will be capable of excessive movement during operation of the motor. The winding forces are also very erratic as the needle travels through the slots and around the ends of the core. These forces can be as high as 8.5 kg/mm^2.

3.5.5 Bobbin Winding

The final method commonly used is bobbin winding. This can be the gentleless process of the five discussed and is used in stepper motors, shaded pole motors, field windings, and armature windings for large synchronous machines.

In this process an insulated bobbin, which is used in the final stator, is placed on a spindle winder and the wire is wound directly on the bobbin. Depending on the design of the motor, the shape of the bobbin can be either full round or rectangular. The winding tension on this process is typically in the 5.5 to 7.1 kg/mm^2 area to wind a good tight coil. However, this force can be reduced without experiencing any significant problems, in that the final turn on the bobbin can be

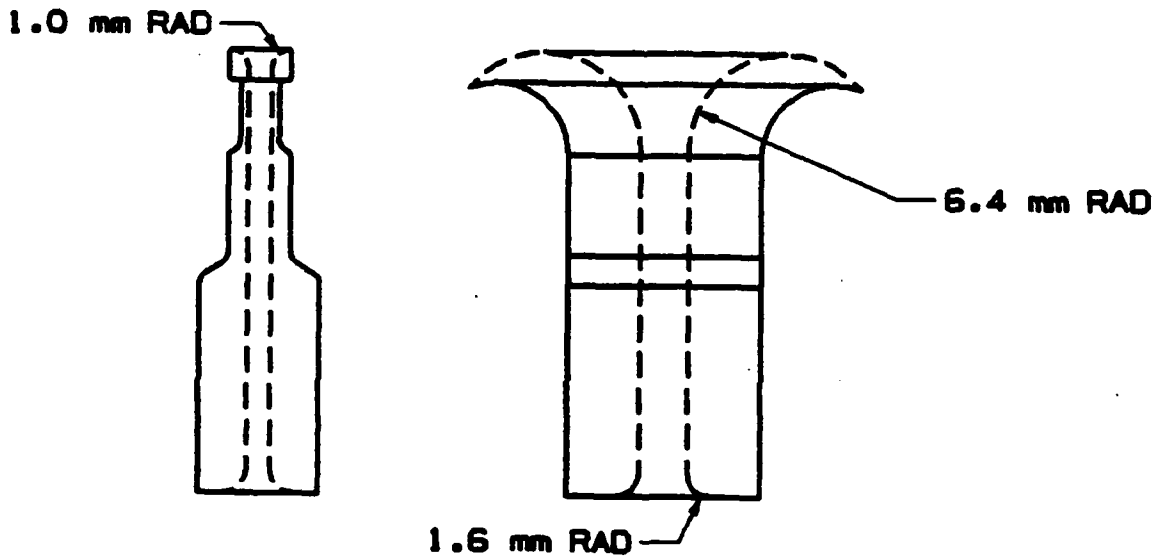

Figure 3.5.9 Winding Needle

secured to the bobbin prior to releasing the tension on the wire, thus eliminating the problems of spring-back. Based on manufacturing experience, a good bobbin wound coil can be made with half this tension.

3.5.6 Winding Process Summary

The needle winding process imposes the highest forces and smallest bending radii on the wire and should be avoided in the design of HTSC machines. The bobbin wind process is the gentleless and maybe the process of chose for HTSC wire. It would be highly desirable to be able to insertion wind the stators in that this is the most widely used and automated process used today.

Based on this analysis, if a HTSC wire is produced with a copper clad or shunt, then the material needs to withstand forces of at least 3 kg/mm^2 and a minimum bending radius of 10 mm.

3.6 Summary

During this quarter, the major activity has been to try and hire a motor designer and mechanical engineer for the project on a full time basis. We now have the motor designer hired, which is of the most importance, and will continue to search for a mechanical engineer.

Consultants have been engaged to begin application studies on available motor technologies and to study physical properties of the HTSC wires for electric machines. The literature research on superconductor motors has also been started, along with a study of the past patent activity throughout the world.

During the next reporting period, we plan to continue our efforts to get a mechanical engineer in place, continue the literature research, finalize the study on past patent activity, report and define HTSC wire properties, and report on initial application designs.

SECTION 4

GENERAL DISCUSSION AND SUMMARY

The program is now fully underway, as the Emerson Motor Division design activities have begun. The wire fabrication task at CPSS and AIResCo is making progress in each separate process step. The raw material for fiber production is now CPSS $YBa_2Cu_3O_{7-x}$ powder, which is produced in adequate quantities to support the program. The quality of the $YBa_2Cu_3O_{7-x}$ powder has improved. Green $YBa_2Cu_3O_{7-x}$ fiber is being continuously produced on spools, with adequate strength for handling. Green fiber diameters are still larger than desired, but are steadily being reduced. We have improved understanding of the binder burnout and sintering as a result of some intensive investigations. Fiber sintering fibers is still being done in a batch mode, using the rapid zone sintering method. The arrival of a continuous furnace at the end of this Quarter places us on the verge of continuous sintering. Continuous silver coated green fiber can be produced. We have made progress toward continuous cladding using the mechanical cladding concept.

An extensive powder optimization study was undertaken to provide an improved $YBa_2Cu_3O_{7-x}$ powder feedstock for the program. Eleven different powders, representing variations in calcination, raw materials, and milling conditions, were prepared and spun into fibers. Particle sizes varied from 0.69 to more than 3 microns. The study uncovered some deleterious effects of anticaking aids used in dry milling. Jet milling was identified as the preferred particle size reduction method, and has been adopted for $YBa_2Cu_3O_{7-x}$ powder production.

The melt spinning process was successfully applied to $YBa_2Cu_3O_{7-x}$ powders at 50 vol% solids loadings. Spools of continuous fiber were produced with diameters ranging between 3 and 15 mils, depending upon drawing conditions. $YBa_2Cu_3O_{7-x}$ fibers were melt spun with several carrier polymer systems, including high density polyethylene and ethylene vinylacetate. Spinning and drawing behavior was found to be sensitive to the milling aids used in powder preparation.

The $YBa_2Cu_3O_{7-x}$ was found to be reactive with organic polymers and processing aids during binder burnout. These reactions were studied in detail. Under certain conditions the reaction can be destroy the specimen, as the copper oxide in $YBa_2Cu_3O_{7-x}$ oxidizes the organic. The reaction of $YBa_2Cu_3O_{7-x}$ powders with 2% stearic acid milling aid is particularly bad. Ethylene glycol milling aid is benign. In fibers, the carrier polymer can react with the $YBa_2Cu_3O_{7-x}$, especially under conditions of slow heating. Ethylene vinyl acetate is more reactive than polyethylene. Stearic acid exacerbates the reaction between the polymers and $YBa_2Cu_3O_{7-x}$. With fast heating, however, these reactions can be avoided, producing sintered filaments with no apparent degradation. Analysis of sintered fiber shows carbon levels at 0.18%, which is the same as the starting powder.

The sintering of variety of $YBa_2Cu_3O_{7-x}$ powders was examined in form of dry spun fibers. Melt spun fibers sinter well, achieving a microstructure consistent with the particle size. Fibers from different carrier polymers sinter similarly, although EVA fibers have less shape retention than HDPE fibers.

The cladding work centered on mechanical cladding of silver treated filaments by solder bonding to copper strips. The silver treatment is now done

continuously. The thin silver coating is co-fired with the $YBa_2Cu_3O_{7-x}$ fiber. Silver-palladium alloy coatings were developed further for higher sintering temperature. Solder run-out during the reflow bonding was eliminated by using a channel shaped copper strip. The components for the surrogate cladding module are still being evaluated.

Aluminum deposits on $YBa_2Cu_3O_{7-x}$ filament surfaces were produced by MOCVD at ATM, but the superconductivity was degraded. Lashmore and Stafford at NIST deposited Al-Mn alloys on filaments by molten salt electrodeposition. The Meissner effect proved that superconductivity was retained, but no resistive transition was found by the transport method, due to a resistive layer between the $YBa_2Cu_3O_{7-x}$ substrate and the metal deposit. Electroless plated copper deposits were obtained on $YBa_2Cu_3O_{7-x}$ filaments at SUNY-Buffalo, but the superconductivity was degraded.

Electrical characterization work focused on methods of making low resistance contacts. A new method has reduced contact resistance of silver pads on $YBa_2Cu_3O_{7-x}$ filaments three orders of magnitude, down to as low as 20 micro ohm/cm2. New software was written for computer controlled determination of critical current and resistive transition.

Emerson Motor Division has begun work on DC heteropolar motor designs and, through Professor Novotny at U. Wisconsin, DC homopolar machines. The mechanical stresses on conventional copper wires during winding have been characterized to determine the mechanical parameters of motor building. A materials property database is being assembled for $YBa_2Cu_3O_{7-x}$, with the major uncertainties being the material's tolerance of time varying magnetic fields and, of course, critical current in magnetic fields.

ATTACHMENT I

REPORT SUMMARY

COMPOSITE CERAMIC SUPERCONDUCTING WIRES FOR ELECTRIC MOTOR APPLICATIONS

Second Quarterly Report on
Contract Number N00014-88-C-0512

December 30, 1988

John W. Halloran, et al., Ceramics Process Systems Corporation,
Cambridge, MA 02139

The program is now fully underway, as the Emerson Motor Division design activities have begun. The wire fabrication task at CPSS and AIResCo is making progress in each separate process step. The raw material for fiber production is now CPSS $YBa_2Cu_3O_{7-x}$ powder, which is produced in adequate quantities to support the program. The quality of the $YBa_2Cu_3O_{7-x}$ powder has improved. Green $YBa_2Cu_3O_{7-x}$ fiber is being continuously produced on spools, with adequate strength for handling. Green fiber diameters are still larger than desired, but are steadily being reduced. We have improved understanding of the binder burnout and sintering as a result of some intensive investigations. Fiber sintering fibers is still being done in a batch mode, using the rapid zone sintering method. A continuous furnace arrived at the end of this Quarter for continuous fiber sintering. Continuous silver coated green fiber can be produced. We have made progress toward continuous cladding using the mechanical cladding concept.

An extensive powder optimization study was undertaken to provide an improved $YBa_2Cu_3O_{7-x}$ powder feedstock for the program. Eleven different powders, representing variations in calcination, raw materials, and milling conditions, were prepared and spun into fibers. Particle sizes varied from 0.69 to more than 3 microns. The study uncovered some deleterious effects of anticaking aids used in dry milling. Jet milling was identified as the preferred particle size reduction method, and has been adopted for $YBa_2Cu_3O_{7-x}$ powder production.

The melt spinning process was successfully applied to $YBa_2Cu_3O_{7-x}$ powders at 50 vol% solids loadings. Spools of continuous fiber were produced with diameters ranging between 3 and 15 mils, depending upon drawing conditions. $YBa_2Cu_3O_{7-x}$ fibers were melt spun with several carrier polymer systems, including high density polyethylene and ethylene vinylacetate. Spinning and drawing behavior was found to be sensitive to the milling aids used in powder preparation.

The $YBa_2Cu_3O_{7-x}$ was found to be reactive with organic polymers and processing aids during binder burnout. These reactions were studied in detail. Under certain conditions the reaction can be destroy the specimen, as the copper oxide in $YBa_2Cu_3O_{7-x}$ oxidizes the organic. The reaction of $YBa_2Cu_3O_{7-x}$ powders with 2% stearic acid milling aid is particularly bad. Ethylene glycol milling aid is benign. In fibers, the carrier polymer can react with the $YBa_2Cu_3O_{7-x}$, especially under conditions of slow heating. Ethylene vinyl acetate is more reactive than polyethylene. Stearic acid exacerbates the reaction between the polymers and $YBa_2Cu_3O_{7-x}$. With fast heating, however, these reactions can be avoided, producing sintered filaments with no apparent degradation. Analysis of sintered fiber shows carbon levels at 0.18%, which is the same as the starting powder.

The sintering of variety of $YBa_2Cu_3O_{7-x}$ powders was examined in form of dry spun fibers. Melt spun fibers sinter well, achieving a microstructure consistent with the particle size. Fibers from different carrier polymers sinter similarly, although EVA fibers have less shape retention than HDPE fibers.

The cladding work centered on mechanical cladding of silver treated filaments by solder bonding to copper strips. The silver treatment is now done continuously. The thin silver coating is co-fired with the $YBa_2Cu_3O_{7-x}$ fiber. Silver-palladium alloy coatings were developed further for higher sintering temperature. Solder run-out during the reflow bonding was eliminated by using a channel shaped copper strip. The components for the surrogate cladding module are still being evaluated.

Aluminum deposits on $YBa_2Cu_3O_{7-x}$ filament surfaces were produced by MOCVD at ATM, but the superconductivity was degraded. Lashmore and Stafford at NIST deposited Al-Mn alloys on filaments by molten salt electrodeposition. The Meissner effect proved that superconductivity was retained, but no resistive transition was found by the transport method, due to a resistive layer between the $YBa_2Cu_3O_{7-x}$ substrate and the metal deposit. Electroless plated copper deposits were obtained on $YBa_2Cu_3O_{7-x}$ filaments at SUNY-Buffalo, but the superconductivity was degraded.

Electrical characterization work focused on methods of making low resistance contacts. A new method has reduced contact resistance of silver pads on $YBa_2Cu_3O_{7-x}$ filaments three orders of magnitude, down to as low as 20 microohm/cm2. New software was written for computer controlled determination of critical current and resistive transition.

Emerson Motor Division has begun work on DC heteropolar motor designs and, through Professor Novotny at U. Wisconsin, DC homopolar machines. The mechanical stresses on conventional copper wires during winding have been characterized to determine the mechanical parameters of motor building. A materials property database is being assembled for $YBa_2Cu_3O_{7-x}$, with the major uncertainties being the material's tolerance of time varying magnetic fields and critical current in magnetic fields.

ATTACHMENT II

ARPA ORDER NUMBER: 9525

PROGRAM CODE NUMBER: 7737

CONTRACTOR: Ceramics Process Systems Corporation
840 Memorial Drive
Cambridge, MA 02139

CONTRACT NUMBER: N00014-88-C-0512

CONTRACT EFFECTIVE DATE: 30 JUNE 1988

CONTRACT EXPIRATION DATE: 31 MARCH 1991

SHORT TITLE OF WORK: High Temperature Superconducting Wire and Motor

PRINCIPAL INVESTIGATOR: John W. Halloran
(617) 354-2020

This is the Second Quarterly Report on a project to develop HTSC wire for an HTSC motor. The wire fabrication task at CPSS and AIResCo is making progress in each separate process step. The raw material for fiber production is an improved $YBa_2Cu_3O_{7-x}$ powder made at CPSS in adequate quantities to support the program. Continuous spools of green $YBa_2Cu_3O_{7-x}$ fiber are being produced. The major effort in fiber spinning is aimed at improving fiber quality and reducing fiber diameter. Binder burnout and sintering has been intensively investigated. Fiber sintering fibers is done rapid zone sintering method. A continuous furnace recieved near the end of this Quarter will be used for continuous sintering. Continuous silver coated green fiber are produced. We have made progress toward continuous cladding using the mechanical cladding concept.

The melt spinning process was successfully applied to $YBa_2Cu_3O_{7-x}$ powders at 50 vol% solids loadings. Spools of continuous fiber were produced with diameters ranging between 3 and 15 mils, with several carrier polymer systems. The $YBa_2Cu_3O_{7-x}$ was found to react with polymers and processing aids during binder burnout under certain conditions. With fast heating, however, these reactions can be avoided, producing sintered filaments with no apparent degradation. Analysis of sintered fiber shows carbon levels at 0.18%, which is the same as the starting powder.

The sintering of variety of $YBa_2Cu_3O_{7-x}$ powders was examined in form of dry spun fibers. Melt spun fibers sinter well, achieving a microstructure consistent with the particle size. Fibers from different carrier polymers sinter similarly, although EVA fibers have less shape retention than HDPE fibers.

The cladding work centered on mechanical cladding of silver treated filaments by solder bonding to copper strips. Thin silver alloy coatings are co-fired with the fiber. Components for a continuous cladding module are being evaluated.

Aluminum deposits on $YBa_2Cu_3O_{7-x}$ filament surfaces were produced by MOCVD at ATM, but the superconductivity was degraded. Lashmore and Stafford at NIST produced Al-Mn electrodeposits on filaments from molten salt. The clad filaments were superconducting, but an insulating layer formed between the $YBa_2Cu_3O_{7-x}$ substrate and the metal deposit. Electroless copper was deposited on $YBa_2Cu_3O_{7-x}$ filaments at SUNY-Buffalo, but the superconductivity was degraded.

Electrical characterization work focused on methods of making low resistance contacts on $YBa_2Cu_3O_{7-x}$ filaments. Contact resistance was reduced to as low as 20 microohm/cm2. New software was written for measuring critical current and resistive transition.

Emerson Motor Division has begun work on DC heteropolar and homopolar motor designs. The mechanical stresses on conventional copper wires during winding have been characterized to determine the mechanical parameters of motor building. A materials property database is being assembled for $YBa_2Cu_3O_{7-x}$, with the major uncertainties being the material's tolerance of time varying magnetic fields and critical current in magnetic fields.

ATTACHMENT III

ARPA ORDER NUMBER: 9525 PROGRAM CODE NUMBER: 7737

CONTRACTOR: Ceramic Process Systems Corporation
840 Memorial Drive
Cambridge, MA 02139

CONTRACT NUMBER: N00014-88-C-0512 CONTRACT AMOUNT: $ 5,509,387.00

EFFECTIVE DATE OF CONTRACT: 30 JUNE 1988

EXPIRATION DATE OF CONTRACT: 31 MARCH 1991

PRINCIPAL INVESTIGATOR: John W. Halloran

TELEPHONE NUMBER: (617) 354-2020

SHORT TITLE OF WORK: High Temperature Superconducting Wire and Motor

REPORTING PERIOD: 1 OCTOBER 1988 through 31 DECEMBER 1988

DESCRIPTION OF PROGRESS

The HTSC ceramic wire will be a flexible composite of many fine ceramic filaments clad with copper. The three basic elements of this method are: 1) spinning polymer-containing "green" fibers; 2) sintering the fibers to make bare superconducting ceramic filaments; and 3) cladding the filaments with copper. The wire fabrication task at CPSS and AIResCo is making progress in each separate process step. The raw material for fiber production is an improved $YBa_2Cu_3O_{7-x}$ powder made at CPSS in adequate quantities to support the program. Continuous spools of green $YBa_2Cu_3O_{7-x}$ fiber are being produced. The major effort in fiber spinning is aimed at improving fiber quality and reducing fiber diameter. Binder burnout and sintering has been intensively investigated. Fiber sintering fibers is done rapid zone sintering method. A belts furnace recieved near the end of this Quarter will be used for continuous sintering. Continuous silver coated green fiber are produce for use in the metal cladding. A continuous cladding method based on the mechanical cladding concept is being developed.

Emerson Motor Division has begun work on DC heteropolar and homopolar motor designs. The mechanical stresses on conventional copper wires during winding have been characterized to determine the mechanical parameters of motor building. A materials property database is being assembled for $YBa_2Cu_3O_{7-x}$, with the major uncertainties being the material's tolerance of time varying magnetic fields and critical current in magnetic fields.

SUMMARY OF SUBSTANTIVE INFORMATION DERIVED FROM SPECIAL EVENTS

Project members attended the several conferences on high temperature superconductivity to keep abreast of current developments.

CHANGE IN KEY PERSONNEL

No change

PROBLEMS ENCOUNTERED AND/OR ANTICIPATED

None

ACTION REQUIRED BY THE GOVERNMENT

None

FISCAL STATUS

1) Amount currently received on contract:		$ 537,124.59
2) Expenditures and commitments to date:		$ 753,820.10
3) Funds required to complete work:		
	through 9/30/89	$ 934,073.00
	through 3/31/91	$ 4,755,567.00